

SIMULATION OF ELECTRICALLY LARGE STRUCTURES IN EMC STUDIES: APPLICATION TO AUTOMOTIVE EMC

THÈSE N° 2957 (2004)

PRÉSENTÉE À LA FACULTÉ SCIENCES ET TECHNIQUES DE L'INGÉNIEUR

Institut des sciences de l'énergie

SECTION D'ÉLECTRICITÉ

ÉCOLE POLYTECHNIQUE FÉDÉRALE DE LAUSANNE

POUR L'OBTENTION DU GRADE DE DOCTEUR ÈS SCIENCES TECHNIQUES

PAR

Abraham RUBINSTEIN

ingénieur électricien, Universidad del Zulia, Maracaibo, Venezuela
et de nationalité colombienne

acceptée sur proposition du jury:

Dr F. Rachidi-Haeri, directeur de thèse

Dr G. Klaus, rapporteur

Dr J.-P. Parmantier, rapporteur

H. Ryser, rapporteur

Prof. A. Skrivervik Favre, rapporteur

Lausanne, EPFL
2004

To Manuel, Marcos and Martha

Summary

The aim of this thesis is the study of the simulation of electrically large structures and the application of the results to automotive Electromagnetic Compatibility (EMC). The theoretical and experimental work carried out has led to the development of computational tools and to the further understanding of the mechanisms involved in the representation of solid surfaces by means of wire-grid simplifications. The work was done in the context of a European project GUIDELINES FOR ELECTROMAGNETIC COMPATIBILITY MODELLING FOR AUTOMOTIVE REQUIREMENTS (*GEMCAR*).

The first two chapters of the thesis contain a description of the *GEMCAR* project, a brief overview of some of the existing numerical methods for electromagnetic simulations (particularly, the ones used in *GEMCAR*), and the explanation of efficient, general simulation strategies that can be applied to different methods. The concept of adaptive sampling and its application are also introduced there. The main original contributions of this thesis are presented in Chapters 3 through 6. They consist of theoretical and experimental work as follows.

We present, in Chapter 3, a modified version of the Numerical Electromagnetics Code (NEC). This version, which we have called Parallel NEC, has been adapted to run on parallel supercomputers, taking advantage of the combined processing power and memory of several processors working as a team. Parallel NEC has been implemented in two different supercomputing architectures to test the portability of the code. The original NEC routines in charge of the calculation and filling of the interaction matrix have been modified to work in a parallel environment. The matrix is now distributed among the available processors and the elements of the matrix are locally and individually calculated by their “owners”. Thus the number of integrals carried out to build the complete matrix equation gets shared, diminishing the necessary runtime for

this time-consuming operation. The system of equations is also solved using a parallel version of the Gauss-Doolittle algorithm. However, the most important feature of Parallel NEC is the possibility to use the distributed memory of the processors. This allows the calculation of problems of a size never achieved before using this numerical method without the need of using disk-space as swap memory. The code has been tested with models containing over 20.000 segments, exhibiting execution times comparable to those obtained with a single-processor PC calculating models of one tenth of that size in terms of the number of segments. Parallel NEC is also able to adapt itself automatically to its environment. It will detect the number of available processors and will take advantage of all available memory and calculating resources.

The validation of Parallel NEC has been carried out in two steps. First, it was validated using simulation results obtained with other numerical methods. Then, it was validated by using experimental data from the GEMCAR project. The experimental setup as well as the validation are presented in Chapter 4.

With the purpose of validating the numerical models developed in GEMCAR, we participated in a number of experimental campaigns carried out at Spiez, Switzerland in 2000 and 2001 using the *VERIFY* (Vertical EMP Radiating Indoor Facility), an EMP simulator belonging to the Swiss Defense Procurement Agency. Measurements of electric and magnetic fields inside a real vehicle (a Volvo S80) featuring different levels of complexity were carried out. These measurements were performed at 8 different points inside the car and at two points on the surface of the body-shell.

The above-mentioned levels of complexity consisted of (1) a “simple test case”, comprising the vehicle body-shell (without all doors or glazing), (2) a “medium complexity case” which, this time, included the doors, and (3) a “complex case”, consisting of the complete car with all mechanical, electrical and electronic equipment installed.

The data used in Chapter 4 refer to the “simple test case”, although the “medium test case” measurements are also available. Other partners of the GEMCAR project carried out experimental testing on the three models using other sources of illumination (see Chapters 1 and 4).

It is interesting to mention for completeness that, as part of the GEMCAR project, a cable harness was installed following the approximate path of the original cabling of

the car, but composed of single wires with 50Ω terminations. Current measurements were made at 4 observation points located at the ends of the branches of the harness. These current measurements are not given here as the subject of this thesis was limited to field measurements and simulations only¹.

The developed code was applied to analyze the penetration of electromagnetic fields inside the vehicle's body shell (i.e., the simple case). The computed results agree well with those obtained with the other methods and with the experimental data obtained from measurements.

The application of the code to such a large problem permitted the observation of some issues raised by the application of the so-called Equal Area Rule (EAR) for the calculation of the segments' lengths and radii.

In Chapter 5, we discuss the wire-grid representation of metallic surfaces in numerical electromagnetic modeling. We present the origins and the evolution of surface wire-grid modeling and, considering two types of geometries, namely (1) a simple cube, and (2) a complex structure represented by the metallic car shell used in Chapter 4, we show that the Equal Area Rule is accurate as long as the wire-grid consists of a simple square mesh. For more complex body-fitted meshes, such as rectangular and triangular grids, the Equal Area Rule appears to be less accurate in reproducing the electromagnetic field scattered by metallic bodies.

In Chapter 6 we present a theoretical development that leads, for the case of a square grid representation of a surface, to the same formula proposed by the Equal Area Rule. This development is, to the best of our knowledge, the first physical and mathematical interpretation of the EAR as of today. Our development shows, however, a different value for the radius of the segments if the representation of the surface uses other polygons, such as in the case of a rectangular or a triangular mesh. To compare the two methods (the traditional versus the new EAR), we carried out a simple numerical test and found that the Equal Area Rule does not always predict the optimum wire radius for the mesh representation of a surface.

¹The interested reader is referred to:

A. Rubinstein, F. Rachidi, D. Pavanello, and B. Reusser. Electromagnetic field interaction with vehicle cable harness: An experimental analysis. *In International Conference on Electromagnetic Compatibility, EMC Europe. Sorrento*, volume 1, Sep 2002. Proceedings.

Résumé

L'objectif de ce travail de thèse est l'étude de la simulation de structures électriquement grandes et l'application des résultats aux problèmes de compatibilité électromagnétique (CEM) dans l'industrie automobile. Les travaux théoriques et expérimentaux effectués ont permis le développement d'outils numériques et l'amélioration de la compréhension des mécanismes impliqués dans la représentation des surfaces solides en utilisant des maillages segmentés. Le travail a été effectué dans le cadre d'un projet Européen GUIDELINES FOR ELECTROMAGNETIC COMPATIBILITY MODELLING FOR AUTOMOTIVE REQUIREMENTS (*GEMCAR*).

Les premiers deux chapitres de ce travail de thèse contiennent une description du projet *GEMCAR*, une brève vue d'ensemble des quelques méthodes numériques existantes pour les simulations électromagnétiques (en particulier, ceux utilisés dans *GEMCAR*), et l'explication d'efficaces stratégies générales de simulation qui peuvent être appliquées aux différentes méthodes. Le concept d'échantillonnage adaptatif et son application y sont aussi introduits. Les principales contributions originales de cette thèse sont présentées dans les chapitres 3 à 6. Elles comportent les parties expérimentales et théoriques suivantes.

Nous avons présenté dans le chapitre 3, une version modifiée du Numerical Electromagnetics Code (NEC). Cette version que nous avons appelé Parallel NEC a été adaptée pour tourner sur des superordinateurs parallèles, profitant de la puissance de calcul et de la mémoire combinés de plusieurs processeurs travaillant en équipe. Parallel NEC a été implémenté sur deux superordinateurs aux architectures différentes pour tester la portabilité du code. Les routines originales du NEC responsables du calcul et de la construction de la matrice d'interaction ont été modifiées pour travailler dans un environnement parallèle. La matrice est désormais distribuée parmi

les processeurs à disposition et les éléments de la matrice sont calculés localement et individuellement par leurs “propriétaires”. De ce fait, le nombre d’intégrales calculées pour compléter l’équation matricielle se partage, diminuant ainsi le temps de calcul nécessaire pour cette longue opération. Le système d’équations est aussi résolu en utilisant une version parallèle de l’algorithme de Gauss-Doolittle. Cependant, la caractéristique la plus importante de Parallel NEC est la possibilité d’utiliser la mémoire partagée des processeurs. Ceci permet le calcul de problèmes d’une dimension jamais réalisée auparavant en utilisant cette méthode numérique sans avoir à utiliser le disque dur comme mémoire virtuelle. Le code a été testé avec des modèles contenant plus de 20.000 segments, montrant des temps d’exécution comparables à ceux obtenus avec un PC monoprocesseur calculant des modèles d’un dixième de cette taille en termes de nombre de segments. Parallel NEC est aussi capable de s’adapter automatiquement à son environnement. Il détecte le nombre de processeurs disponibles et profite de toute la mémoire et des ressources de calcul.

La validation de Parallel NEC a été réalisée en deux étapes. Premièrement, il a été validé en utilisant des résultats de simulations obtenus avec d’autres méthodes numériques. Puis, il a été validé en utilisant des données expérimentales provenant du projet GEMCAR. La configuration expérimentale ainsi que la validation sont exposées dans le chapitre 4.

Afin de valider les modèles numériques développés dans GEMCAR, nous avons participé à un certain nombre de campagnes expérimentales réalisées à Spiez, Suisse en 2000 et 2001 en utilisant le *VERIFY* (Vertical EMP Radiating Indoor Facility), un simulateur EMP appartenant au Groupement de l’Armement Suisse. Des mesures de champs électrique et magnétique ont été effectuées dans une véritable automobile (une Volvo S80) avec différents niveaux de complexité. Ces mesures ont été effectuées en 8 points différents dans la voiture et en deux points sur la surface de la carrosserie.

Les niveaux de complexité mentionnés précédemment consistent en (1) un “cas de test simple”, comprenant la carcasse du véhicule (sans les portes ni les vitres), (2) un “cas de complexité moyenne” avec cette fois-ci les portes et (3) un “cas complexe”, consistant en une voiture complète avec tous les équipements mécaniques, électriques et électroniques installés.

Les données utilisées dans le chapitre 4 se rapportent au “cas de test simple” bien que les mesures du “cas de complexité moyenne” soient aussi disponibles. D’autres partenaires du projet GEMCAR ont réalisé des tests expérimentaux sur les trois modèles utilisant d’autres types de sources d’illumination (voir chapitres 1 et 4).

Il est intéressant de mentionner que dans le cadre du projet GEMCAR, un câblage a été installé suivant un chemin approché à celui du câblage original de la voiture, mais composé d’un seul fil terminé avec 50Ω . Des mesures de courant ont été prélevées à 4 points d’observation localisés aux extrémités des branches du câble. Ces mesures de courant ne sont pas présentées ici puisque le sujet de cette thèse a été limité exclusivement aux mesures et simulations de champs électromagnétiques¹.

Le code développé a été appliqué pour analyser la pénétration de champs électromagnétiques dans la carcasse du véhicule. Les résultats numériques sont en bon accord avec ceux obtenus en utilisant d’autres méthodes numériques et avec les données expérimentales.

L’application du code sur un problème de telles dimensions a permis l’observation de quelques problèmes provenant de l’utilisation de la dite Equal Area Rule (EAR) pour le calcul de la longueur et le rayon des segments représentant une surface métallique.

Dans le chapitre 5, nous discutons la représentation des surfaces métalliques par un maillage de conducteurs (wire-grid) dans la simulation numérique. Nous avons présenté les origines et l’évolution de la modélisation de surfaces par des maillages, considérant deux types de géométries, à savoir (1) un cube simple, et (2) une structure complexe représentée par la carrosserie métallique de la voiture utilisée dans le chapitre 4. Nous montrons que l’Equal Area Rule est précise pour un maillage carré. Pour des maillages plus complexes et plus adaptés aux contours du modèle, tels que les maillages triangulaires, l’Equal Area Rule semble être moins exacte pour reproduire le champ électromagnétique au voisinage des objets métalliques.

Dans le chapitre 6, nous présentons un développement théorique qui mène, pour le cas de la représentation d’une surface par un maillage rectangulaire, à la même

¹Le lecteur intéressé est référé à :

A. Rubinstein, F. Rachidi, D. Pavanello, and B. Reusser. Electromagnetic field interaction with vehicle cable harness: An experimental analysis. *In International Conference on Electromagnetic Compatibility, EMC Europe. Sorrento*, volume 1, Sep 2002. Proceedings.

formule proposée par l'Equal Area Rule. Ce développement est, au meilleur de notre connaissance, la première interprétation physique et mathématique de l'EAR de nos jours. Notre développement montre, cependant, une valeur différente pour les rayons des segments si la représentation de la surface utilise un maillage triangulaire. Pour comparer les deux méthodes (la traditionnelle vs. la nouvelle EAR), nous avons réalisé un test numérique simple. Bien que les résultats ne soient pas concluants, ils suggèrent que la nouvelle EAR (NEAR) donne de meilleurs résultats.

Remerciements

Le travail dans le monde scientifique est une source inépuisable de satisfactions. Cependant, la récolte du fruit de l'effort intellectuel, dont la culture peut tarder des années, demande parfois beaucoup de patience et d'optimisme face aux adversités. J'ai eu la chance de trouver en mon directeur de thèse, le Dr. Farhad Rachidi, une source elle aussi inépuisable de patience et de optimisme dont j'ai eu besoin au cours des dernières quatre années pour finir mon travail. Farhad a converti les obstacles en points d'appui et m'a fait profiter de ses vastes connaissances et de ses compétences et de son incroyable qualité humaine. Merci Farhad. Un grand merci au Professeur Alain Germond, directeur du laboratoire de réseaux électriques (LRE) pour m'avoir accueilli dans son laboratoire. Merci au Professeur Michel Ianoz pour ses conseils et son soutien.

Le Professeur Marcos Rubinstein est mon frère. Il ne se souvient probablement pas, mais un jour, quand j'avais plus ou moins 8 ans, chez des amis à Maracay, au Venezuela, il a trouvé dans une chambre, un Apple[[et il m'a appelé pour que je voie pour la première fois de ma vie un ordinateur. Là, sous mon regard émerveillé et stupéfié, il m'a fait un cadeau dont il n'a certainement jamais pris conscience ; il a rédigé en quelques secondes deux lignes dans une langue incompréhensible (un petit logiciel en BASIC) qui a rempli l'écran avec des centaines de fois mon prénom. Ce jour là, j'ai été contaminé par la fièvre des ordinateurs, par la folie de la technologie. Plus tard, quand j'avais 11 ans, il m'a fait cadeau d'un Commodore 64, mon premier ordinateur. Il a trouvé la manière de me faire venir en Suisse en 1996 faire un stage au LRE, ce qui m'a ouvert les portes pour venir faire mon doctorat en 2000. Il a aussi proposé des idées brillantes pour mon travail de thèse et il a donné les dernières corrections au manuscrit. Pour tout ça, et pour beaucoup plus, merci Marcos.

Mon travail de thèse a été développé dans le cadre d'un projet européen (GEM-

CAR) financé partiellement par l'office fédéral de l'éducation et de la science (OFES) à qui je transmets mes remerciements les plus amples.

Je voudrais remercier également tous les membres du projet GEMCAR, qui ne m'ont jamais fait sentir comme un étudiant. Ils ont partagé avec moi leur expérience et ils ont toujours écouté avec sincère intérêt ce que j'avais à dire. Un grand merci en particulier au Dr. Jean-Philippe Parmantier de l'ONERA, France, qui a été membre du jury de ma thèse et m'a proposé des bonnes idées qui ont amélioré la qualité de mon travail. Au Dr. Alastair Ruddle de MIRA, UK, le coordinateur de GEMCAR, pour sa confiance et son soutien. Un grand merci à Xavier Ferrières de l'ONERA, pour son aide au développement des différents modèles utilisés dans le projet et dans la thèse. Je tiens à remercier aussi le Dr. Magnus Granström de Volvo, Suède, pour son aide avec des données concernant la Volvo S80, indispensables pour l'écriture de ce travail.

Un grand merci également aux MM. Markus Nyffeler et Beat Reusser du Regroupement de l'Armement Suisse (NEMP Labor Spiez) pour leur soutien et pour leur collaboration dans l'utilisation du générateur d'impulsions VERIFY.

Mes plus sincères remerciements au Professeur Juan Mosig pour avoir accepté la présidence du jury ainsi qu'aux membres du jury, Prof. Anja Skrivervik, Dr, J.P. Parmantier, M. Heinrich Ryser et Dr. Georg Klaus pour leurs suggestions et remarques constructives.

A mes amis et collègues du LRE : Anne-Claude Maillefer, Davide Pavanello, Elvira Kägi-Kolisnychenko, José Luis Bermudez, Rachid Cherkaoui, Emanuel Petrache, Pierre Zweiacker, Elena Vdovina, Ana Vukicevic et Alexandre Oudalov. Je tiens à exprimer mes remerciements les plus sincères à notre secrétaire, Andrée Moinat, qui a toujours rendu plus facile, le côté compliqué du travail au laboratoire (affaires de bureau). Un merci très spécial aussi à mon collègue de bureau et mon ami, Emmanuel Marthe, pour son aide et soutien avec les ordinateurs et particulièrement avec L^AT_EX.

Je remercie mes amis, qui se trouvent malheureusement très loin. Il a été très dur de les quitter pour traverser l'océan et parcourir les quelques 10000 Km qui nous séparent. J'ai eu néanmoins la chance d'avoir près de moi, par longues périodes pendant la rédaction de cette thèse, des personnes que j'aime profondément et de tout mon cœur. Merci Mary Liz d'être resté chez-nous l'été dernier, de m'avoir fait partager le bonheur

de ta grossesse, de remplir de bon humour ces jours difficiles du commencement de la rédaction du manuscrit. Merci pour ton amitié sincère et pour ton soutien, et pour les merveilleux moments que nous avons, autant de fois, partagés avant et après mon départ de Maracaibo. Merci aussi de m'avoir appelé en plus d'une occasion, ton meilleur ami. Merci à toi et aussi à Mario pour partager avec moi l'arrivée de votre fille, Ema Lucia. Merci Mario pour me faire part de tes rêves et tes préoccupations et pour me faire profiter de la bonté et la générosité qui te caractérisent. Ma chère Maria, merci pour prendre la relève après le départ de Mary Liz l'an dernier, mais surtout merci pour tout ce que tu as toujours fait pour moi, depuis le mois de septembre 1986, quand nous nous sommes rencontrés. Merci de supporter mon manque de patience plus des fois qu'il n'en a été juste et d'être toujours là quand j'en ai eu besoin. Merci d'avoir fait ce long voyage et d'être encore aujourd'hui, malgré le temps et la distance, mon amie inconditionnelle.

Je te remercie maman, pour être si fière de mes frères et de moi et surtout pour le dire à haute voix. Merci pour cette force et cette énergie que tu as toujours montré. Je disais à l'époque, quand je te voyais travailler si dure, puis, arriver à la maison t'occuper de tout (y compris moi), que tu étais inépuisable et que ça ne t'arrivait jamais d'être fatiguée. Aujourd'hui je comprends que ça t'arrivé tous les jours. Tu devais être très fatiguée, mais tu travaillais et tu t'occupais de moi, malgré ta fatigue, parce que tu m'aimes. Merci Martha, Manuel et Marcos pour m'avoir permis de profiter de ma place de cadette. Vous m'avez tous apporté votre aide et votre soutien et vous le faites toujours comme si j'étais un enfant. Il est vraiment délicieux de se sentir le petit de la maison avec deux frères et une sœur comme vous.

Je l'ai déjà dis, il est très dur de quitter son pays, ses amis. Il est encore plus dur de quitter sa famille. Il est dur parfois d'accepter les différences d'une nouvelle culture, une langue étrangère, de tout recommencer. Je te remercie Virginia d'avoir traversé tout ça, rien que pour moi, pour la très simple raison d'être à mon côté. Et je sais qu'il n'est pas toujours évident d'être à mon côté. Merci de récolter les mangues vertes et mures avec moi.

Contents

Summary	i
Résumé	v
Remerciements	ix
List of Figures	xvii
List of Tables	xxi
1 Introduction	1
1.1 Motivation	1
1.2 The GEMCAR Project	4
1.3 Organization of the Thesis	10
2 Numerical Methods and Simulation Strategies Applied to the Problem of Interest	15
2.1 Introduction	15
2.2 Modeling Methodology	16
2.3 Modeling Functional EMC Performance	17
2.4 Capabilities of Numerical Techniques	19
2.4.1 Time and Frequency Domain Techniques	19
2.4.2 Types of Simulations	20
2.5 Methods applied within GEMCAR	22
2.5.1 The Finite-Difference Time-Domain (FDTD)	22
2.5.2 The Transmission Line Matrix (TLM)	25

2.5.3	The Boundary Element Model (BEM)	27
2.5.4	The Method of Moments (MoM)	28
2.6	Combining Different Methods	31
2.6.1	Multiple Domain Approach	31
2.6.2	Hybridization approach	31
2.7	Efficient Frequency Selection	32
2.7.1	Adaptive Sampling	32
2.7.2	The Blumer Index	33
2.8	Comparison of GEMCAR Numerical Methods for a Biconilog Antenna	34
2.9	Conclusions	36
3	Development of an Optimized Parallel Numerical Electromagnetics Code based on NEC2	41
3.1	Introduction	41
3.2	Parallel Implementation of NEC	43
3.2.1	Structure of NEC	43
3.2.2	Two-Dimensional Block-Cyclic Decomposition	45
3.2.3	Parallelization Strategy	49
3.3	Test and Performance	51
3.3.1	The Swiss-T1 Parallel Supercomputer	51
3.3.2	The Eridan Parallel Supercomputer	52
3.3.3	Performance of Parallel NEC	55
3.4	Conclusions	59
4	Validation of Parallel NEC	63
4.1	Introduction	63
4.2	Description of the Configuration	64
4.2.1	Numerical Validation of Parallel NEC	68
4.2.2	Experimental Results	72
4.2.3	Discussion on Meshing Issues	73
4.3	Conclusions	77

5	The Wire-Grid Representation of Solid Metallic Surfaces using the MoM	81
5.1	Introduction	81
5.2	The Equal Area Rule	83
5.3	A Numerical Example using Parallel NEC	85
5.4	Conclusions	88
6	Improved Surface Modelling. The New Equal Area Rule (NEAR)	93
6.1	Introduction	93
6.2	Theoretical basis for the classical Equal Area Rule (EAR) and proposed New Equal Area Rule (NEAR)	94
6.3	Application to other patterns	98
6.4	Comparison Between the Classical and the New EARs	101
6.4.1	The Radius Predicted by the Classical Equal Area Rule (EAR)	101
6.4.2	The Radius Predicted by the New Equal Area Rule (NEAR) . .	102
6.5	Conclusions	103
7	Conclusions and Perspectives	109
	Appendix	113
	Glossary of Terms	123
	Curriculum vitae	127

List of Figures

1.1	Electromagnetic environment of a modern car	2
1.2	Internal cabling of a Volvo S80. Courtesy of Volvo Car Corp	3
1.3	Background and expertise of GEMCAR partners	6
1.4	Field Measurement points defined in the GEMCAR Project	6
1.5	Logperiodic antenna used in the GEMCAR project	8
1.6	Biconilog antenna used in the GEMCAR project	9
1.7	VERIFY EMP Simulator	10
2.1	Strategy for EMC performance prediction using separated methods (adapted from [3])	19
2.2	FDTD basic cubic cell	23
2.3	Mesh of a Volvo S80 for a FDTD calculation	25
2.4	A so-called Symmetrical Condensed Node in the TLM method. The node is at the intersection point of the six transmission lines leading to the neighboring nodes	26
2.5	Mesh of a Volvo S80 for a TLM calculation	27
2.6	Mesh of a Volvo S80 for a BEM calculation	28
2.7	MoM Mesh of a Volvo S80	30
2.8	Example of GEMCAR's hybrid FV/FDTD mesh (adapted from [3])	32
2.9	Relative field strength at a measuring point in front of the antenna	35
2.10	MoM (NEC) model of the GEMCAR Biconilog Antenna	35
3.1	Flow diagram of NEC2. Adapted from [1]	46
3.2	Flow diagram of the developed Parallel NEC. Shaded: modified or newly created parallel code. Adapted from [8]	47

3.3	Distribution of matrix among 4 processors	48
3.4	Calculation of an upper triangular matrix	49
3.5	Swiss-T1 calculation server	52
3.6	Swiss-T1 calculation server architecture	53
3.7	The TNet switches with 12 ports each	53
3.8	Eridan calculation server	54
3.9	Eridan calculation server architecture	54
3.10	mesh of the simplified car consisting of 6753segments used for performance comparisons	55
3.11	Matrix factorization time as a function of number of processors for the Swiss-T1 parallel supercomputer	57
3.12	Total run time as a function of number of processors for the Swiss-T1 parallel supercomputer	57
3.13	NEC mesh of the considered geometry consisting of 23449 segments used for performance comparisons	58
4.1	Vehicle models	64
4.2	Field Measurement Points defined in the GEMCAR Project	64
4.3	VERIFY EMP Simulator	65
4.4	Cartography of the incident filed of the VERIFY EMP simulator	66
4.5	Vertical electric field inside the working volume of the simulator	67
4.6	Measurement points for current at the cable harness	67
4.7	Thomson Electric and Magnetic Field Sensors used for the EMP simulator measurements	68
4.8	Test car inside the simulator (side illumination)	69
4.9	Illustration of the four measurements points inside the vehicle (front illumination)	69
4.10	Vertical electric field component measured at Points P3, P4, P5 and P6. Front illumination	70
4.11	Vertical electric field component measured at Points P3, P4, P5 and P6. Side illumination	71

4.12	Meshing of the different numerical methods used for validation (Adapted from [10])	72
4.13	Comparison of the numerical results from different methods	73
4.14	Normalized vertical electric field E_z at points P3, P4, P5, and P6. Comparison between measurements and simulations (using parallel NEC) for front illumination. The fields are normalized with respect to the incident field located at the centre of the EMP simulator	74
4.15	Normalized vertical electric field E_z at points P3, P4, P5, and P6. Comparison between measurements and simulations (using parallel NEC) for side illumination. The fields are normalized with respect to the incident field located at the centre of the EMP simulator	75
4.16	Comparison of measurement and simulation for the two different meshes. Adapted from [11]	76
5.1	Four single wires representing a solid square patch. Adapted from [9]	84
5.2	Surface area of a wire. Adapted from [9]	84
5.3	Equal Area Rule for an arbitrarily shaped mesh. Adapted from [9]	85
5.4	Cube with rectangular Mesh. Adapted from [9]	87
5.5	Cube with triangular Mesh. Adapted from [9]	87
5.6	Simulated E-field as a function of the wire radius for a rectangular (squared) and a triangular meshes. Adapted from [9]	89
6.1	Scattered field generated by a perfect conductor in response to an incident electric field	95
6.2	A wire grid representation of the slab using rectangles	96
6.3	Geometry of the problem for one of the segments	96
6.4	Surface chosen for the derivation of the NEAR formula for a triangular mesh	99
6.5	(a) The triangular mesh corresponding to the surface under consideration and (b) the geometry of one triangle	99
6.6	Model of an octahedron meshed with a triangular grid	101
6.7	Triangular mesh of a face of the Octahedron	102

6.8	Comparison of the total E field calculated using the Classical (EAR) and the New (NEAR) formulas	104
1	Flow diagram for the use of the Blumer Index. Adapted from [1]	114
2	Plots of (a) the spectral magnitude of the damped sine waveform, and (b) the magnitude derivative of the spectrum. Adapted from [1]	116
3	Event flow for determining new frequency points in the spectrum. Adapted from [1]	117
4	Spectral magnitude for iterations 1 - 8 (note that there is also a spectral point at $\omega_{min} = 0$, which is not evident on the log-log plots). Adapted from [1]	118
5	Frequency spectrum of the vehicle simulation after each iteration	120

List of Tables

1.1	GEMCAR consortium. Adapted from [8]	5
1.2	Electrical specifications of VERIFY	11
2.1	Classification of model types required to predict functional performance of vehicle electrical systems (adapted from [3])	18
2.2	Relative merits of simulation techniques (adapted from [3])	20
3.1	Timing and memory as a function of the number of processors for a 6753 segments test case on the Swiss-T1 parallel supercomputer	56
3.2	Timing and memory as a function of the number of processors for a 23449 segments test case. Asterisks are used where the results could not be obtained due to early interruption of the program	58
4.1	Electrical specifications of VERIFY	65
1	Blumer index for the spectrum of Figure 4 as a function of the iteration number	117
2	Blumer index for the spectra of Figure 5 as a function of the number of iterations	119

Chapter 1

Introduction

1.1 Motivation

The world is living a technological revolution in which regular people find themselves submerged in a universe of state of the art gadgets. Just by holding a cellular phone to make a call or entering some public areas, where freely available Internet access can be found by means of Wireless LAN (WLAN) or Bluetooth, we are surrounded by sources of electromagnetic interference, the main study subject of Electromagnetic Compatibility (EMC). From this fact, and the arrival of electric and hybrid cars, the automotive industry has been moving in the past few years towards the inclusion of EMC testing as a requirement for the commercialization of new models (see Figure 1.1).

In the automobile industry, the production of a new model requires the construction of a prototype that is subjected to different tests, from security to stability to radiation immunity. Data collected in this experimental phase, may (and often does) lead to changes in design, so that a new prototype is built and, again, taken into the study phase. This is clearly an expensive process.

For many years now, the aeronautics industry has made a particular effort to include numerical simulation into the design process, since the reliability of a plane has always been considered as paramount [1]. At the same time, the automobile industry has been undergoing an increase in on-board technology. The latest models of essentially all car manufacturers rely on advanced electronic circuits for the control

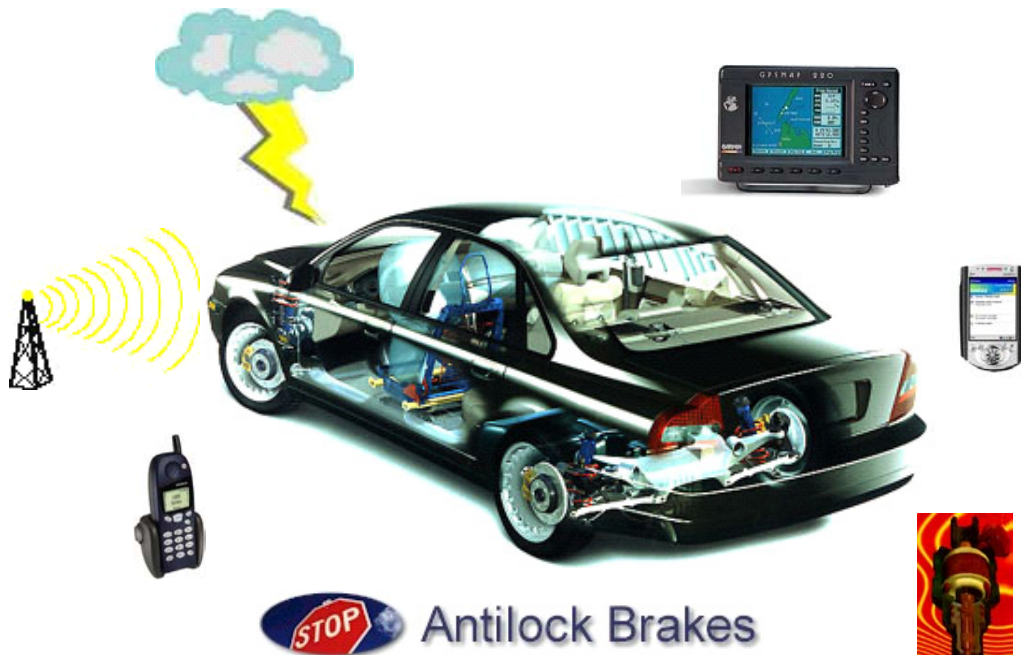


Figure 1.1: Electromagnetic environment of a modern car

and monitoring of critical tasks that were performed by electro-mechanic parts in the past. The “drive by wire” automobile is already a reality and several concept cars don’t even have a steering wheel, gas or brake pedal. Today, people drive cars with satellite global positioning systems (GPS), high-tech entertainment devices, wireless interacting systems and computer controlled brains for the optimization of fuel injection, breaks, steering, alarms, etc. This translates into a dramatic increase in the number of onboard circuits and the length of installed wires. As an example, a Volvo S80 features 1.2 km of electric cabling connecting dozens of electronic circuits by means of several hundred different wires (see Figure 1.2). These cables connecting different equipment play a dominant role in the quality (or lack thereof) of vehicles from a point of view of electromagnetic compatibility. They represent, in fact, a privileged path for the emission, reception and guidance of perturbations [2]. Additionally, studies have shown that the conducting body-shell of an automobile does not represent an efficient shield for the protection of cabling and electronic equipment from external incident electromagnetic fields. Experimental data show that, in some cases, the presence of the car may result in an enhancement of the induced currents in the wiring system [3].

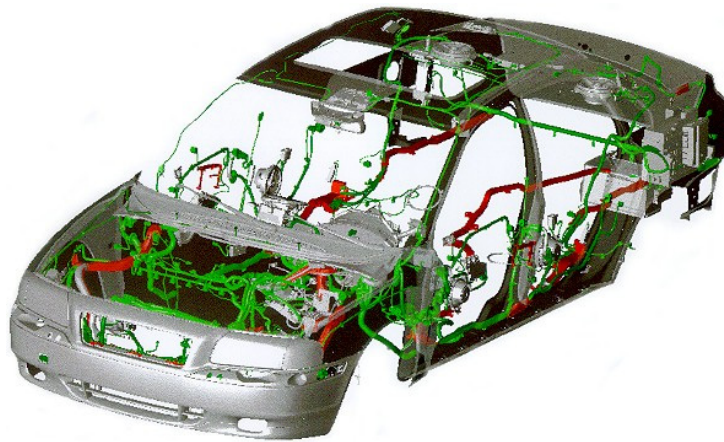


Figure 1.2: Internal cabling of a Volvo S80. Courtesy of Volvo Car Corp

Although it may still be seen as a recent problem, the subject is gaining importance, as evidenced by the fact that more and more international conferences and symposia are dedicating sessions to automotive EMC. International European projects such as AutoEMC [4] and GEMCAR [5], Ph.D. theses (e.g. [1] and [2]) as well as papers published in international journals such as [6] and [7], also support this fact.

Just as the aerodynamics and mechanical tests have been, in part, substituted by very efficient and reliable numerical simulations, the aim of the car industry is to reduce to the minimum the test-error-correct-test loop in the design phase of the electrical and electronic circuits by bringing the biggest part of the electromagnetic immunity tests to the computer in the form of simulations.

A problem inherent to the automotive industry derives from the fact that car manufacturers have to face delivery times which are significantly shorter than those dealt with in the aeronautics industry. Even though the calculation tools are perfectly suitable for both industries, the application of those tools may vary considerably when they are being used in the automobile design environment.

A number of methods are available for EM modeling. Some of them have already been applied and validated by EMC modeling experts in the aerospace industry. Each method has shown to have its advantages and disadvantages from the point of view of precision, nature of the evaluated model, computer requirements, preconditioning of the model, postprocessing of the results, etc. There is no clear winner. In fact, several

numerical methods are often applied to different parts and variations of a model, in order to obtain the best combination of accuracy and calculation time.

The development in the area of personal computers has given a new face to numerical modeling in general. The analysis of simple structures, such as antennas and some rough 3D models that begun years ago as the work of experts using very expensive computational equipment and specialized software, is becoming today a normal task carried out by radio amateurs and electronics enthusiasts using simple home PCs. Additionally, the use of more sophisticated computer resources and mathematical routines that take advantage of the latest architectures of processors, allows the study of more complex structures at a reasonable price. However, despite all these advances in computing technology, the application of some of the existing numerical methods to electrically large structures is still a challenge.

1.2 The GEMCAR Project

Most of the work presented in this thesis has been carried out in the framework of the GEMCAR project[5]. The project, which stands for Guidelines for Electromagnetic Compatibility Modelling for Automotive Requirements is a collaborative research project supported by the European Commission and the Swiss Federal Office for Education and Science. Taking into account the already mentioned matureness of the aeronautics and aerospace industries in the field of EMC modeling, the consortium included aerospace organizations working in collaboration with automotive companies. The project consortium comprised nine organisations drawn from five European countries, as shown in table 1.1. The aim of GEMCAR is the practical application of some of the different numerical methods to the automotive industry, including the development of the proper mesh of the 3D structure for each of the numerical methods considered, the study of the level of complexity required by the model, the computing requirements and limitations of each numerical method and the accuracy of the results for different configurations. The practical modeling issues established are the following:

- the requirements for EMC modelling in automotive applications
- the level of model detail that is required

Partner	Role	Country
MIRA	Coordinator	UK
CETIM	Principal contractor (industry)	France
EADS	Principal contractor (industry)	France
EPFL	Principal contractor (academic)	Switzerland
Hevrox	Principal contractor (industry)	Belgium
ONERA	Principal contractor (industry)	France
QuinetiQ	Principal contractor (industry)	UK
Volvo	Principal contractor (industry)	France
Ford	Assistant contractor (to MIRA)	UK

Table 1.1: GEMCAR consortium. Adapted from [8]

- the uses and potential benefits of automotive EMC modelling
- how to maximize the efficiency of vehicle scale simulations

With these objectives in mind, the partners were selected to provide an inter-complementary range of skills: electromagnetic modeling, EMC measurements and system integration expertise (see Figure 1.3). The contribution of the EPFL as the academic partner of GEMCAR included EMC measurements using an EMP simulator and electromagnetic modeling with the Numerical Electromagnetics Code (NEC), a numerical tool based on the Method of Moments (MoM) (see Subsection 2.5.4 and Chapters 3 and 4). It is within this context that most of the work presented in this thesis is centered. The goals were achieved by means of experimental testing, numerical modeling and comparison of experimental data and simulated results. Measurements of electric and magnetic fields inside a real vehicle (a Volvo S80) featuring different levels of complexity were carried out in order to obtain the data to validate the numerical models. These measurements were executed at 8 different points inside the car identified as points P1 to P8 in Figure 1.4. The vertical electric field was also measured at two points on the surface of the body of the car, identified as points Q1 and Q2 in the same figure.

The different levels of complexity mentioned above consisted of (1) a “simple test case”, comprising the vehicle body-shell (without all doors or glazing) and a simple harness (single conductor with branches and terminations) (2) a “medium complexity

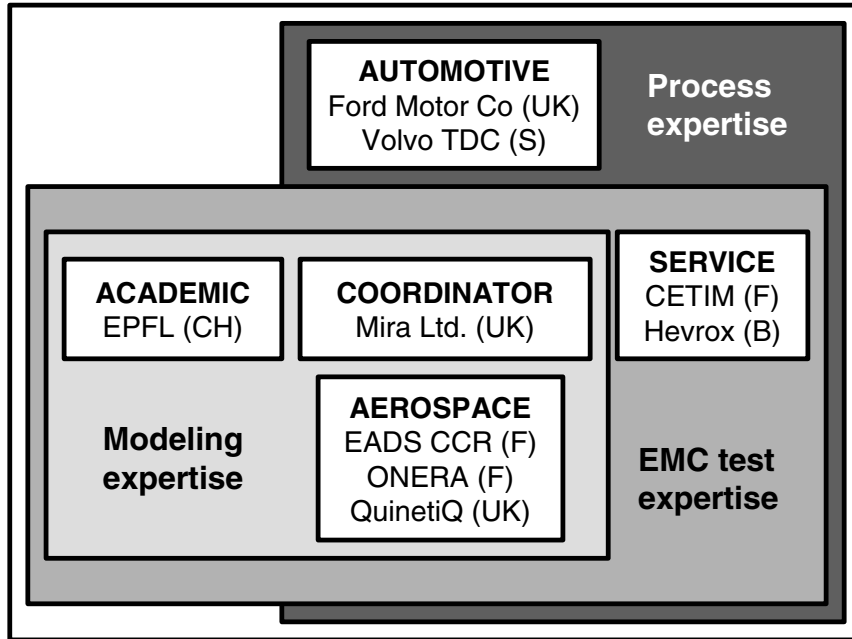


Figure 1.3: Background and expertise of GEMCAR partners

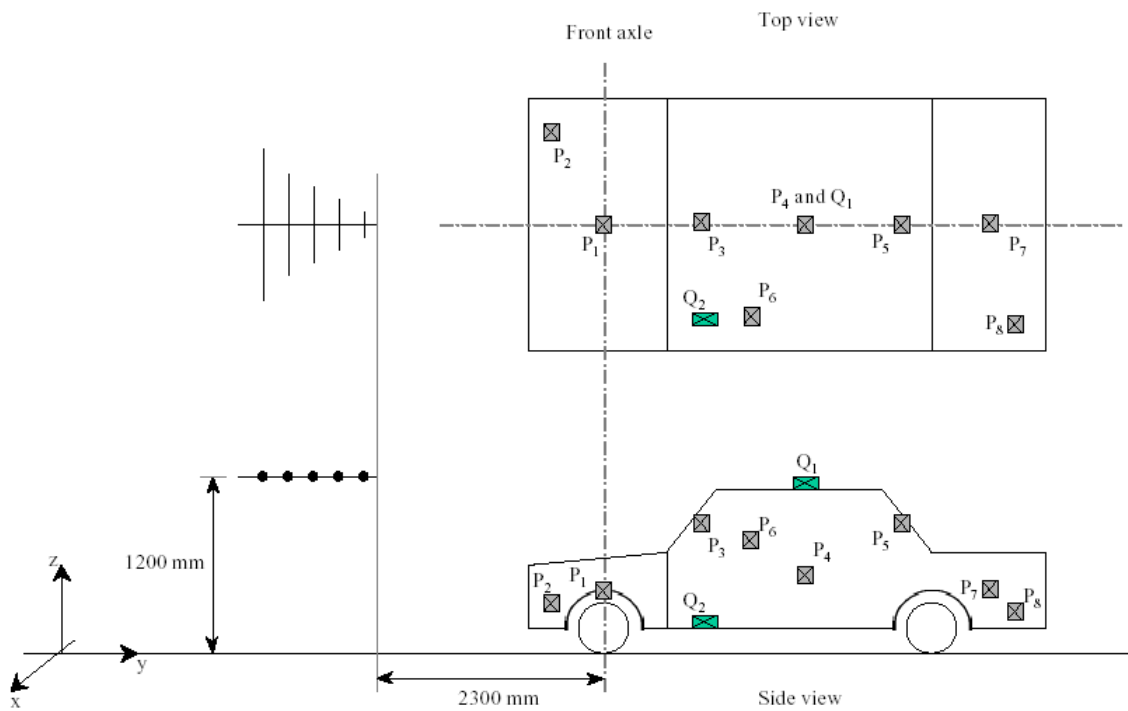


Figure 1.4: Field Measurement points defined in the GEMCAR Project

case” which this time included the doors (see Figure 4.1) and (3) a “complex case”, consisting of the total car with every mechanical, electrical and electronic equipment installed.

Three different sources were used to illuminate the car: (1) an EMCO log-periodic dipole array antenna (type: 3146, bandwidth 200-1000 MHz, Figure 1.5), (2) an EMCO biconilog antenna (type: 3143, bandwidth: 20-1000 MHz, Figure 1.6) and (3) the *VERIFY* EMP simulator belonging to the Swiss Defence Procurement Agency, located at Spiez (see Figure 1.7 and Table 1.2). In cases (1) and (2), the tests were carried out in different testing environments such as a semi anechoic chamber (SAC), a fully anechoic chamber (FAC) and some tests were carried out using an open air test site (OATS). Most of the data used in this thesis were collected with the *VERIFY* EMP Simulator.

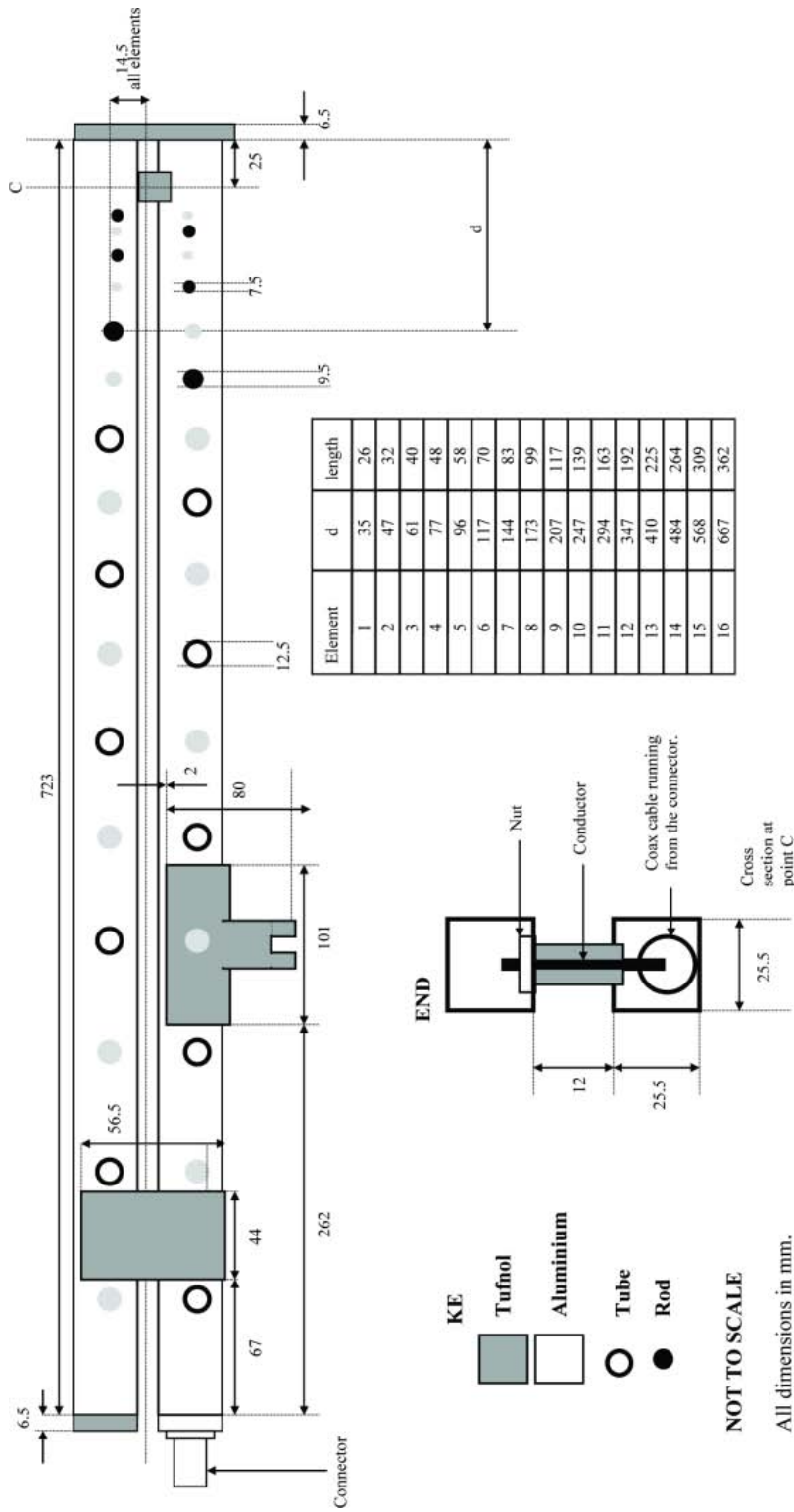


Figure 1.5: Logperiodic antenna used in the GEMCAR project

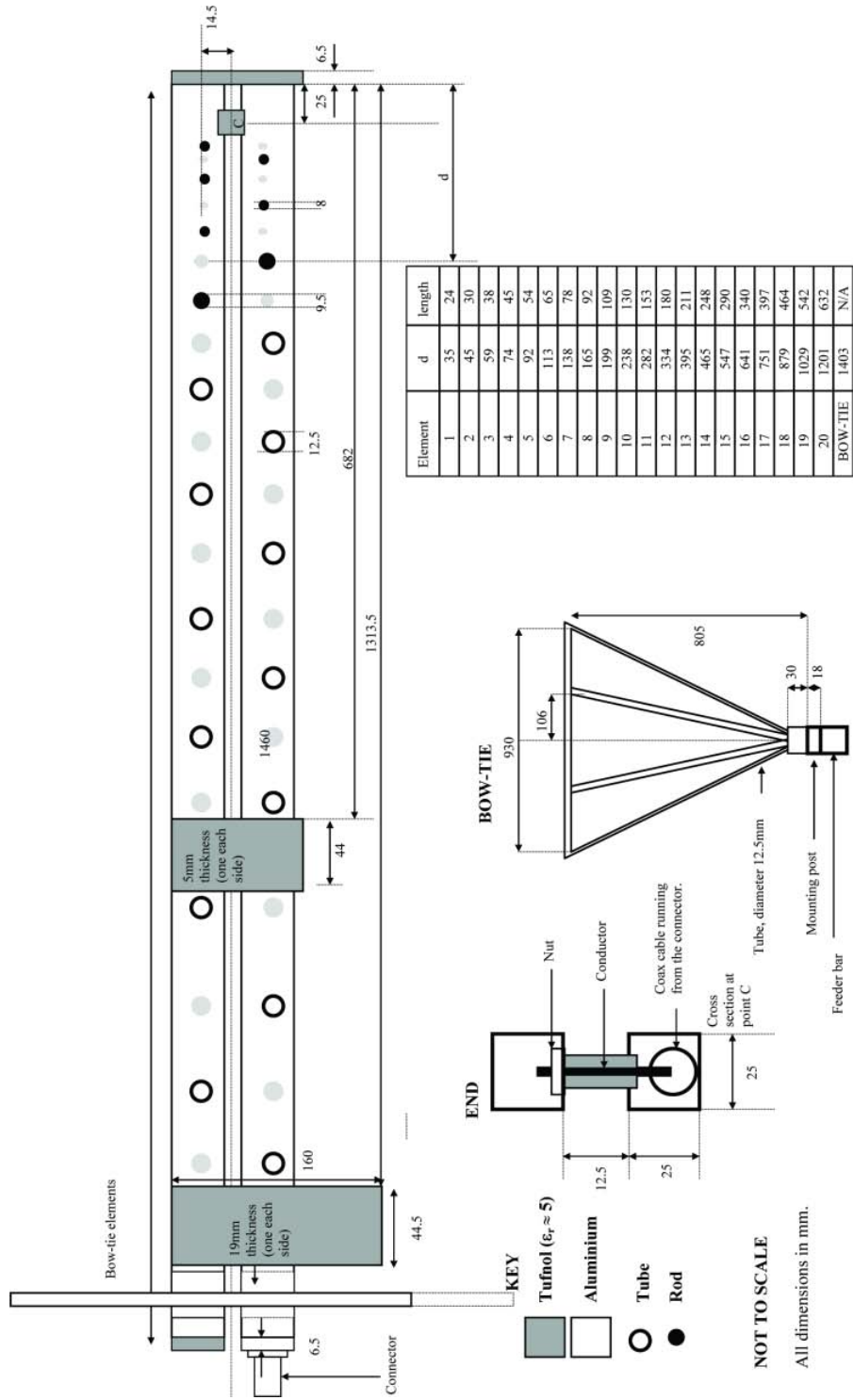


Figure 1.6: Biconilog antenna used in the GEMCAR project



Figure 1.7: VERIFY EMP Simulator

Currents induced on a test harness installed inside the car were also measured but they are not the subject of study of this thesis ¹.

1.3 Organization of the Thesis

This thesis is organized in 7 chapters. After this brief introductory chapter, Chapter 2 presents a theoretical description of the numerical models used in the GEMCAR project. Results of simulations from all of the methods are used in chapters 2 and 4 for comparison purposes. This thesis concentrates on the study and implementation of the Method of Moments (MoM).

Chapter 3 describes the development of a new version of the Numerical Electromagnetics Code (NEC) capable of running on parallel supercomputers. Large structures which exceed currently available computer resources are analyzed, and timing and memory results are presented in Chapter 4, where the code is applied to analyze the penetration of electromagnetic fields inside a vehicle. The computed results are tested using experimental data obtained using the simple model of the GEMCAR project vehicle (consisting essentially of the body shell) illuminated by the VERIFY EMP simulator.

¹A preliminary analysis of the effects of the measured currents can be found in [3]

Pulse Generator Voltage Range (V_{max} = voltage to produce maximum field level)	0.3 V_{max} - V_{max}
Antenna Impedance	$100\Omega \pm 20\%$
Polarity	plus or minus
Max. Pulse Rate	1 pulse per minute
Shot-to-shot Reproducibility in E and H Fields	$\pm 10\%$ for 20 shots
Misfire/Self-fire Rate	$< 5\%$
Field Characteristics in Working Volume:	
Amplitude	30-100 kV/m; 79-265 A/m
Prepulse	$< 10\%$
Risetime (10-90 %)	0.9 nsec (+0.1/-0.2 ns) smooth rise
Duration (FWHM)	24 nsec (-0 nsec/+12 nsec)
Amplitude variation over any vertical plane in working volume	$\pm 10\%$ of geometric center
Spectrum:	
DC - 500 MHz	$\leq \pm 6$ dB from theoretical
500 MHz - 1 GHz	$\leq \pm 12$ dB from theoretical

Table 1.2: Electrical specifications of VERIFY

Chapter 5 deals with the wire-grid representation of metallic surfaces in numerical electromagnetic modeling. We discuss in particular the adequacy of the well-known and widely used Equal Area Rule (EAR) to calculate the radii of wire-grid models.

Chapter 6 presents a derivation and possible physical interpretation of the wire-grid simulation of surfaces. In that chapter, we propose a preliminary new formulation for obtaining the appropriate radii for the meshed surface.

Finally, conclusions and proposed future work are presented in Chapter 7.

Bibliography

- [1] Laurent Paletta. *Démarche topologique pour l'étude des couplages électromagnétiques sur des systèmes de câblages industriels de grande dimension*. PhD thesis, Université Paris XI - Orsay, September 1998.
- [2] Nicolas Ribière-Tharaud. *Amélioration des méthodes de qualifications des véhicules automobiles en CEM. Applications aux faisceaux de câbles*. PhD thesis, Université de Paris-Sud - U.F.R. Scientifique d'Orsay, May 2001.
- [3] A. Rubinstein, F. Rachidi, D. Pavanello, and B. Reusser. Electromagnetic Field Interaction with Vehicle Cable Harness: An Experimental Analysis. In *International Conference on Electromagnetic Compatibility, EMC Europe. Sorrento*, volume 1, Sep 2002. Proceedings.
- [4] EMC simulation for automotive applications. Web Page. <http://www.esi-group.com/autoEMC/AutoEMC.htm>.
- [5] Guidelines for ElectroMagnetic Compatibility Modelling for Automotive Requirements (GEMCAR). Web Page. <http://www.gemcar.org>.
- [6] F. Canavero, J.-C. Kedzia, P. Ravier, and B. Scholl. Automotive EMC: Numerical simulation for early EMC design of cars. In *4th European Conference on Electromagnetic Compatibility, (Brugge, Belgium)*, pages 32–39, 11-15 September 2000. Tutorials.
- [7] A. Ruddle, D. Ward, A. Williams, and A. Duffy. Objective validation of automotive EMC models. In *1998 IEEE International Symposium on Electromagnetic Compatibility*, volume 1, pages 475–479, 1998.

- [8] A. Ruddle. The EU Framework V Project “GEMCAR”: Guidelines for Electromagnetic Compatibility Modelling for Automotive Requirements. In *EMC Zurich’03 Conference Proceedings*, 2003.

Chapter 2

Numerical Methods and Simulation Strategies Applied to the Problem of Interest

2.1 Introduction

The objective of this chapter is to briefly present the numerical methods used within the GEMCAR project and the strategies for improving the efficiency of vehicle-level EMC simulations. We will concentrate in this chapter on the calculation element only. No consideration is given here to the equally important model building aspects of the problem (i.e., geometric descriptions, mesh generation, identification of material properties) or the engineering processes that are required to integrate EMC modeling with wider vehicle engineering tasks [1]. Some of these aspects, are covered in Chapter 5 for the Method of Moments. In this context, the notion of improved “efficiency” includes:

- the capability to perform a calculation that is perhaps not achievable with a single tool or technique
- improvements in the accuracy of the results
- approaches allowing easy modification of parameters associated with the model
- reductions in the duration, scope and number of models that are required

These goals can be achieved by working on three main areas: (1) Optimizing the algorithms used in the simulation software, (2) combining numerical techniques to exploit the strengths of different approaches and (3) improving the modeling methodology to obtain the maximum benefit from each simulation.

Within this thesis, it was not possible to investigate all types of improvements as well as all numerical methods available. Nevertheless, the main ones applied in the GEMCAR project will be described. The mathematical basis of the Method of Moments (MoM) is developed here in this chapter since this method, being the base of the Numerical Electromagnetics Code (NEC) [2], is of special interest for this thesis. Three other methods were used in GEMCAR. Of those, only two, FDTD and TLM, are fundamentally different from the Method of Moments and, for that reason, they will be explained in some detail. The third method, the BEM, will only be described briefly since it is closely related to the Method of Moments.

2.2 Modeling Methodology

Computing requirements, such as memory or calculating power, are intimately bound to the approach that is used in building and exploiting EMC models (e.g., the selection of a particular numerical method or tool). This is particularly important for full 3D field calculations, which are extremely demanding in terms of runtime and memory [3]. In some cases, however, models can be simplified, depending on the purpose of the simulations and, as a result, the computer requirements are reduced. For 3D simulations, the model complexity determines the memory requirements and calculation time. The Method of Moments, for example, exhibits a quadratic dependence of the growth of the memory requirements with the number of segments representing the model [4]. For experimental validation purposes, it is essential to include a realistic representation of the antenna that is used to illuminate the real system in order to effectively replicate the test conditions [3]. This inevitably increases the size of the model and the resources required for the simulation. Once validation has been achieved, it is possible to use simpler antenna models since these can remain virtual.

The primary aims of adopting numerical modeling are to reduce dependence on

physical testing, to improve understanding of physical tests, to facilitate the analysis of “un-testable” scenarios and to provide a tool that can be used to guide design choices, even before any physical hardware is available for testing [3].

Thus, model validation is an important prerequisite that should lead eventually to the unleashing of the true benefits of modeling, which only become available when the simulation results are trusted without reference to practical measurements. Although simulations will not replace testing for compliance with standards, it is likely that EM modeling will have a strong impact on the definition of test conditions, regarding, for example, radiated immunity, illumination antenna definition, optimization of on-board antennas, and emission and intra-system EMC.

2.3 Modeling Functional EMC Performance

The calculation of electromagnetic interactions and coupling between cables and equipment within their housing (e.g., the geometrically complex vehicle body-shell from GEMCAR) is an essential part of the analysis that allows the prediction of functional EMC effects. A single monolithic simulation for such purposes is not always a practicable proposition. The combined use of modeling techniques represents a viable approach to developing a functional EMC model. In a number of cases, hybridization can also be considered [5]. For building an EMC model, we can consider a range of modeling techniques operating at a number of different levels as outlined in Table 2.1 [3]. Hybridization requires the integration of circuit behavior (a “class D” model) with the electromagnetic performance of the vehicle installation (a “class A” model). It is possible to include cable models within some 3D field modeling schemes (the “self-consistent” approach), which should provide a more rigorous solution, but an approximation that treats the behavior of the cables separately (the “separated” method) may offer some advantages in terms of computational efficiency. The “separated method”, also referred to as “weak hybridization”, requires the use of two-dimensional “class B” and one-dimensional “class C” models (see Table 2.1) in order to determine the transmission line parameters for the various elements of the network and the propagation characteristics of its branches. It is important to notice, however, that the better part of the

Model class	Model order	Model nature	Objectives
A	3D + time or frequency	Electromagnetic - volume or surface meshing	3D electromagnetic field distribution and related parameters (eg. antenna characteristics)
B	2D static	Electrostatic - planar or peripheral meshing	Lumped circuit models of transmission line segments (valid for small spacing)
C	1D + time or frequency	Transmission line - linear meshing	Accounting for wave propagation effects on transmission lines (length and termination load dependent)
D	0D + time or frequency	Circuit simulation - lumped element behavioral models	Device physics in circuit models, but no account of physical layout

Table 2.1: Classification of model types required to predict functional performance of vehicle electrical systems (adapted from [3])

computational effort goes to the full 3D field computations. Linking different “class A” models may maximize the efficiency of field calculations, particularly for electrically large systems, such as vehicles at high frequencies. A representative scheme for modeling functional performance using the “separated method” is illustrated in Figure 2.1, which outlines the necessary interactions between the various model classes [3]. A “class A” model, containing a three-dimensional representation of the vehicle and an external source of electromagnetic noise can be used for calculating the field distribution along the harness path. A coupling model can then be used to link these fields, as distributed sources, to the wiring system and, therefore, to the “class C” model. The harness information (“class C” model) together with the distributed sources (from “class A” model) provide the wave propagation information necessary for sub-system hardware performance analysis. Wave propagation may also be calculated from a “class B” and a “class C” models as already mentioned.

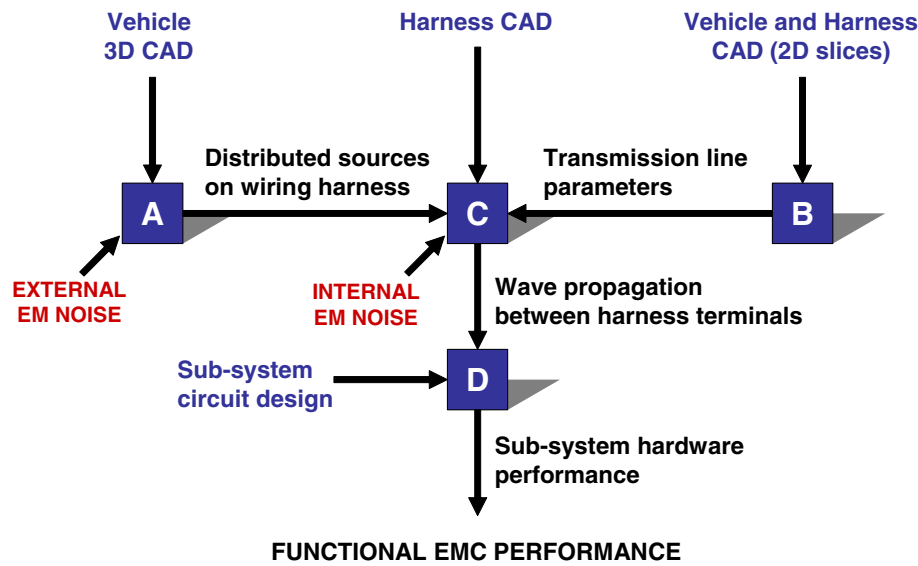


Figure 2.1: Strategy for EMC performance prediction using separated methods (adapted from [3])

2.4 Capabilities of Numerical Techniques

The purpose of this section is to provide an overview of the main capabilities of the numerical techniques, identified in Section 2.3, that can be employed in the analysis of vehicle-level EMC. As it is not possible to exploit a “class C” model without input from a “class B” model (using the designations illustrated in Figure 2.1), the combination of these two can be described more conveniently as “cable network” simulation [6].

The methods will be classified in terms of the operational domain of the simulation (i.e., time or frequency) and the nature of the simulation (3D field, cable network and electrical circuit codes). Some of these techniques are briefly described in the next section.

2.4.1 Time and Frequency Domain Techniques

The relative merits of simulations in the time and frequency domains are summarized in Table 2.2. It can be seen that both, time and frequency domain techniques, offer

Operational domain	Advantages	Disadvantages
Time	<ul style="list-style-type: none"> • Good description of transients • Non-linear problems (sparks, non linear equipment) • Frequency spectrum with only one event • calculation time depend-ing on the size of the mesh 	<ul style="list-style-type: none"> • Difficulty to account for frequency dependence of materials (cables, absorbers, soils) • Difficulty to have a multi-excitation problem • Accommodating multiple-domain approaches (signal processing requirements)
Frequency	<ul style="list-style-type: none"> • Accounting for frequency dependent materials • Simultaneous application of multiple sources 	<ul style="list-style-type: none"> • Calculations made at each frequency • The frequency step required to generate a precise spectrum

Table 2.2: Relative merits of simulation techniques (adapted from [3])

their own advantages, and that neither provides an ideal approach for all types of problems [3].

2.4.2 Types of Simulations

2.4.2.1 Three-dimensional numerical codes

These are numerical codes that solve Maxwell's equations on an approximation of the scattering geometry. This geometry is represented in a discrete form, generally described as a "mesh". Numerous methods have been developed to solve Maxwell's equations in both, the time and the frequency domain. In principle, they can solve any kind of problem since Maxwell's equations account for the overall coupling within the geometry in a global sense. For classification purposes, a useful distinction can be drawn between volume and surface meshing techniques.

- **Volume meshing techniques** such as FDTD, TLM, FEM or Finite-Volume Time-Domain (FVTD) are based on computing fields over the entire object and

its surrounding environment (in theory, the entire space). The advantage of these methods is that they easily account for complex spatial variations in the electrical properties (e.g., permittivity, conductivity) of the modeled volume. However, special techniques such as absorbing boundary conditions are required to truncate the workspace to ensure computational tractability. In the past ten years, the “perfectly matched layer” (PML) has demonstrated considerable promise [3]. Nevertheless, those layers still present instabilities under specific conditions that could be overcome with more sophisticated schemes.

- **Surface meshing techniques** such as the MoM are based on computing parameters only over the surfaces of the objects of interest. They are very well suited to the solution of integral equations in either the frequency or the time domain, and they automatically take into account radiation effects. The main limitation of these techniques lies in the memory requirements, because a dense matrix containing the interaction between the different cells needs to be stored [3]. Modeling dielectric materials is also more of a challenge in surface meshing techniques than it is in the case of volume meshing techniques. Recently, the Fast Multi-pole Method (FMM), which is based on optimizing the product of matrices and vectors, has shown dramatic improvements for Radar Cross Section (RCS) calculations [7]. However, the application of the method for EMC at high frequencies is not obvious with the forms of integral equations that are currently used (EFIE - Electric, MFIE - Magnetic, CFIE - Combined Field Integral equations).

2.4.2.2 Cable Network Codes

Cable network codes are numerical codes that determine the response of a network under certain conditions. These codes should not be confused with methods that allow the calculation of 3D fields such as the TLM method that we will describe in Subsection 2.5.2. The gain compared to 3D codes mainly comes from the avoidance of time-consuming field computations. Versions are available in both the time and the frequency domain. A higher efficiency is obtained when the branches can be approximated as multiconductor transmission lines. In this case, the calculation is not made on

the geometry but on equivalent electrical models of cables (per-unit-length impedance and admittance parameters), connections (electrical circuits) and sources (equivalent voltage and current generators). The field distribution local to the cable is determined from an electrostatic model and the subsequent calculations are essentially limited to longitudinal propagation, transmission and reflection effects [3].

2.4.2.3 Electrical Circuit Codes

Electrical circuit codes are computer codes that are able to calculate the response of any electric circuit. We find codes both in the time and the frequency domain. Public domain versions, such as SPICE, developed at the University of California, Berkeley, and numerous commercial products are widely available. However, they are generally not suitable for EMC purposes due to their requirements in terms of memory and performance, and to the fact that EMC effects need to be included in the form of lumped circuit elements, which do not necessarily reflect the actual interference mechanisms.

2.5 Methods applied within GEMCAR

2.5.1 The Finite-Difference Time-Domain (FDTD)

This method is based, in its original form, on the discretization of the space to be modeled into cubic cells (see Figures 2.2 and 2.3). Maxwell's curl equations are then written for each of the three dimensional Cartesian components, yielding a system of six scalar equations 2.1a through 2.2c.

$$\frac{\partial H_x}{\partial t} = \frac{1}{\mu} \cdot \left(\frac{\partial E_y}{\partial z} - \frac{\partial E_z}{\partial y} - \rho' H_x \right) \quad (2.1a)$$

$$\frac{\partial H_y}{\partial t} = \frac{1}{\mu} \cdot \left(\frac{\partial E_z}{\partial x} - \frac{\partial E_x}{\partial z} - \rho' H_y \right) \quad (2.1b)$$

$$\frac{\partial H_z}{\partial t} = \frac{1}{\mu} \cdot \left(\frac{\partial E_x}{\partial y} - \frac{\partial E_y}{\partial x} - \rho' H_z \right) \quad (2.1c)$$

$$\frac{\partial E_x}{\partial t} = \frac{1}{\varepsilon} \cdot \left(\frac{\partial H_z}{\partial y} - \frac{\partial H_y}{\partial z} - \sigma E_x \right) \quad (2.2a)$$

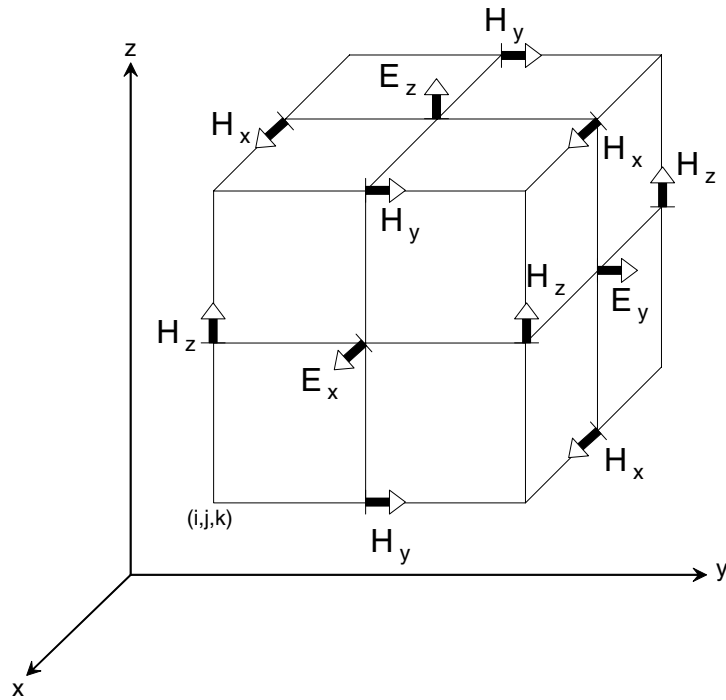


Figure 2.2: FDTD basic cubic cell

$$\frac{\partial E_y}{\partial t} = \frac{1}{\varepsilon} \cdot \left(\frac{\partial H_x}{\partial z} - \frac{\partial H_z}{\partial x} - \sigma E_y \right) \quad (2.2b)$$

$$\frac{\partial E_z}{\partial t} = \frac{1}{\varepsilon} \cdot \left(\frac{\partial H_y}{\partial x} - \frac{\partial H_x}{\partial y} - \sigma E_z \right) \quad (2.2c)$$

where E_x , E_y and E_z and H_x , H_y and H_z are the components in the three-dimensional rectangular coordinate system (x, y, z) of the electric and magnetic fields, respectively, μ is the magnetic permeability in henrys per meter, ρ' is an equivalent magnetic resistivity in ohms per meter and σ is the electric conductivity in siemens per meter.

These equations are then set up in their discrete form in space and time, and applied to the sides of each cell. One obtains thus Equations 2.3 and 2.4, which represent time stepping relations that can be used to calculate the magnetic field H in terms of the components of the electric field E at the previous time step, and the electric field E in terms of the magnetic field H at the previous time step.

$$H_x|_{i,j,k}^{n+1/2} = \left(\frac{1 - \frac{\rho'_{i,j,k}\Delta t}{2\mu_{i,j,k}}}{1 + \frac{\rho'_{i,j,k}\Delta t}{2\mu_{i,j,k}}} \right) H_x|_{i,j,k}^{n-1/2} + \left(\frac{\frac{\Delta t}{\mu_{i,j,k}}}{1 + \frac{\rho'_{i,j,k}\Delta t}{2\mu_{i,j,k}}} \right) \cdot \left(\frac{E_y|_{i,j,k+1/2}^n - E_y|_{i,j,k-1/2}^n}{\Delta z} - \frac{E_z|_{i,j+1/2,k}^n - E_z|_{i,j-1/2,k}^n}{\Delta y} \right) \quad (2.3a)$$

$$H_y|_{i,j,k}^{n+1/2} = \left(\frac{1 - \frac{\rho'_{i,j,k}\Delta t}{2\mu_{i,j,k}}}{1 + \frac{\rho'_{i,j,k}\Delta t}{2\mu_{i,j,k}}} \right) H_y|_{i,j,k}^{n-1/2} + \left(\frac{\frac{\Delta t}{\mu_{i,j,k}}}{1 + \frac{\rho'_{i,j,k}\Delta t}{2\mu_{i,j,k}}} \right) \cdot \left(\frac{E_z|_{i+1/2,j,k}^n - E_z|_{i-1/2,j,k}^n}{\Delta x} - \frac{E_x|_{i,j,k+1/2}^n - E_x|_{i,j,k-1/2}^n}{\Delta z} \right) \quad (2.3b)$$

$$H_z|_{i,j,k}^{n+1/2} = \left(\frac{1 - \frac{\rho'_{i,j,k}\Delta t}{2\mu_{i,j,k}}}{1 + \frac{\rho'_{i,j,k}\Delta t}{2\mu_{i,j,k}}} \right) H_z|_{i,j,k}^{n-1/2} + \left(\frac{\frac{\Delta t}{\mu_{i,j,k}}}{1 + \frac{\rho'_{i,j,k}\Delta t}{2\mu_{i,j,k}}} \right) \cdot \left(\frac{E_x|_{i,j+1/2,k}^n - E_x|_{i,j-1/2,k}^n}{\Delta y} - \frac{E_y|_{i+1/2,j,k}^n - E_y|_{i-1/2,j,k}^n}{\Delta x} \right) \quad (2.3c)$$

$$E_x|_{i,j,k}^{n+1} = \left(\frac{1 - \frac{\sigma_{i,j,k}\Delta t}{2\varepsilon_{i,j,k}}}{1 + \frac{\sigma_{i,j,k}\Delta t}{2\varepsilon_{i,j,k}}} \right) E_x|_{i,j,k}^n + \left(\frac{\frac{\Delta t}{\varepsilon_{i,j,k}}}{1 + \frac{\sigma_{i,j,k}\Delta t}{2\varepsilon_{i,j,k}}} \right) \cdot \left(\frac{H_z|_{i,j+1/2,k}^{n+1/2} - H_z|_{i,j-1/2,k}^{n+1/2}}{\Delta y} - \frac{H_y|_{i,j,k+1/2}^{n+1/2} - H_y|_{i,j,k-1/2}^{n+1/2}}{\Delta z} \right) \quad (2.4a)$$

$$E_y|_{i,j,k}^{n+1} = \left(\frac{1 - \frac{\sigma_{i,j,k}\Delta t}{2\varepsilon_{i,j,k}}}{1 + \frac{\sigma_{i,j,k}\Delta t}{2\varepsilon_{i,j,k}}} \right) E_y|_{i,j,k}^n + \left(\frac{\frac{\Delta t}{\varepsilon_{i,j,k}}}{1 + \frac{\sigma_{i,j,k}\Delta t}{2\varepsilon_{i,j,k}}} \right) \cdot \left(\frac{H_x|_{i,j,k+1/2}^{n+1/2} - H_x|_{i,j,k-1/2}^{n+1/2}}{\Delta z} - \frac{H_z|_{i+1/2,j,k}^{n+1/2} - H_z|_{i-1/2,j,k}^{n+1/2}}{\Delta x} \right) \quad (2.4b)$$

$$E_z|_{i,j,k}^{n+1} = \left(\frac{1 - \frac{\sigma_{i,j,k}\Delta t}{2\varepsilon_{i,j,k}}}{1 + \frac{\sigma_{i,j,k}\Delta t}{2\varepsilon_{i,j,k}}} \right) E_z|_{i,j,k}^n + \left(\frac{\frac{\Delta t}{\varepsilon_{i,j,k}}}{1 + \frac{\sigma_{i,j,k}\Delta t}{2\varepsilon_{i,j,k}}} \right) \cdot \left(\frac{H_y|_{i+1/2,j,k}^{n+1/2} - H_y|_{i-1/2,j,k}^{n+1/2}}{\Delta x} - \frac{H_x|_{i,j+1/2,k}^{n+1/2} - H_x|_{i,j-1/2,k}^{n+1/2}}{\Delta y} \right) \quad (2.4c)$$

Notice that, at each time step, only one of the fields (E or H) is calculated in terms

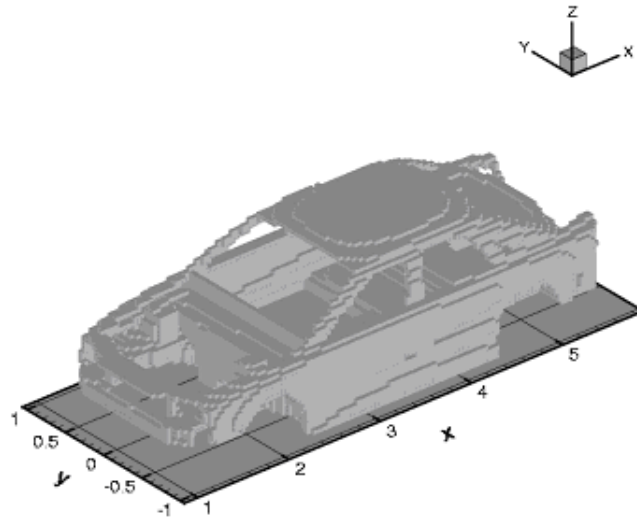


Figure 2.3: Mesh of a Volvo S80 for a FDTD calculation

of the other one. The solution is thus obtained in what is termed a “leapfrogging” manner. The stepping solution does not require the inversion of any matrices and only the instantaneous values of the fields are kept in memory at each time step. Details of this method are given in the original paper by Yee [8] and in [9].

2.5.2 The Transmission Line Matrix (TLM)

The TLM method is essentially used in the time domain. It is based on an intuitive application of wave propagation in space. It assumes that electric and magnetic fields propagate within the medium through virtual transmission lines which are placed between nodes once the complete volume to be modeled has been discretized into a Cartesian grid (see Figure 2.5). The voltages and currents in the transmission lines are related to the electric and magnetic fields, respectively. In order to account for different propagation characteristics for differently polarized waves, two transmission lines are used for two perpendicular polarizations. The most commonly used node, known as the *Symmetrical Condensed Node* is illustrated in Figure 2.4.

As time progresses, pulses propagate out of each node along all of the transmission lines attached to it. Due to mismatches in the impedances, when a pulse arrives at a given node from a source node, part of its energy will reflect back towards the source

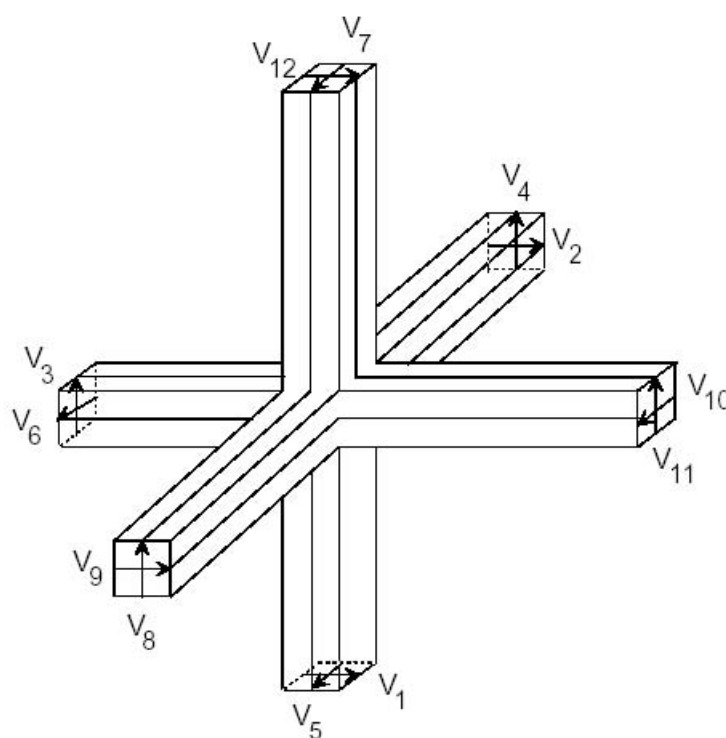


Figure 2.4: A so-called Symmetrical Condensed Node in the TLM method. The node is at the intersection point of the six transmission lines leading to the neighboring nodes

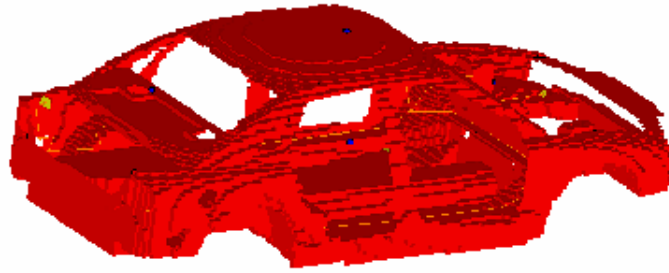


Figure 2.5: Mesh of a Volvo S80 for a TLM calculation

node and part of it will be transmitted into the other transmission lines at the destination node. Note that reflections may occur even if the material is uniform since, even if the characteristic impedance of all the lines is the same, say Z_0 , a wave that reaches a node will see an impedance of $Z_0/5$, which corresponds to the parallel combination of the impedances of the other five transmission lines at that node. In general, a scattering matrix at each node is used to calculate the fraction of the incident fields that is reflected and transmitted into the other transmission lines. Losses are modeled either by using lossy transmission lines or by introducing lossy stubs. Boundaries are modeled by introducing load impedances at the nodes. A conductor, for example, will be modeled by way of a short circuit. To model infinite volumes, the outer boundaries are made into absorbing walls by matching the boundary nodes using the characteristic impedance of the incoming transmission lines.

More information about this method can be found in [10, 11, 12, 13, 14, 15].

2.5.3 The Boundary Element Model (BEM)

The Boundary Element Model (BEM) solves partial differential equations (PDEs) using mesh elements by means of the weighted residual technique. It is a particular case of the MoM (see 2.5.4) that defines the expansion and weighting functions only on a boundary surface, (i.e., only the boundary of the domain of interest requires discretization. See Figure 2.6). If the domain is either the interior or exterior to a volume, then only the surface is divided into mesh elements. For this reason, the computational advantages of the BEM over other methods can be considerable. The approach uses the simplest elements, is relatively easy to apply, and is versatile and efficient [16].

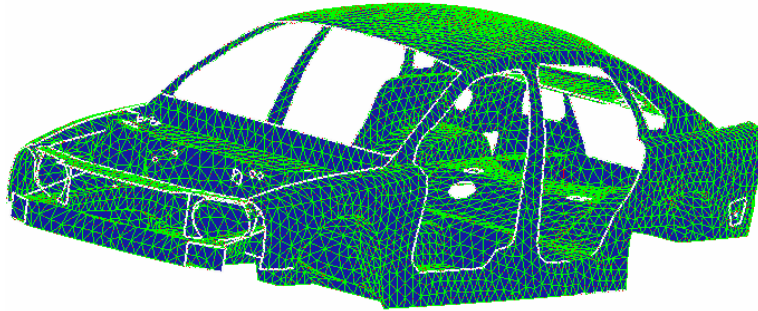


Figure 2.6: Mesh of a Volvo S80 for a BEM calculation

2.5.4 The Method of Moments (MoM)

Numerous problems in physics and engineering can be reduced to the need to solve equations of the form

$$\mathcal{L}(f) = e \quad (2.5)$$

where \mathcal{L} is a linear operator, f is an unknown function and e is a known source function [17].

One can readily find cases that involve the solving of Equation 2.5 in the field of electromagnetics, as illustrated, for example, by Poisson's equation in electrostatics, where the linear operator is the Laplacian, the function f is the electric potential, and the known function e is proportional to the charge.

If the linear operator involves integrals, Equation 2.5 is usually known as an integral equation. Integral equations are commonly found in scattering problems in electromagnetics that can be solved using the Method of Moments (see Figure 2.7). This technique, which we will introduce in what follows, allows for the numerical estimation of the function f in the integral equation.

We will use an analogy with vectors in an n -dimensional space since that is a good way to understand the principle of the Method of Moments.

Think of the functions f and e in Equation 2.5 as vectors. We will use arrows to distinguish them from the functions. Our task is to find \vec{f} . If a suitable base composed

of n linearly independent vectors \vec{f}_i can be found, the vector \vec{f} can be expressed as

$$\vec{f} = \sum \alpha_i \vec{f}_i \quad (2.6)$$

where α_i are unknown constants and \vec{f}_i are the known functions of our base.

Substituting Equation 2.6 into Equation 2.5 and making use of the linearity properties of the operator, we obtain

$$\sum \alpha_i \mathcal{L}(\vec{f}_i) = \vec{e} \quad (2.7)$$

The problem of finding \vec{f} has now reduced to the problem of finding the values of α_i since, with those, we can use Equation 2.6 to obtain \vec{f} .

To find the α_i coefficients, we first find a second, different n -dimensional base composed of the vectors \vec{w}_j . If we now perform the dot product of Equation 2.7 by \vec{w}_j , we obtain

$$\sum \alpha_i \mathcal{L}(\vec{f}_i) \cdot \vec{w}_j = \vec{e} \cdot \vec{w}_j \quad (2.8)$$

Note that, the dot (or scalar) products $\mathcal{L}(\vec{f}_i) \cdot \vec{w}_j$ and $\vec{e} \cdot \vec{w}_j$ represent known scalars. Equation 2.8 represents therefore a system of n equations with n unknowns (α_i) and it can, therefore, be written in matrix form and solved using standard numerical techniques.

To illustrate the construction of the matrix, we will consider a 3-dimensional space. From Equation 2.8, with $N = 3$ we have

$$\begin{aligned} \alpha_1 \mathcal{L}(\vec{f}_1) \cdot \vec{w}_1 + \alpha_2 \mathcal{L}(\vec{f}_2) \cdot \vec{w}_1 + \alpha_3 \mathcal{L}(\vec{f}_3) \cdot \vec{w}_1 &= \vec{e} \cdot \vec{w}_1 \\ \alpha_1 \mathcal{L}(\vec{f}_1) \cdot \vec{w}_2 + \alpha_2 \mathcal{L}(\vec{f}_2) \cdot \vec{w}_2 + \alpha_3 \mathcal{L}(\vec{f}_3) \cdot \vec{w}_2 &= \vec{e} \cdot \vec{w}_2 \\ \alpha_1 \mathcal{L}(\vec{f}_1) \cdot \vec{w}_3 + \alpha_2 \mathcal{L}(\vec{f}_2) \cdot \vec{w}_3 + \alpha_3 \mathcal{L}(\vec{f}_3) \cdot \vec{w}_3 &= \vec{e} \cdot \vec{w}_3 \end{aligned} \quad (2.9)$$

This equation can be written in matrix notation as

$$[G][I] = [E] \quad (2.10)$$

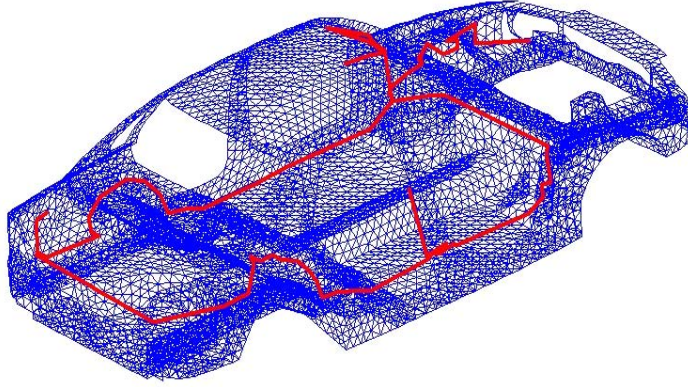


Figure 2.7: MoM Mesh of a Volvo S80

where,

$$G = \begin{bmatrix} \mathcal{L}(\vec{f}_1) \cdot \vec{w}_1 & \mathcal{L}(\vec{f}_2) \cdot \vec{w}_1 & \mathcal{L}(\vec{f}_3) \cdot \vec{w}_1 \\ \mathcal{L}(\vec{f}_1) \cdot \vec{w}_2 & \mathcal{L}(\vec{f}_2) \cdot \vec{w}_2 & \mathcal{L}(\vec{f}_3) \cdot \vec{w}_2 \\ \mathcal{L}(\vec{f}_1) \cdot \vec{w}_3 & \mathcal{L}(\vec{f}_2) \cdot \vec{w}_3 & \mathcal{L}(\vec{f}_3) \cdot \vec{w}_3 \end{bmatrix} \quad (2.11)$$

$$I = \begin{bmatrix} \alpha_1 \\ \alpha_2 \\ \alpha_3 \end{bmatrix} \quad (2.12)$$

and

$$E = \begin{bmatrix} \vec{e} \cdot \vec{w}_1 \\ \vec{e} \cdot \vec{w}_2 \\ \vec{e} \cdot \vec{w}_3 \end{bmatrix} \quad (2.13)$$

When the Method of Moments technique is applied to functions, the dot products become inner products and the basis vectors become basis functions. Theoretically the number of functions that form the basis would have to be infinite. In practice, one uses a finite number that approximate the functions sufficiently well. The matrix $[G]$ is known as the *interaction matrix*.

The MoM is the numerical method used on the Numerical Electromagnetics Code (NEC), of special interest for this thesis (see Chapters 3 and 4).

2.6 Combining Different Methods

2.6.1 Multiple Domain Approach

The term “multiple domain” is used here to describe the application of different tools to different parts of a problem. Using this approach, the calculation of each part can be achieved separately at different times. Partial solutions are then linked through data files which have been calculated by the elementary tools. In the following sections, two main types of linking techniques are described [3].

2.6.1.1 Link through scattering matrices

Each part of the problem is characterized by scattering (S), impedance (Z) or admittance (Y) matrices [3]. A network formulation is used to describe the full wave interactions between the different parts [18, 19]. This technique leads to a network resolution such as the BLT equation [20]. The technique may be applied to decompose a 3D geometry. The problem in that case is that large files have to be stored. Since time, space and frequency steps are calculated independently by each one of the tools, interpolation in these three parameters is often necessary to make the different files fit with each other and with the specifications of the global calculation. All those considerations may explain why this approach has not caught on yet in the computational electromagnetics community.

2.6.1.2 Link through incident fields

The link through incident fields is based on the field-to-transmission-line formalisms [21, 22, 23]. Its interest is for calculating the response of a complex wiring system illuminated by an incident field (the field in the absence of the wiring). This technique has been applied with success in GEMCAR [5] and in different contexts [24].

2.6.2 Hybridization approach

The word “hybridization” (or more precisely “strong hybridization”) is used here to describe different numerical techniques that are merged inside a single source code. This technique is currently applied in 3D codes, for example in the hybrid FDTD/FVTD

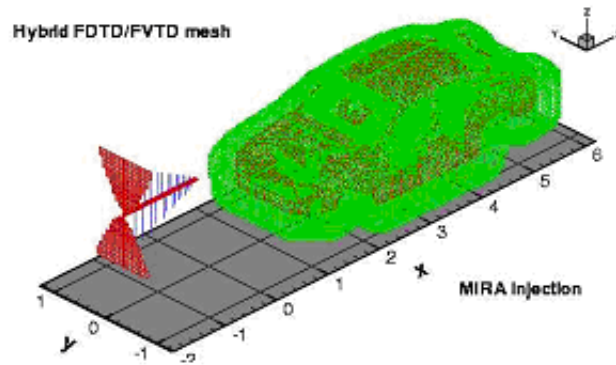


Figure 2.8: Example of GEMCAR’s hybrid FV/FDTD mesh (adapted from [3])

code [5] developed in the framework of GEMCAR. A hybrid code applies different numerical methods simultaneously. Unlike the multiple-domain technique approach, no big files need to be stored by one of the methods for use by the other methods. On the other hand, if something in the geometry is modified locally, the entire calculation has to be performed again, which is not the case with a multiple-domain technique.

2.7 Efficient Frequency Selection

2.7.1 Adaptive Sampling

This section draws heavily from [25]. Data acquisition systems used for frequency domain measurements are usually programmed to measure response data at equally-spaced, linear or logarithmic steps. Dividing the total frequency range into several bands with different subdivision schemes is also possible.

This sampling schemes, however, may fail to efficiently or accurately represent a spectrum. In the vicinity of spectral peaks, for example, it is essential to sample a large number of data points in order to observe the changes in magnitude and phase of the function. On the other hand, where the function changes less rapidly (i.e., away from spectral peaks), it should be possible to use a lower number of data points and still properly represent the spectrum.

Blumer [26] uses the concept of *adaptively sampling* a spectrum. He showed that it is possible to numerically calculate the spectra of the transient response of transmission lines with high accuracy using an unequal sample spacing, that is to say, a non

uniform sampling step spectrum with fewer spectral points. This, of course, reduces the calculation time.

In what follows, we will describe the Blumer Index which can be used as a figure of merit to evaluate the accuracy of a discrete spectral representation.

2.7.2 The Blumer Index

We wish to approximate a continuous spectrum $F(\omega)$ from $\omega = 0$ to ∞ by way of a discrete function $F(\omega_i)$ from $\omega_i = \omega_{min}$ to ω_{max} . Errors in this representation arise from

- truncating the infinite spectrum at the lower and upper frequencies $\omega_i = \omega_{min}$ and ω_{max}
- undersampling the spectrum.

For a continuous spectrum $F(\omega)$, we know that the energy contained in the spectrum is given by [27]:

$$W = \frac{1}{2\pi} \int_{-\infty}^{\infty} |F(\omega)|^2 d\omega \quad (2.14)$$

If the spectrum is causal, it must obey the Hilbert transform relationships [28] [26]. This implies that the following relationship between the real and imaginary parts of the spectrum must hold [29]:

$$\int_0^{\infty} |\operatorname{Re}(F(\omega))|^2 d\omega = \int_0^{\infty} |\operatorname{Im}(F(\omega))|^2 d\omega \quad (2.15a)$$

For a discrete spectrum, the relationship in 2.15a will not be exact due to the errors mentioned above. In that case, this relationship becomes

$$\sum_{\omega=\omega_{min}}^{\omega_{max}} |\operatorname{Re}(F(\omega))|^2 \Delta\omega \approx \sum_{\omega=\omega_{min}}^{\omega_{max}} |\operatorname{Im}(F(\omega))|^2 \Delta\omega \quad (2.15b)$$

As the sampling density (for measured data) or the number of calculated points increases, and by increasing the limits of integration, the numerical representation becomes more accurate and the difference between the left and right terms in Equation 2.15b approaches zero.

Finally, the accuracy of the measured or numerically calculated spectrum is defined by the *Blumer index* as

$$B = \left\{ 1 - \left| \frac{\int_0^\infty |\operatorname{Re}(F(\omega))|^2 d\omega - \int_0^\infty |\operatorname{Im}(F(\omega))|^2 d\omega}{\int_0^\infty |\operatorname{Re}(F(\omega))|^2 d\omega + \int_0^\infty |\operatorname{Im}(F(\omega))|^2 d\omega} \right| \right\} \times 100\% \quad (2.16)$$

expressed as a percentage. A Blumer index B of a 100%, indicates that Equation 2.15a is satisfied. However, errors in the spectrum will cause this parameter to be less than 100%. Its value obtained by numerically calculating the indicated integrals will provide an indication of the quality of the spectrum.

The Appendix explains the use of the Blumer index and shows examples of its application.

2.8 Comparison of GEMCAR Numerical Methods for a Biconilog Antenna

Figure 2.9 illustrates the degree of correlation that can be obtained between measured fields computed results obtained from the different numerical methods used in GEMCAR. Measurements were obtained in the calibration phase of the project using the Biconilog antenna shown in Figure 1.6. Figure 2.10 shows a 3D representation of the NEC geometry for the antenna model.

Although differences are observed, mostly at higher frequencies, the overall agreement among the results obtained using the different techniques and the measurements is good, despite major differences in their formulations. However, the amount of effort involved in developing the models and in obtaining the results varies considerably from one method to the other. It is particularly known that the NEC code is very powerful for antenna simulation and less suited than the other codes for the simulation of surfaces and 3D structures. Chapter 3 explains the development of a parallel version of NEC, capable of dealing with problems less natural to the original NEC's mathematical formulation.

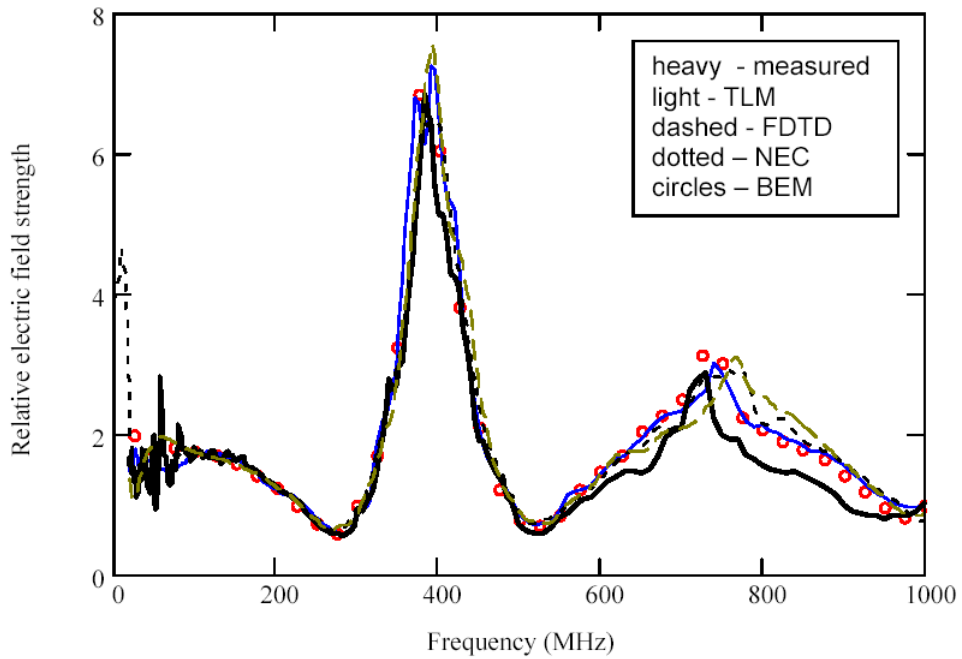


Figure 2.9: Relative field strength at a measuring point in front of the antenna

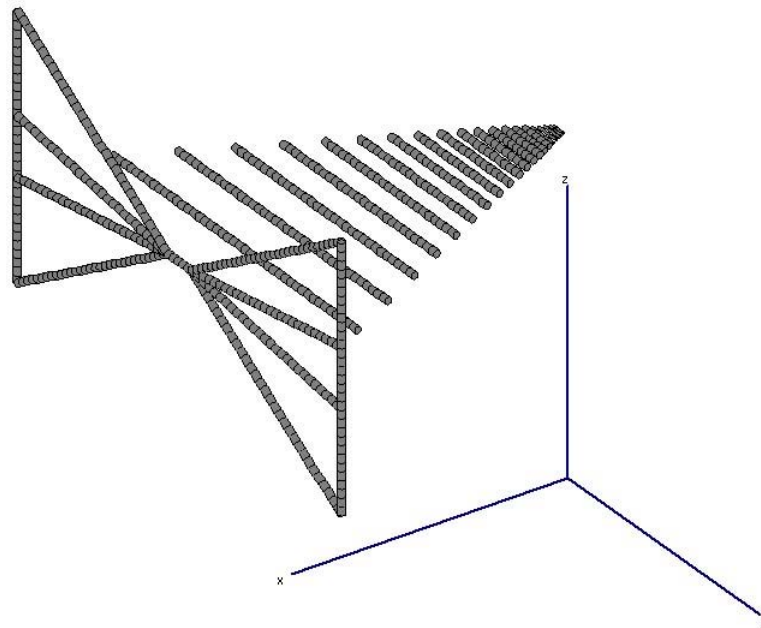


Figure 2.10: MoM (NEC) model of the GEMCAR Biconilog Antenna

2.9 Conclusions

In this chapter, we have presented the different numerical methods used in the GEM-CAR project, including the Method of Moments, on which parallel NEC (described in Chapter 3) is based. We have given an example of how all of the methods satisfactorily agree for a simple antenna model, despite the differences in their numerical formulation. We have shown efficient simulation strategies and we have emphasized the interest of combining different numerical methods. After having presented the specificity of modeling EMC performance of a system, we discussed the capabilities of currently available numerical techniques. This led us to analyze how to improve the efficiency of the calculations made by one technique and how to combine those techniques.

Many numerical tools are now mature enough to treat complex problems, but they are still limited when it comes to treating large systems. In those cases, one must think of combining the tools, using whichever one is appropriate for solving each of the specific problems. Three types of numerical codes suitable for three types of problems were identified: (1) 3D codes that allow the calculation of fields everywhere in a complex 3-Dimensional structure, (2) cable network codes that calculate the response of a complex network integrating the incident field on its running paths and (3) electrical circuit codes that allow the calculation of the response on complex circuit terminations, even if these are non linear.

Finally, the concept of Adaptive Sampling was explained and the Blumer index was presented as a tool for analyzing the quality of a spectrum.

Bibliography

- [1] A. Ruddle. The EU framework V project GEMCAR: Practical Aspects of the Whole Vehicle Electromagnetics Models. In *Proceedings of GEMCAR workshop at the 15th Zurich International EMC Conference*, 2003.
- [2] G. Burke and A. Poggio. Numerical electromagnetics code - method of moments. In *Report No. UCID-18834*, 1981. Livermore CA: Lawrence Livermore National Laboratory.
- [3] J. P. Parmantier, A. Ruddle, and X. Ferrières. The EU framework V project GEMCAR: Efficient Simulation Strategies. In *Proceedings of GEMCAR workshop at the 15th Zurich International EMC Conference*, 2003.
- [4] A. Rubinstein, F. Rachidi, M. Rubinstein, and B. Reusser. A Parallel Version of NEC for the Analysis of Large Structures. In *IEEE Transactions on Electromagnetic Compatibility*, volume EMC-45, pages 177–188, May 2003.
- [5] X. Ferrières, J.P. Parmantier, and S. Bertuol. Modeling EM coupling onto Vehicle wiring based on the combination of a hybrid FV/FDTD Method and a cable network method. In *EMC Zurich'03 Conference Proceedings*, 2003.
- [6] C-R-Paul. *Analysis of Multiconductor Transmission Lines*. John Wiley & Sons, New-York, 1994.
- [7] R. Coifman, V. Rokhlin, and S.W. Wandzura. The Fast multipole method for the wave equation : A pedestrian description. *IEEE Trans. Antenna Propagation*, AP-35(3):7–12, June 1993.

-
- [8] K. S. Yee. Numerical solution of initial boundary value problems involving Maxwell's equations in isotropic media. *IEEE Trans. Antennas and Propagation*, 14:302–307, 1966.
- [9] A. Taflove. *Computational Electrodynamics: The Finite-Difference Time-Domain Method*. Artech House, Norwood, MA. USA, 1995.
- [10] P. B. Johns and R. L. Beurle. Numerical solution of two-dimensional scattering problems using a transmission-line matrix. In *Proceedings IEE*, volume 118, pages 1023–1208, 1971.
- [11] P. B. Johns. The art of modelling. In *Electronics and Power*, volume 25, pages 565–569, 1979.
- [12] P. B. Johns. A Symmetrical Condensed Node for the TLM Method. *IEEE Trans. Microwave Theory Tech.*, MTT-35:370–377, Apr. 1987.
- [13] W. J. R. Hofer. *Numerical Techniques for Microwave and Millimeter-Wave Passive Structures*. John Wiley & Sons, 1989.
- [14] W. J. R. Hofer. Time domain electromagnetic simulation for microwave CAD applications. *IEEE Transactions on MTT*, 40(7):1517–1527, 1992.
- [15] C. Christopoulos. *The Transmission-Line Modeling Method*. IEEE Press / Oxford University Press, 1995.
- [16] V. Prasad Kodali. *Engineering Electromagnetic Compatibility. Principles, Measurements, Technologies, and Computer Models*. IEEE Press, second edition, 2001.
- [17] R. F. Harrington. *Field Computation by Moment Methods*. IEEE Press - Oxford University Press, 1993.
- [18] J.P. Parmantier, V. Gobin, F. Issac, I. Junqua, Y. Daudy, and J.M. Lagarde. An Application of the Electromagnetic Topology Theory on the Test-bed Aircraft. In *Interaction Notes*. EMPTAC, November 1993. Note 506.

- [19] J.P. Parmantier, V. Gobin, F. Issac, I. Junqua, Y. Daudy, and J.M. Lagarde. ETE III: an Application of the Electromagnetic Topology Theory on the Test-bed Aircraft. In *Interaction Notes*. EMPTAC, November 1996. Note 506.
- [20] C.E. Baum. The Theory of Electromagnetic Interference Control. In *Modern Radio Science 1990*, pages 87–101. Oxford University Press, 1990.
- [21] F.M. Tesche, M.V. Ianoz, and T. Karlsson. *EMC Analysis Methods and Computational Models*. John Wiley & Sons, 1997.
- [22] A.K. Agrawal, H.J. Price, and S.H. Gurbaxani. Transient Response of Multiconductor Transmission Lines Excited by a Nonuniform Electromagnetic Field. *IEEE Trans. on EMC*, 22(2):119–129, May 1980.
- [23] F. Rachidi. Formulation of Field to Transmission Line Coupling Equations in Terms of Magnetic Excitation Field. *IEEE Trans. on EMC*, 35(3), August 1993.
- [24] L. Paletta, J.P. Parmantier, F. Issac, P. Dumas, and J.C. Alliot. Susceptibility analysis of wiring in a complex system combining a 3D solver and a transmission-line network simulation. *IEEE Trans. on EMC*, pages 309–317, May 2002.
- [25] F. M. Tesche. Suggestions for the Implementation of an Adaptive, Nonuniform Sampling Scheme for CW Data Acquisition. In *Internal Report for the Swiss Defense Procurement Agency*, Dallas, TX, 1995.
- [26] W. Blumer and W. Johl. Coupling to Transmission Line Systems: Theoretical Background and TLS Code. In *Supplement to the Proceedings of the 11th International Zurich Symposium on EMC*, pages 7–9, March 1995.
- [27] A. Papoulis. *The Fourier Integral and its Applications*. McGraw Hill, New York, 1962.
- [28] F. M. Tesche. On the Use of the Hilbert Transform for Processing Measured CW Data. *IEEE Transactions on EMC*, 34(3), August 1992.
- [29] G. Arfken. *Mathematical Methods for Physicists, Third Edition*. Academic Press, San Diego, 1985.

Chapter 3

Development of an Optimized Parallel Numerical Electromagnetics Code based on NEC2

3.1 Introduction

The Numerical Electromagnetics Code (NEC) is a user-oriented computer code based on the Method of Moments (introduced in Chapter 2) and written in FORTRAN for the analysis of the electromagnetic response of antennas and other metal structures [1, 2, 3]. It has been widely used with great success for radio communications testing as well as antenna design and EMC. With its ability to represent models by means of wires, the code should also allow the simulation of very complex 3D structures [1]. NEC also allows the use of patches for the representation of surfaces, although constraints imposed by the code limit the application of this technique.

NEC produces an interaction matrix representing the system of integral equations needed to obtain the currents and fields. The number of elements in this matrix depends on the number of segments and patches that conform the model to be evaluated. This matrix is then reduced using LU factorization and, together with the excitation vector, the final solution to the integral equations is obtained [1].

For a model consisting of N segments, a good approximation to the amount of memory in bytes required by NEC is given by this expression:

$$Mem = N^2 \cdot 16 \text{ bytes} \quad (3.1)$$

Notice the quadratic dependence of the growth of the memory requirements with the number of segments. The required amount of memory becomes important on many current computers at around 2000 segments since, for that particular case, approximately 64 MB of RAM are necessary to complete program execution. With 128 MB of RAM, the number of segments that fit in memory will not even reach 3000. In order to run even larger models, virtual memory can be used but at a very high price in terms of execution time. The use of the hard disk, by means of a swap file, will slow down the execution of NEC to unpredictable values (see Section 3.3). An ‘out of core’ routine is embedded into NEC to optimize performance in these cases. The matrix is cut into pieces that are stored on the hard disk, following a special pattern. The operating system can then use all available RAM and NEC will take care of disk swapping. The out of core routine requires about four times the normal RAM and, as a consequence, enormous swap files are created [1].

One might think that having as much memory as needed is the best way to assure optimal execution. However, operating systems are not capable of managing all the memory one would be prepared to buy. A version of NEC compiled for a very large number of segments will fail to start because operating systems are unable to allocate it in memory. Excell et al. [4] presented a modified version of NEC to optimize performance on a four-processor Cray X-MP computer. This is a shared memory machine with a low degree of parallelism. Nitch and Fourié [5, 6] re-implemented NEC using *C++* and produced a modified version capable of running in parallel.

In this chapter, a parallel version of the Numerical Electromagnetics Code (NEC) is presented [7] [8]. The parallel version of NEC presented here works on distributed memory parallel supercomputers and it is portable to any platform supporting typical message passing parallel environments such as MPI (Message Passing Interface) and PVM (Parallel Virtual Machine). It is entirely based on the original NEC core written in FORTRAN, and it does not require any modifications to be made to classic NEC input files. The output files have also an identical format to those produced by the original NEC, so that any existing NEC post-processing tools may be used. Some small

models have been tested in both, the original NEC and the proposed parallel version and the numerical results were found to be identical.

The parallel implementation is thoroughly described in Section 3.2. The code is implemented on two supercomputers belonging to the Swiss Federal Institute of Technology, and its performance in terms of memory and solution time is presented in Section 3.3. A short summary and conclusions are given in Section 3.4.

3.2 Parallel Implementation of NEC

3.2.1 Structure of NEC

Computer resources at the time NEC was written were very different from those available today. With almost 10'000 lines, this code has been conceived for linear operation.

In NEC, a hybrid coupled form of the Electric Field Integral Equation (EFIE) and the Magnetic Field Integral Equation (MFIE) is solved using a form of the Method of Moments (see 2.5.4).

For an observation point \vec{r} on wire surfaces, the integral equations are [1]:

$$\begin{aligned} -\hat{s} \cdot \vec{E}^I(\vec{r}) &= \frac{-j\eta}{4\pi k} \int_L I(s) \left(k^2 \hat{s} \cdot \hat{s} - \frac{\partial^2}{\partial s \partial s} \right) g(\vec{r}, \vec{r}') ds \\ &\quad - \frac{j\eta}{4\pi k} \int_{S_1} \vec{J}_s(\vec{r}') \cdot \left[k^2 \hat{s} - \nabla' \frac{\partial}{\partial s} \right] g(\vec{r}, \vec{r}') dA' \end{aligned} \quad (3.2)$$

and, for an observation point \vec{r} on surfaces excluding wires [1]:

$$\begin{aligned} \hat{t}_2(\vec{r}) \cdot \vec{H}^I \vec{r} &= -\frac{1}{4\pi} \hat{t}_2(\vec{r}) \cdot \int_L I(s) (\hat{s}' \times \nabla' g(\vec{r}, \vec{r}')) ds \\ &\quad - \frac{1}{2} \hat{t}_1(\vec{r}) \cdot \vec{J}_s(\vec{r}) - \\ &\quad \frac{1}{4\pi} \int_{S_1} \hat{t}_2(\vec{r}) \cdot \left[\vec{J}_s(\vec{r}') \times \nabla' g(\vec{r}, \vec{r}') \right] dA' \end{aligned} \quad (3.3)$$

and:

$$\begin{aligned} \hat{t}_1(\vec{r}) \cdot \vec{H}^I \vec{r} &= -\frac{1}{4\pi} \hat{t}_1(\vec{r}) \cdot \int_L I(s) (\hat{s}' \times \nabla' g(\vec{r}, \vec{r}')) ds \\ &\quad - \frac{1}{2} \hat{t}_2(\vec{r}) \cdot \vec{J}_s(\vec{r}) - \\ &\quad \frac{1}{4\pi} \int_{S_1} \hat{t}_1(\vec{r}) \cdot \left[\vec{J}_s(\vec{r}') \times \nabla' g(\vec{r}, \vec{r}') \right] dA' \end{aligned} \quad (3.4)$$

where \vec{E}^I and \vec{H}^I are incident electric and magnetic fields, respectively, \vec{J}_s is the surface current density, I is the filamentary current,

$$g(\vec{r}, \vec{r}') = \frac{\exp(-jk|\vec{r} - \vec{r}'|)}{|\vec{r} - \vec{r}'|} = \text{Green function in free space,}$$

$$k = \omega\sqrt{\mu_0\epsilon_0} = \text{wave vector in free space,}$$

$$\eta = \sqrt{\frac{\mu_0}{\epsilon_0}} = \text{wave impedance in free space,}$$

s = distance parameter along the wire axis at \vec{r} and

\hat{s} = unit vector tangent to the wire axis at \vec{r}

and where \hat{t}_1 and \hat{t}_2 are vectors tangential to the surface and perpendicular to each other, so that,

$$\hat{t}_1(\vec{r}_0) \times \hat{t}_2(\vec{r}_0) = \hat{n}(\vec{r}_0)$$

with \hat{n} being the unit vector normal to the surface at \vec{r} .

In Equations 3.2 to 3.4, the primed coordinates refer to the sources and the unprimed coordinates refer to the observation points.

Equations 3.2, 3.3 and 3.4 are solved in NEC using the Method of Moments (see 2.5.4).

Figure 3.1 shows the original flow diagram of NEC. Some parts of the code, mainly the data input routines were suitable for use in parallel environments. For the calculation of the interaction matrix elements as well as the matrix equation resolution, several other routines were adapted. Figure 3.2 shows a modified version of the flow diagram of the main section of NEC reflecting the changes imposed by the parallelization process. NEC is globally composed of two parts: (1) the input section (on the left hand side of Figure 3.2), which reads in geometrical information about the model and stores the cards that dictate additional model information, program commands and directives of execution; and (2) the calculation section (on the right hand side of the figure), which computes the coefficients to produce $[G]$ for the matrix equation $[G][I] = [E]$, where $[G]$ is the so-called interaction matrix, holding geometrical and electromagnetic information about the structure, $[I]$ is a vector holding the current on each element and $[E]$ represents the excitation vector (see Subsection 2.5.4). This section of the code also solves this equation by means of the Gauss-Doolittle matrix-triangulation

method. The method has been divided into two routines. The first carries out an LU decomposition of the interaction matrix $[G]$ [1], which is then passed to a second routine together with the excitation vector $[E]$ to determine the solution of the system. The better part of the computational effort goes into factoring $[G]$ into $[L]$ and $[U]$. In fact, the computation of the elements of the interaction matrix $[G]$ and the solution of the matrix equation are the two most time-consuming steps in calculating the response of a structure, often accounting for over 90 % of the computation time [1]. For that reason, the parallelization effort was concentrated on that part of the code.

3.2.2 Two-Dimensional Block-Cyclic Decomposition

A parallel implementation of the LU decomposition and the parallel solution of the system of equations require the distribution of the information stored in the matrices among the available processors. This means that matrices $[G]$ and $[E]$ need to be cut into smaller sub-matrices that will be local to each processor. In order to evenly distribute the calculation effort among all available processors, this distribution must follow a special pattern known as the two-dimensional block-cyclic distribution or decomposition [9].

Consider, for instance, a parallel computer with 4 processors labelled from 0 to 3 and a matrix to be distributed. At first, one would be tempted to think that the most logical way to distribute the information among the 4 processors would follow the layout shown in Figure 3.3(a). Figure 3.3(b) shows the result of applying the two-dimensional block cyclic distribution with the same number of processors to the same matrix. Processor 0 holds the shaded parts of the matrix. As it can be seen, the block cyclic decomposition is a “far from intuitive” form of distribution for the matrices. The implementation of the Gaussian Elimination algorithm, a key component of the Gauss-Doolittle numerical method, iterates on the matrix by rows and columns, from left to right, and from top to bottom to obtain the triangular form of the interaction matrix. Starting with a given matrix

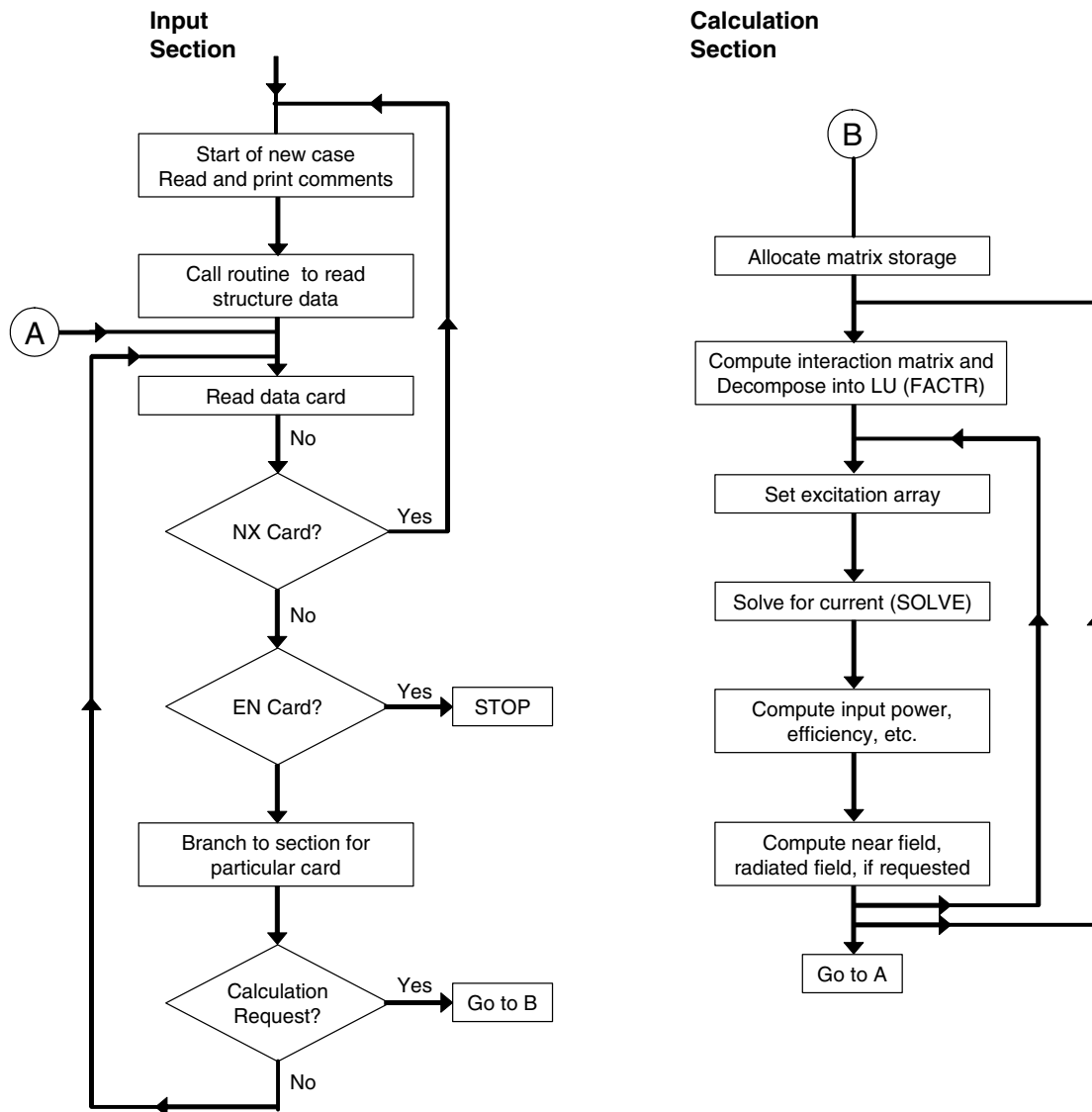


Figure 3.1: Flow diagram of NEC2. Adapted from [1]

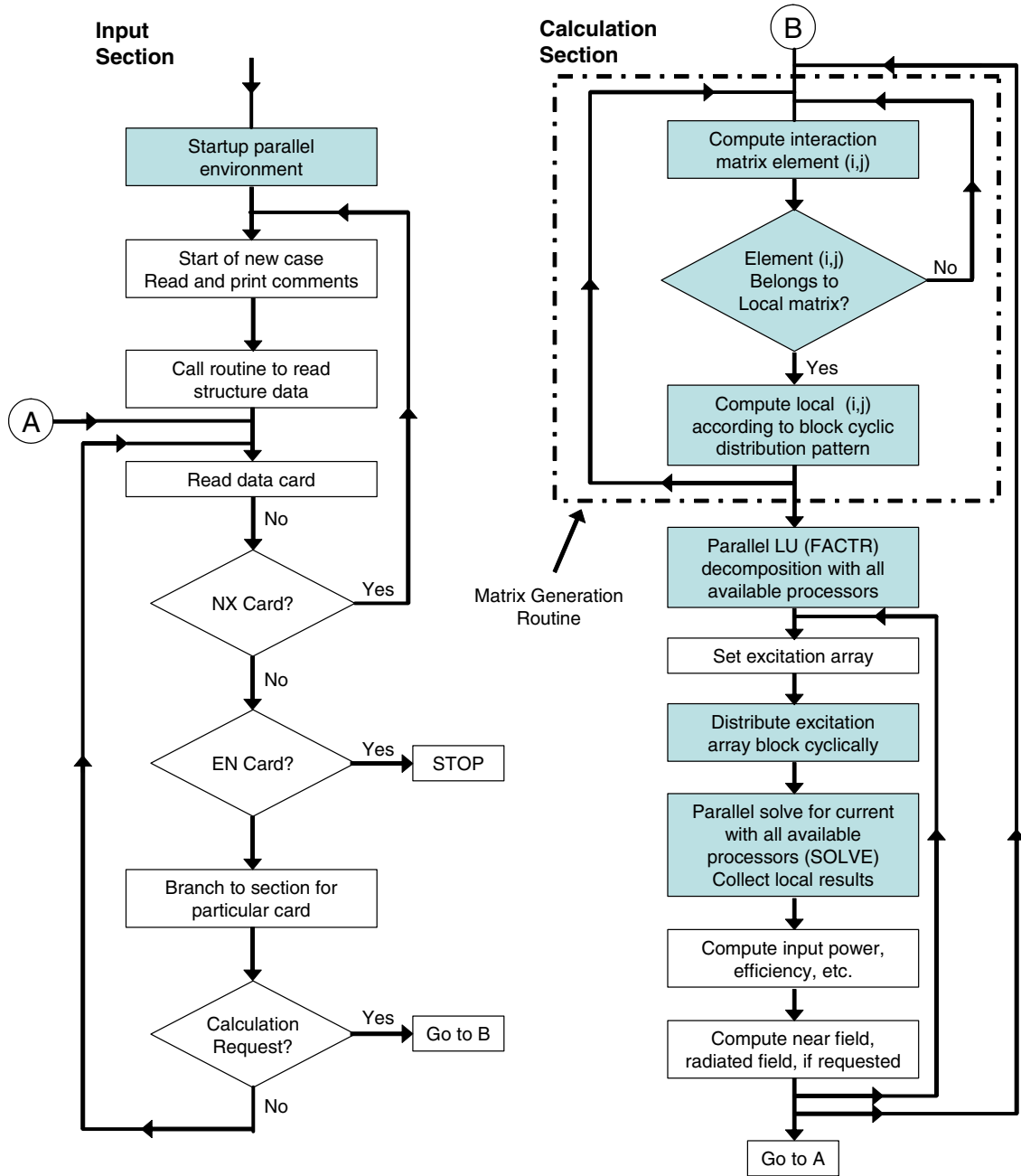
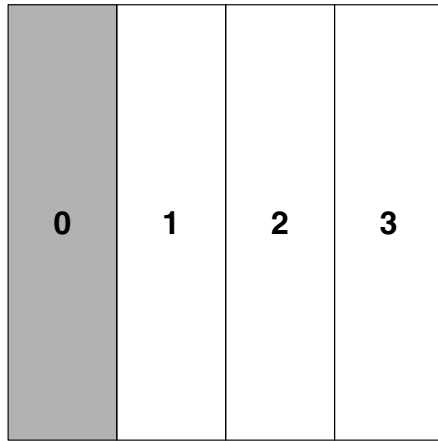
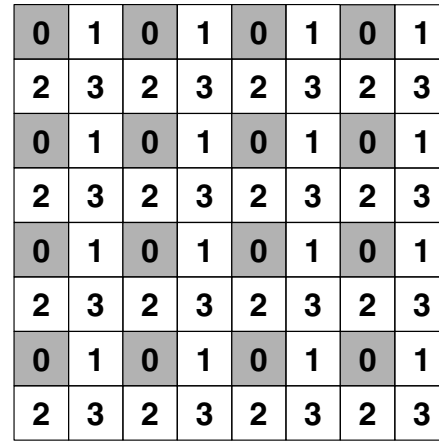


Figure 3.2: Flow diagram of the developed Parallel NEC. Shaded: modified or newly created parallel code. Adapted from [8]



(a) One-dimensional column distribution



(b) Two-dimensional block cyclic distribution

Figure 3.3: Distribution of matrix among 4 processors

$$\begin{pmatrix} a_{11} & a_{12} & \dots & a_{1n} \\ a_{21} & a_{22} & \dots & a_{2n} \\ \vdots & \vdots & \ddots & \vdots \\ a_{n1} & a_{n2} & \dots & a_{nn} \end{pmatrix} \quad (3.5)$$

After one iteration of the algorithm, the first element of the diagonal holds a 1, the rest of the elements of that column have become 0 and all of the other elements of the matrix have been transformed by the linear operations. At this phase, the matrix looks like this

$$\begin{pmatrix} 1 & a'_{12} & \dots & a'_{1n} \\ 0 & a'_{22} & \dots & a'_{2n} \\ \vdots & \vdots & \ddots & \vdots \\ 0 & a'_{n2} & \dots & a'_{nn} \end{pmatrix} \quad (3.6)$$

The state of the system at the end of a particular iteration, still far from the end, could be represented by Figure 3.4. If one uses the one-dimensional column distribution (Figure 3.3(a)), after a certain number of iterations, all elements in the leftmost group, labelled 0, would belong to the “already calculated” area of Figure 3.4, thus, leaving processor 0 idle during a significant part of the calculation time. Once all the elements that correspond to processor 1 have been calculated, this processor,

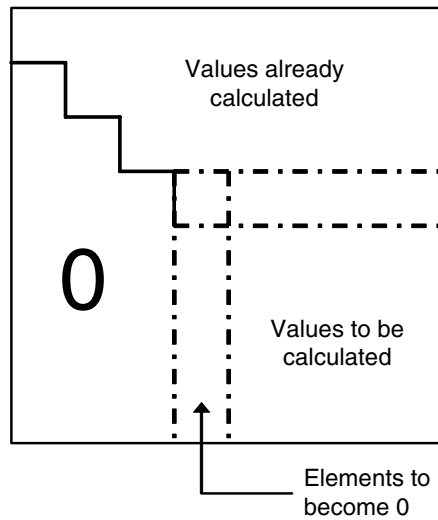


Figure 3.4: Calculation of an upper triangular matrix

too, will become idle, for the remainder of the calculation time. The same type of reasoning may be applied in turn to the other two processors. On the other hand, the use of the two-dimensional block cyclic decomposition in Figure 3.3(b) assures that, on average, all of the processors contribute to the final solution from the beginning to the end of the algorithm. Better performance may be obtained if the processor grid is square since, this way, it is easier to achieve a more equitable distribution of the calculation load. Since the number of processors may vary from one machine to another, a square processor grid remains a desirable condition rather than a requisite and, in practice, the grid is made as square as possible. This is achieved by way of an automatic calculation of the squarest possible processor grid on the running platform performed at the beginning of the developed parallel NEC and used to declare and start the parallel environment. The block cyclic decomposition used in the developed parallel NEC is based on the SCALAPACK library [10], a very powerful, freeware, parallel implementation of a subset of routines contained in the Linear Algebra Package (LAPACK).

3.2.3 Parallelization Strategy

Clearly, the construction of the interaction matrix on a single computer to be distributed later among the computers in the grid would not solve the memory problem.

A new implementation of the matrix filling routine had to be written in order to produce an already distributed matrix as it is being calculated. After execution of the input section in Figure 3.2, every processor on the grid holds the information needed to calculate the elements of $[G]$. One newly created function indicates to each processor of the cluster if the element (i, j) being calculated corresponds to its local sub-matrix. If this is the case, a subroutine will calculate the local values of (i, j) for the same element so that it can be assigned to the corresponding local matrix. At the end of the modified matrix generation routine indicated in Figure 3.2, each processor will hold its local version of the interaction matrix without the need for explicit communication operations among the processors. The dimensions of the interaction matrix array are assigned at runtime based on the calculated dimensions of the local sub-matrices, which depend on the number of processors in use. The code adapts automatically to the environment and to the number of processors. The dimensions of the rest of the arrays need to be indicated at compilation time ¹.

The LU decomposition in NEC is carried out in the matrix factorization routine (called FACTR). After this routine is executed, the interaction matrix $[G]$ can be expressed as:

$$[G] = [L][U] \quad (3.7)$$

and the matrix equation becomes:

$$[L][U][I] = [E] \quad (3.8)$$

The solution is then computed in the solving routine (called SOLVE), solving for $[F]$ by forward substitution in

$$[L] = [F][E] \quad (3.9)$$

and solving for $[I]$ by backward substitution in

$$[U] = [I][F] \quad (3.10)$$

¹NEC reads all the geometrical and electromagnetic information from the input file before calculating the interaction matrix. This information is stored in arrays which, in the proposed parallel version of NEC, remain identical to the original version. Since these arrays are passed to subroutines using common blocks, their dimensions need to be explicitly declared at compilation time.

Both the FACTR and SOLVE routines have been rewritten to produce parallel equivalents.

Vector $[E]$ needs to be block-cyclically distributed as well. This task is carried out by a routine that automatically assigns values and indices. After the solution $[I]$ is found, data are put back together by means of a block-cyclic composition routine and all of the processors become aware of the solution. Normal program execution can continue and solutions can be printed to the output file.

As a consequence of the matrix distribution among the processors, in the parallel version of NEC, the memory requirements for each one of the local sub-matrices are inversely proportional to the number of processors. For example, a model consisting of 11500 segments requires approximately 2 GB of RAM running on only 1 processor. If 16 processors with 128 MB of RAM each are used to solve the same problem, the memory gets shared and the model can be successfully executed without swapping matrix information between memory and disk. As a general rule, an estimate of the memory requirements in bytes at a local node for the parallel version of NEC can be calculated using this expression:

$$Mem = \frac{N^2 \cdot 16}{P} \quad (3.11)$$

where P is the number of processors being used at runtime.

3.3 Test and Performance

Testing was carried out using one regular PC with a PIII processor running the original sequential version of NEC2 [1] at 750 MHz with Windows NT 4.0 and 256 MB of RAM. The parallel version of NEC was implemented on 2 distributed memory machines, the Swiss-T1 [11] and Eridan [12].

3.3.1 The Swiss-T1 Parallel Supercomputer

Parallel NEC was originally developed and tested using the Swiss-T1 [11], one of the fastest supercomputers in Switzerland. The Swiss-T1 features 35 Compaq DS20E dual Alpha processor boxes at 500 MHz each (Figs. 3.5 and 3.6). They all have 1 GB of RAM

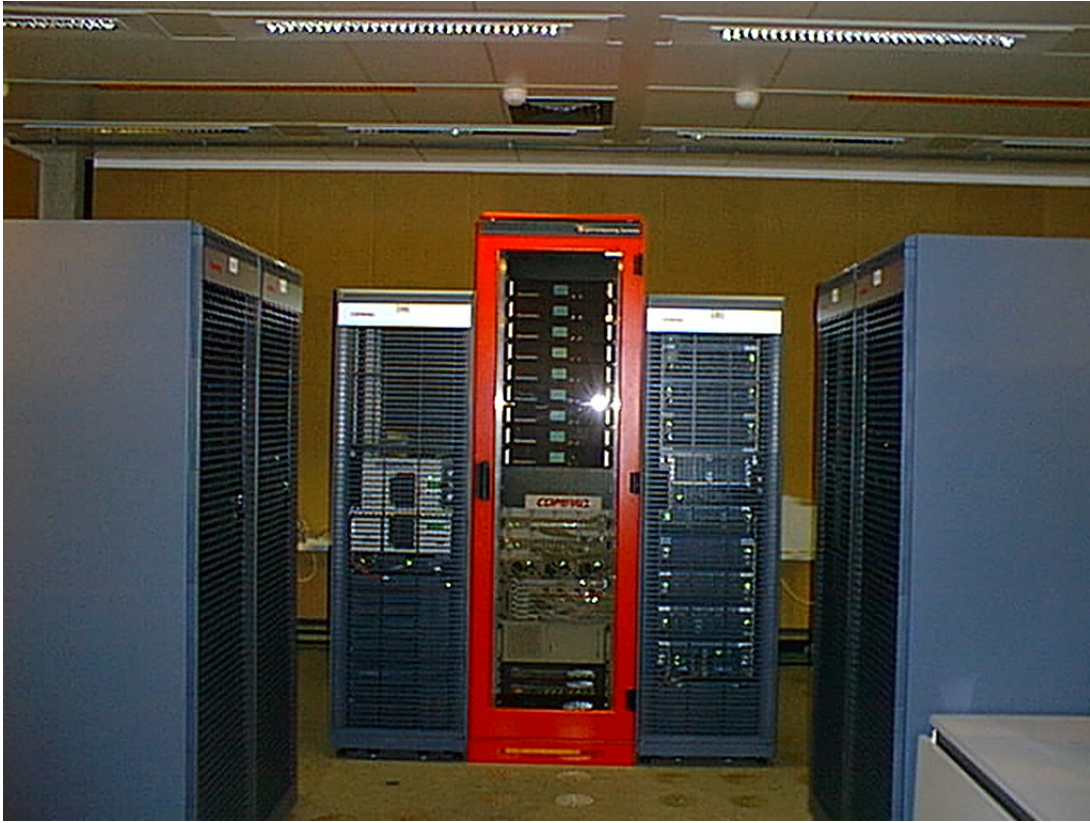


Figure 3.5: Swiss-T1 calculation server

and two 9.1 GB SCSI-U2 hard disks. Two of those boxes are used as an interactive front-end, another one for upgrades, development and maintenance, and the other 32 are used as calculation nodes. This 64-processor calculation part is connected by a Tnet network (Figure 3.7, which is a reliable, high performance, low latency network to build supercomputing clusters.

3.3.2 The Eridan Parallel Supercomputer

The Eridan supercomputer [12] has 128 MIPS R14000 RISC super-scalar CPU's running at 500 MHz each and distributed among 32 nodes. Each processor has 512 Mbytes of RAM for a total of 64 Gbytes. The total capacity of the hard disks goes up to 1.5 TB for system and users (Figs. 3.8 and 3.9).

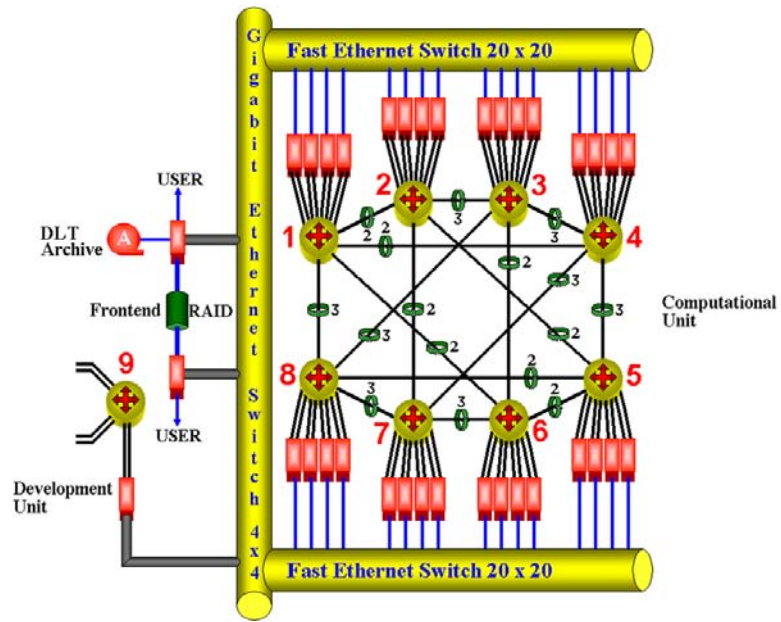


Figure 3.6: Swiss-T1 calculation server architecture



Figure 3.7: The TNet switches with 12 ports each



Figure 3.8: Eridan calculation server

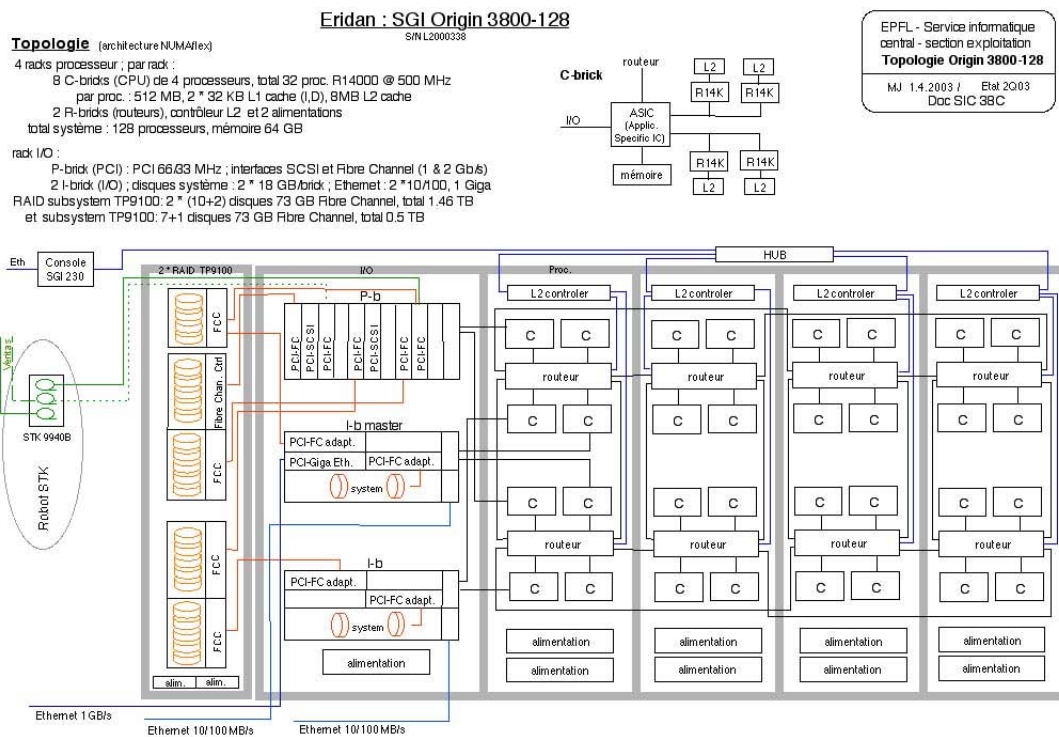


Figure 3.9: Eridan calculation server architecture

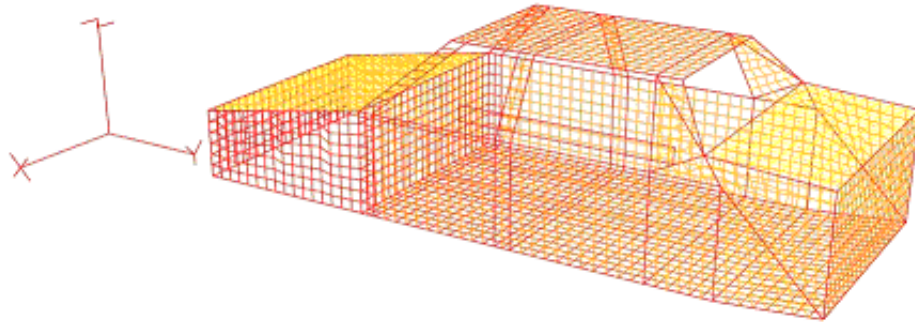


Figure 3.10: mesh of the simplified car consisting of 6753 segments used for performance comparisons

3.3.3 Performance of Parallel NEC

The first NEC input file used for testing, a rectangular wiregrid representation of a car, consisted of 6753 segments. Figure 3.10 shows a 3D plot of this simple model. In this case, the Eridan computer was only used to test portability of the code. On the Swiss-T1, the same input file was executed with 4, 8, 16, 24, 32 and 36 processors. The numerical results from both computers were found to be the same within working precision. For Eridan, no timing or memory results are presented here. Table 3.1 shows the relation of the number of processors on the Swiss-T1 with matrix filling, matrix factorization and run times, local memory and total memory.

On the PC, it was specified that the maximum core storage should be limited to 2000 segments since the total model requires about 700 MB. This would leave enough space for the operating system and services and should allow flawless calculation using the out of core routine included in NEC and described in Section 3.1. Two frequency steps were calculated. Examining Table 3.1, it can be seen that the use of only 4 processors reduces run time to a small fraction of the original running on the PC, only 1.9%. This is mainly due to the fact that the PC is forced to use disk swapping. Per processor memory behaves as expected. It is important to notice that the memory used by each single processor depends on the particular dimensions of its local matrix, and that the values given in the table are the largest. The total memory for each parallel configuration is higher than the PC's theoretical requirements because the rest of the arrays that are used in the parallel version need to be declared with the total

Number of Processors	Matrix Filling Time	Matrix Factorization time	Run Time (2 freq. steps)	Mem/processor (MB)	Total Memory (MB)
1 - PC	10 min	6 h 47 min	14 h 6 min	62 ^a	2790
4 - T1	2 min 56 sec	5 min 24 sec	16 min 7 sec	193.9	769.34
8 - T1	2 min 42 sec	2 min 45 sec	11 min 37 sec	104.4	816.04
16 - T1	2 min 34 sec	1 min 31 sec	8 min 52 sec	57.28	883.76
24 - T1	2 min 50 sec	1 min 39 sec	8 min 29 sec	39.55	905.81
32 - T1	2 min 33 sec	2 min 33 sec	8 min 16 sec	33.72	1019.45
36 - T1	3 min	1 min 3 sec	8 min 34 sec	28.45	988.57

Table 3.1: Timing and memory as a function of the number of processors for a 6753 segments test case on the Swiss-T1 parallel supercomputer

^aApproximation based on a core storage of 2000 segments

size of the model. In Figures 3.11 and 3.12, the matrix factorization time and the total run time as a function of the number of processors are presented. From these figures, we observe that the use of too large a number of processors can compromise the total run time. It was noticed that, for this particular experiment, the matrix filling time did not respond linearly to the number of processors whereas the factorization and solution routines did. This may be due to the fact that the matrix filling does not use any parallel-optimized functions or routines but it depends on the particular configuration of the parallel cluster and the number of elements in the matrix, making it hard to predict the execution time as a function of the number of processors.

A larger structure consisting of 23449 segments, a more complex representation of a car using a triangular grid was also tested (see Figure 3.13). With this number of segments, approximately 8.4 GB of RAM are required. The total execution time on the Swiss-T1 with 32 processors was about 68 minutes for one frequency step. This example cannot be executed on a PC, unless disk swapping is used. For such a case over 35 GB of disk space would be needed. The same file was launched on the PC and program execution was stopped after 168 hours. No solution was produced. Table 3.2 summarizes information about matrix filling time, matrix factorization time, total run time and memory.

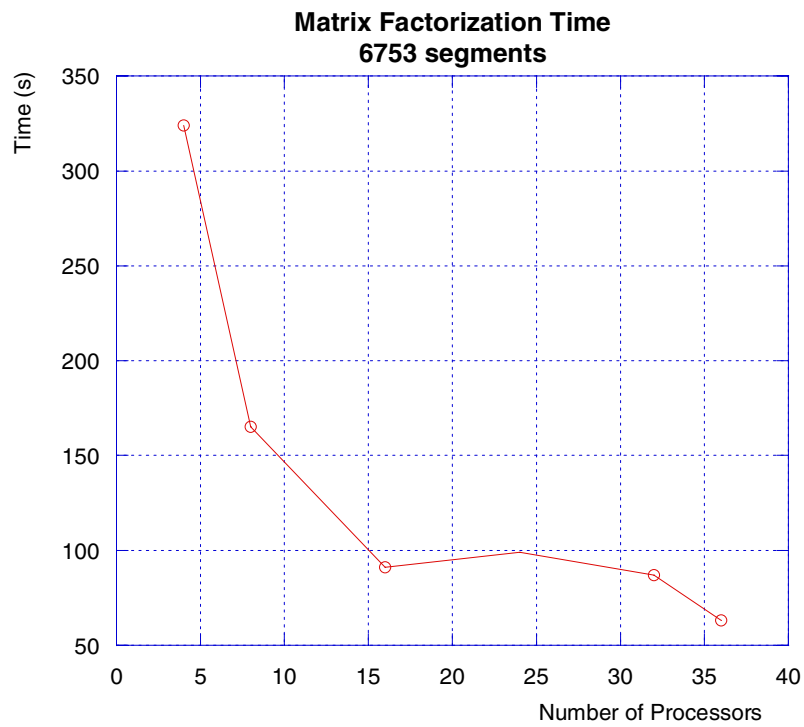


Figure 3.11: Matrix factorization time as a function of number of processors for the Swiss-T1 parallel supercomputer

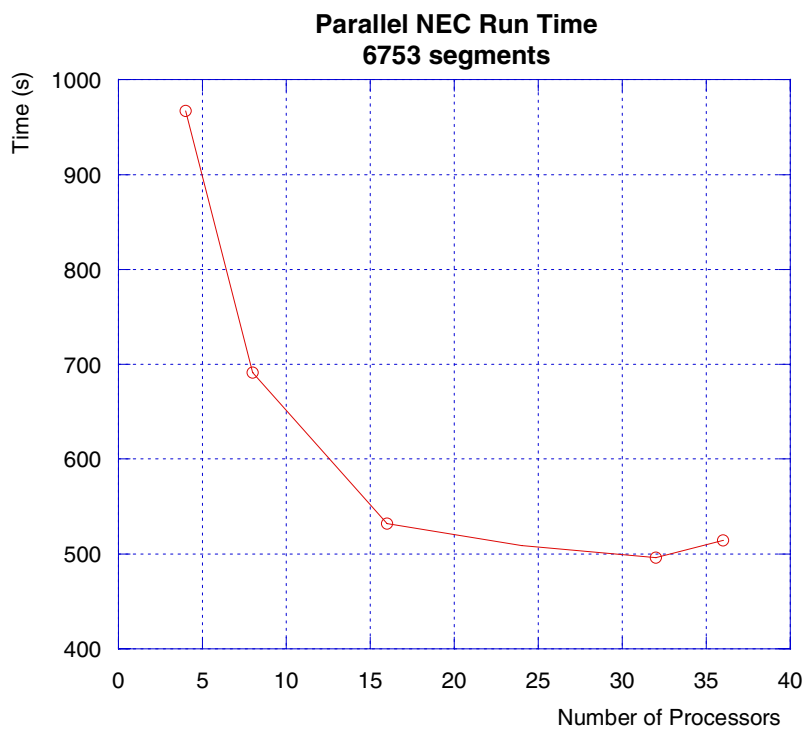


Figure 3.12: Total run time as a function of number of processors for the Swiss-T1 parallel supercomputer

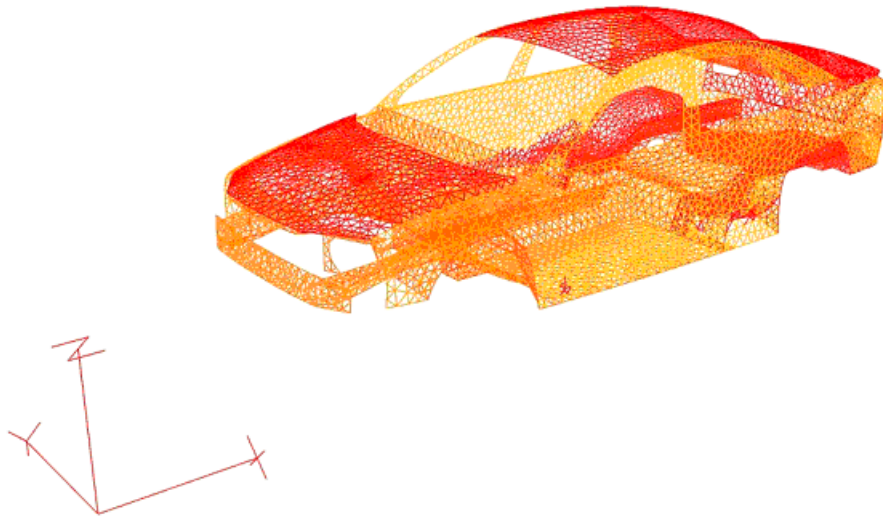


Figure 3.13: NEC mesh of the considered geometry consisting of 23449 segments used for performance comparisons

Number of Processors	Matrix Filling Time	Matrix Factorization Time	Run Time (1 freq. step)	Mem/processor (MB)	Total Memory (MB)
1 - PC	*****	*****	Stopped after 168 h	*****	~ 36000
32 - T1	35 min 50 sec	32 min 10 sec	68 min 24 sec	282.72	8940.32

Table 3.2: Timing and memory as a function of the number of processors for a 23449 segments test case. Asterisks are used where the results could not be obtained due to early interruption of the program

3.4 Conclusions

In this chapter, a parallel version of the Numerical Electromagnetics Code (NEC) which makes it possible to simulate larger structures than ever before has been proposed.

The use of a memory distributed system allows the sharing of memory and computing power. The matrix solving routines, based on the Gauss-Doolittle matrix-triangulation algorithm, are executed by several processors working together as a team. Optimal performance requires a very specific distribution of the matrix elements known as the bi-dimensional block-cyclic distribution. Assuming the array of processors as a two-dimensional grid, it has been shown that a rectangular distribution assures a theoretically-optimal load balance among the processors.

The code is portable to any platform supporting typical message passing parallel environments such as MPI and PVM where it could be executed on heterogeneous clusters of computers running on different operating systems. The Parallel NEC was implemented in two different supercomputing architectures, both based on memory distributed parallel arrays of processors, but featuring different architectures, processor types, and operating systems. Different FORTRAN compilers were used to obtain the developed parallel NEC executables on both machines, in order to test portability to an even higher level.

The possibility of running very complex models without the use of disk swapping produces appreciable speed improvements. Memory sharing also allows the execution of models that are impossible to run on current single processor machines.

Bibliography

- [1] G. Burke and A. Poggio. Numerical electromagnetics code - method of moments. In *Report No. UCID-18834*, 1981. Livermore CA: Lawrence Livermore National Laboratory.
- [2] A. J. Poggio and E. K. Miller. *Computer Techniques for Electromagnetics*, chapter 4. Summa, 1987.
- [3] T. R. Ferguson, T. H. Lehman, and R. J. Balestri. Efficient Solution of Large Moments Problems: Theory and Small Problem Results. In *IEEE Transactions on Antenna Propagation*, pages 230–235, March 1976.
- [4] P. S. Excell, G. J. Porter, Y. K. Tang, and K. W. Yip. Re-working of two standard moment-method codes for the execution on parallel processors. In *International Journal of Numerical Modelling: Electronic Networks, Devices and fields*, 1995. Vol 8.
- [5] D.C. Nitch and A.P.C. Fourié. Parallel implementation of NEC. In *Applied Computational Electromagnetics Society (ACES) Journal*, March 1994. Vol 9.
- [6] D.C. Nitch, A.P.C. Fourié, and J. S. Reeve. Running SuperNEC on the 22 Processor IBM-SP2 at Southampton University. In *Applied Computational Electromagnetics Society (ACES) Journal*, pages 99–106, 1998. Vol 13.
- [7] A. Rubinstein, F. Rachidi, and M. Rubinstein. Development of an Optimized Parallel Numerical Electromagnetics Code (NEC) and Its Implementation on the Swiss-T1 and Eridan Parallel Supercomputers. In *Annual Review of Progress in Computational Electromagnetics. Monterey*, 18-22 March 2002.

-
- [8] A. Rubinstein, F. Rachidi, M. Rubinstein, and B. Reusser. A Parallel Version of NEC for the Analysis of Large Structures. In *IEEE Transactions on Electromagnetic Compatibility*, volume EMC-45, pages 177–188, May 2003.
- [9] J. Dongarra, R. van de Geijn, and D. Walker. A look at scalable dense linear algebra libraries. In *Scalable High Performance Computing Conference Proceedings*, pages 372–379, 1992. Vol 13.
- [10] L. S. Blackford, J. Choi, A. Cleary, E. D’Azevedo, J. Demmel, I. Dhillon, J. Dongarra, S. Hammarling, G. Henry, A. Petitet, K. Stanley, D. Walker, and R. C. Whaley. *ScaLAPACK Users’ Guide*. Society for Industrial and Applied Mathematics, 1997.
- [11] The Swiss-T1 parallel supercomputer. Web Page. <http://tone.epfl.ch>.
- [12] The Parallel calculation server Eridan. Web Page. <http://sewww.epfl.ch/SIC/SE/servcentraux/origin.html>.

Chapter 4

Study of the Field Penetration Inside a Vehicle Illuminated by an EMP Simulator. Validation of Parallel NEC

4.1 Introduction

The automobile industry has been increasing the amount of on-board technology. Modern cars exhibit navigation systems, high-tech entertainment devices, and computer-controlled optimization of fuel injection, brakes, etc. As a consequence, the study of the EMC phenomena in automobiles becomes indispensable (e.g. [1, 2]). In order to test the developed parallel NEC code presented in Chapter 3, experimental data obtained in the framework of the European GEMCAR (Guidelines for Electromagnetic Compatibility Modelling for Automotive Requirements) project were used. GEMCAR was introduced in Section 1.2.

The computed results were validated using (1) other numerical methods used in GEMCAR and briefly described in Chapter 2 and (2) experimental data obtained using the VERIFY EMP simulator belonging to the Swiss Defense Procurement Agency. The VERIFY simulator generates a vertically-polarized electric field with a rise time of 0.9 ns and a Full Width at Half Maximum (FWHM) of 24 ns. Measurements of electromagnetic fields inside a stripped-down car (consisting essentially of the body shell) were performed considering two types of illumination, front and side.

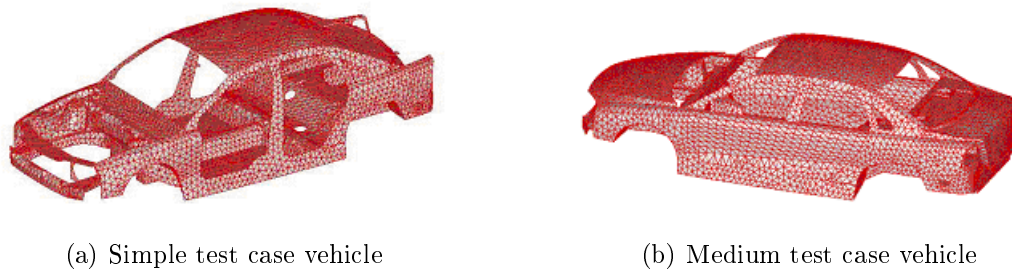


Figure 4.1: Vehicle models

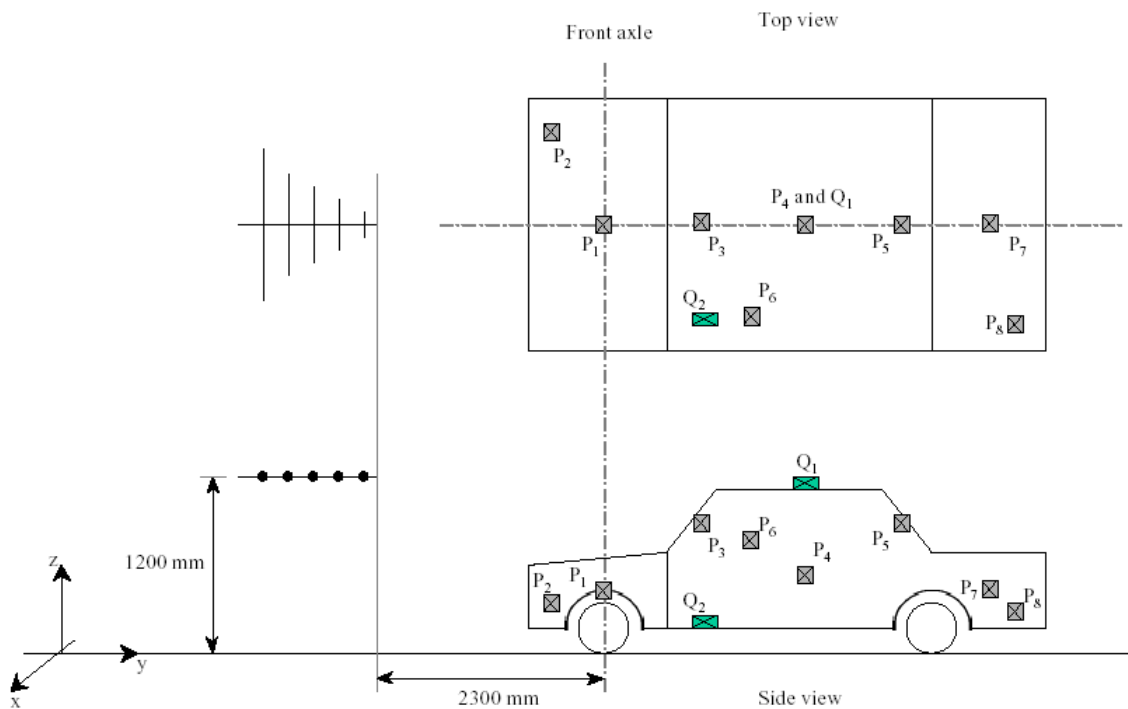


Figure 4.2: Field Measurement Points defined in the GEMCAR Project

4.2 Description of the Configuration

Measurements of electric and magnetic fields inside a real vehicle (a Volvo S80) featuring different levels of complexity (see Figure 4.1) were carried out in order to obtain the data to validate the numerical models. These measurements were carried out at 8 different places inside the car identified as points P1 to P8. Two surface fields were also measured, identified as points Q1 and Q2 (Figure 4.2).

The data used in this section were collected with the *VERIFY* EMP Simulator (See Figure 4.3 and Table 4.1) and they refer to the “simple test case”, as described in Section 1.2.



Figure 4.3: VERIFY EMP Simulator

Pulse Generator Voltage Range (V_{max} = voltage to produce maximum field level)	$0.3 V_{max} - V_{max}$
Antenna Impedance	$100\Omega \pm 20\%$
Polarity	plus or minus
Max. Pulse Rate	1 pulse per minute
Shot-to-shot Reproducibility in E and H Fields	$\pm 10\%$ for 20 shots
Misfire/Self-fire Rate	$< 5\%$
Field Characteristics in Working Volume:	
Amplitude	30-100 kV/m; 79-265 A/m
Prepulse	$< 10\%$
Risetime (10-90 %)	0.9 nsec (+0.1/-0.2 ns) smooth rise
Duration (FWHM)	24 nsec (-0 nsec/+12 nsec)
Amplitude variation over any vertical plane in working volume	$\pm 10\%$ of geometric center
Spectrum:	
DC - 500 MHz	$\leq \pm 6$ dB from theoretical
500 MHz - 1 GHz	$\leq \pm 12$ dB from theoretical

Table 4.1: Electrical specifications of VERIFY

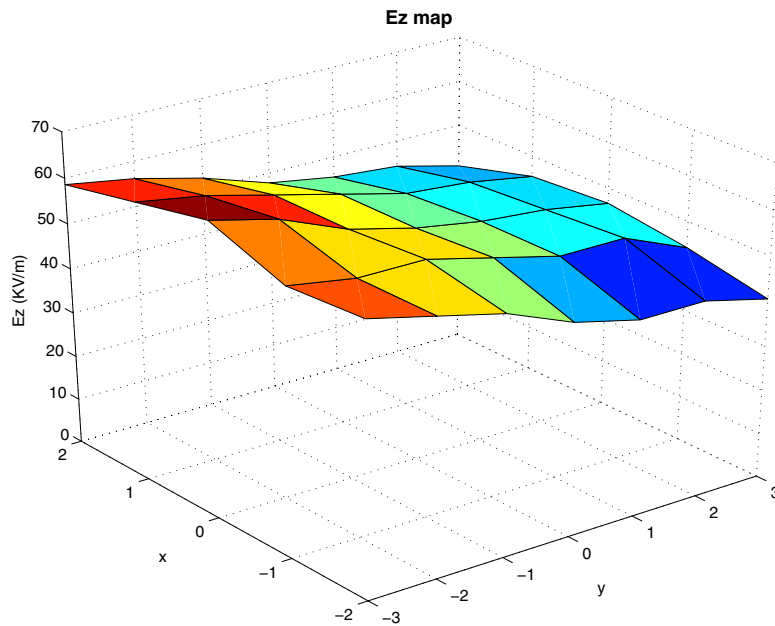


Figure 4.4: Cartography of the incident field of the VERIFY EMP simulator

A cartography of the E-field produced by the EMP simulator was created by taking several measurements at a height of 1 m above the ground and at square intervals of 1 m. This grid was used to check the homogeneity of the produced field, by taking the peak value of each sample and representing it in a 3-D plot showing the peak values of E_z as a function of the position inside the working volume (see Figure 4.4).

The incident (vertical) electric field, measured in absence of any test object, is presented in Figure 4.5.

The cable harness was installed following an approximate path of the original cabling of the car but it was composed of single wires with 50Ω terminations. Current measurements were taken at 4 observation points (see Figure 4.6) located at the ends of the branches of the harness. No current simulations are given as they do not represent the subject of study of this thesis. The interested reader is referred to [2].

For the electric and magnetic field measurements we used Thomson MELOPEE-E1602 (E field) and H1602 (H field) sensors (see Figure 4.7), designed for measuring free space electric and magnetic fields, sinusoidal or pulsed, up to 1.2 GHz.

The data acquisition system featured a fiber optics link between the sensors and a digitizer with a sampling rate of 2 GSamples/s.

The car was placed inside the working volume of the EMP simulator (Figure 4.8)

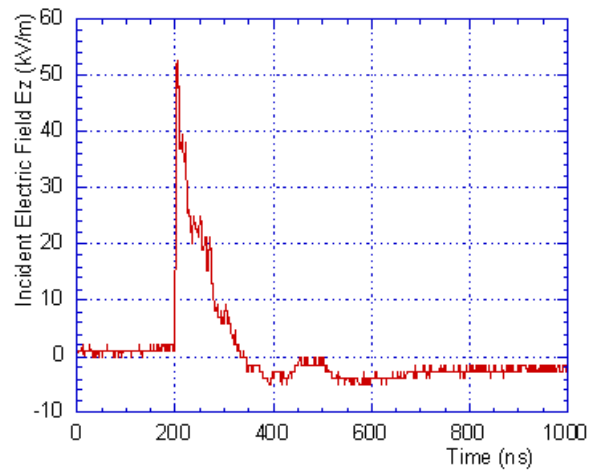


Figure 4.5: Vertical electric field inside the working volume of the simulator

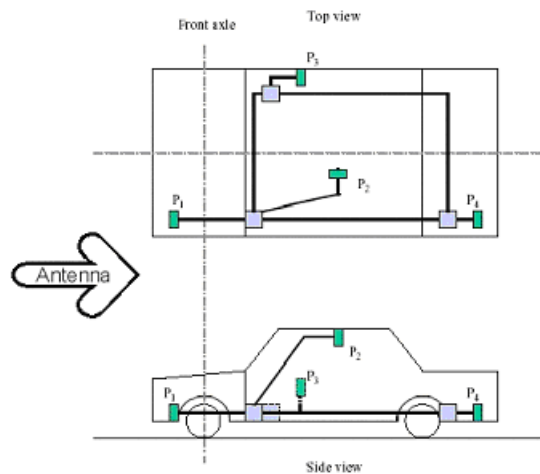


Figure 4.6: Measurement points for current at the cable harness



Figure 4.7: Thomson Electric and Magnetic Field Sensors used for the EMP simulator measurements

and four points, P3, P4, P5 and P6 (see Figure 4.9) out of the total ten (see Figure 4.2) were selected in the passengers' compartment for the experimental validation of Parallel NEC. Figures 4.10 and 4.11 present the waveforms of the vertical component of the electric field measured at points P3 to P6 for front and side illuminations, respectively. A thorough analysis of the experimental data may be found in [3].

4.2.1 Numerical Validation of Parallel NEC

As a first step in validating the code, numerical results obtained using the parallel NEC have been compared to those obtained using other, well known numerical techniques (TLM [4, 5]), hybrid FV/FDTD [6] and BEM [7]). The point used for comparison was P4, located at the centre of the vehicle. The geometrical data for the simulated car were obtained from a CAD file. This file was manipulated to represent the stripped-down model of the test car (i.e. only the body shell) and it was adapted to fit particular requirements of each individual method. The 3D representation of one of the NEC input files has already been show in Figure 4.12(d). This model was converted and



Figure 4.8: Test car inside the simulator (side illumination)

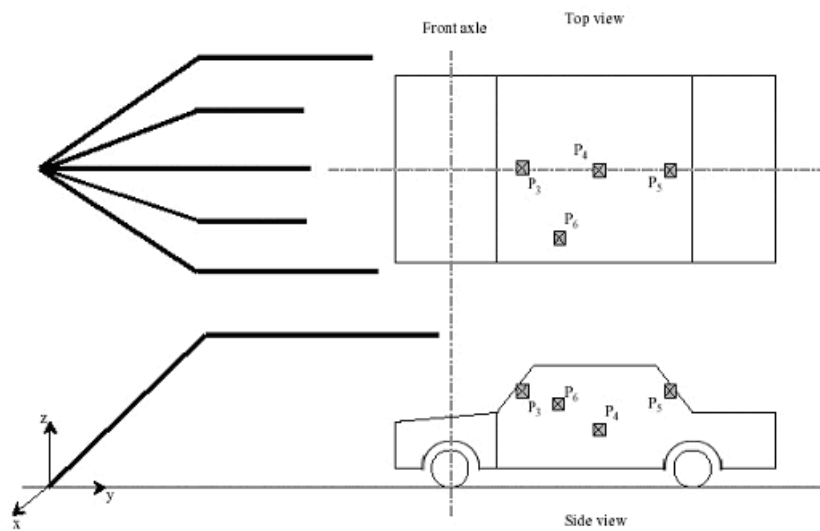


Figure 4.9: Illustration of the four measurements points inside the vehicle (front illumination)

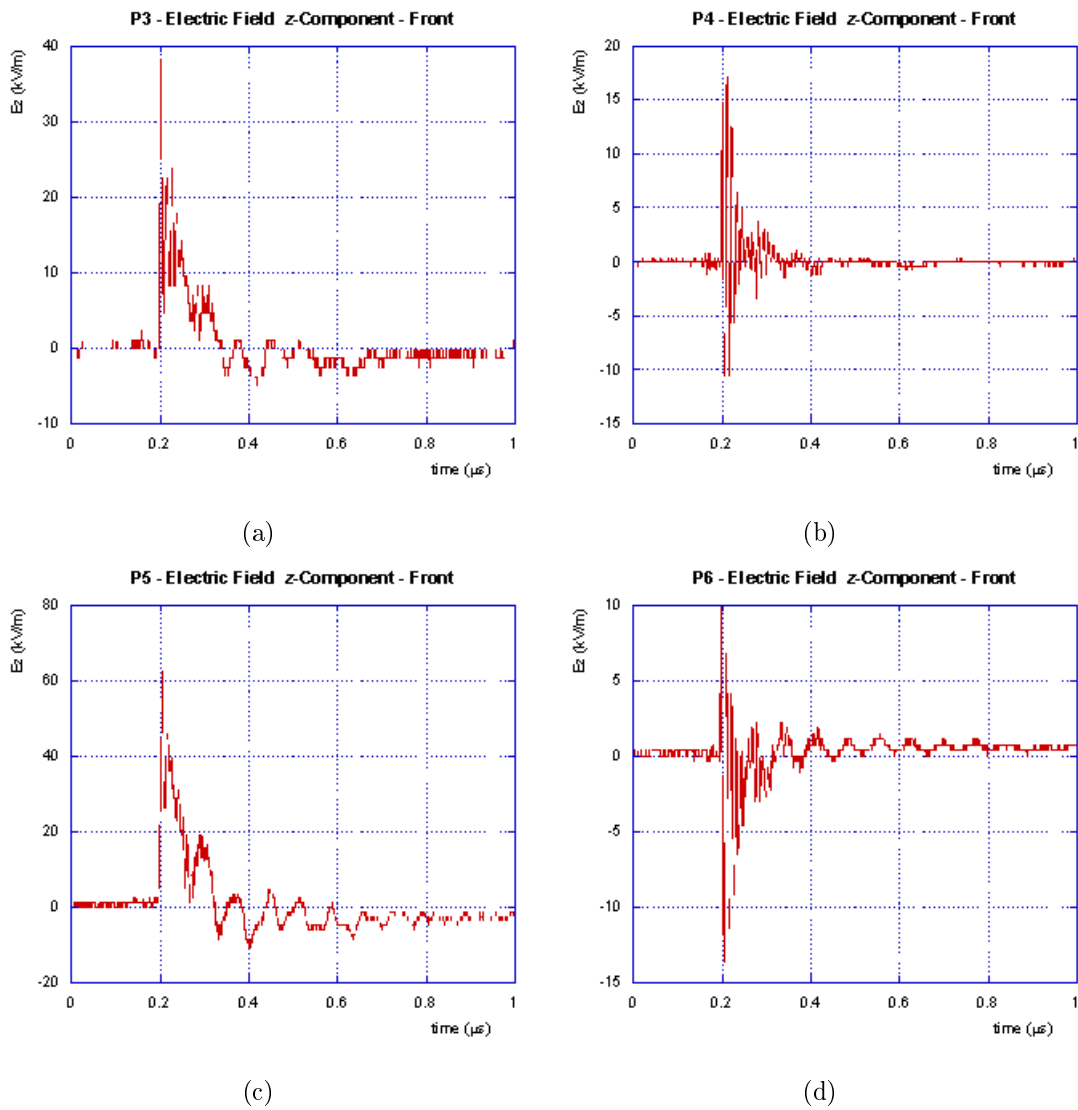


Figure 4.10: Vertical electric field component measured at Points P3, P4, P5 and P6. Front illumination

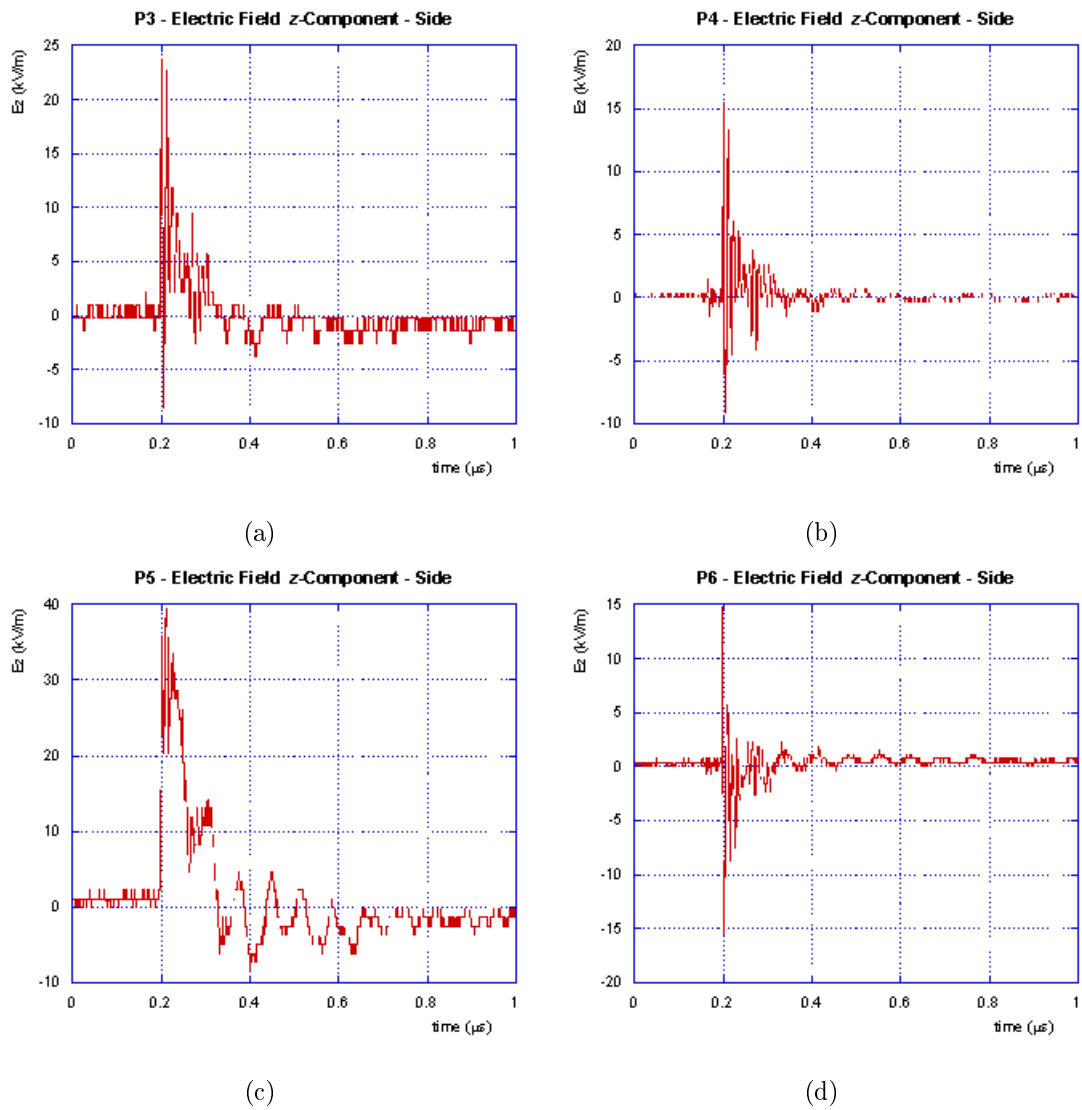


Figure 4.11: Vertical electric field component measured at Points P3, P4, P5 and P6. Side illumination

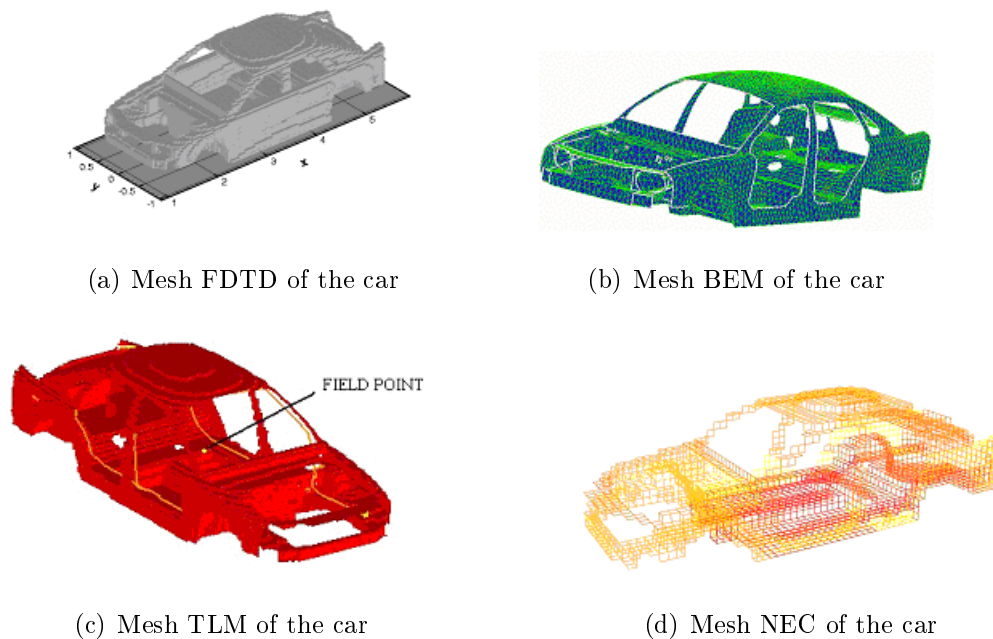


Figure 4.12: Meshing of the different numerical methods used for validation (Adapted from [10])

adapted from the TLM version of the CAD data. The excitation was provided by a simulated unitary, vertically polarized plane wave produced by NEC. Figure 4.12 shows the adapted meshing of the model for each numerical method applied and Figure 4.13 shows a comparison of the simulation results at point P4 for a front illumination [7, 8, 9]. An excellent agreement was found.

4.2.2 Experimental Results

4.2.2.1 Comparison with Experimental Data

Since NEC is a frequency domain tool, the measured data were converted to the frequency domain using the FFT, and incident field measurements performed in the absence of any object inside the simulator were used to properly adapt the simulations to the excitation. The NEC model consisting of almost 8000 segments was run on 16 processors. The average run time for one frequency step was 7 minutes.

Figures 4.14 and 4.15 show comparisons of measurements and simulations for the vertical component of the electric field at the four observation points defined inside the car for both, front and side illumination. The fields are normalized with respect

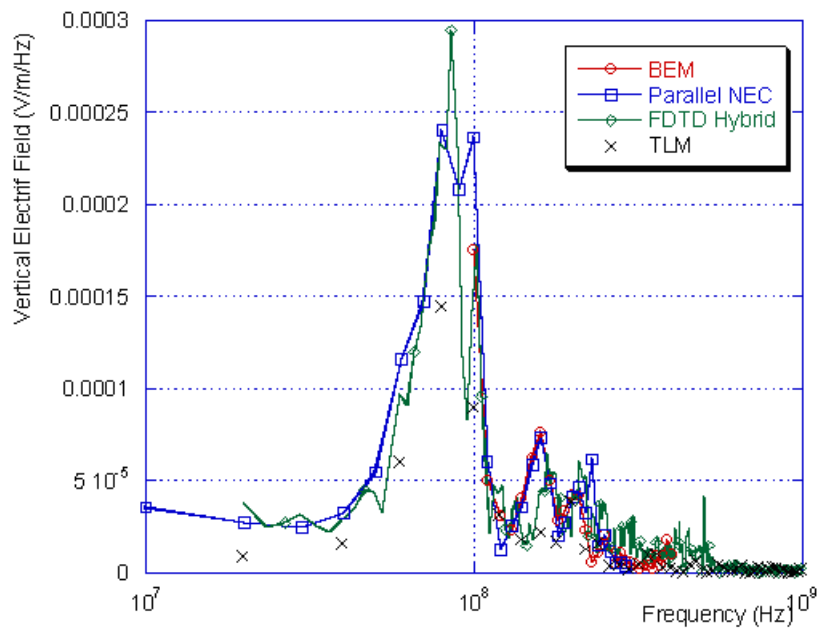


Figure 4.13: Comparison of the numerical results from different methods

to the incident field located at the centre of the EMP simulator. We can see that the simulations are in very good agreement with the measurements for the considered frequency range. The differences can be explained, at least in part, by the fact that the geometry of the model is a simplified approximation of the real geometry of the vehicle. There exists also an uncertainty associated with the definition and placement of the observation points and with the fact that the applied field used in the experiment is not a perfectly uniform plane wave.

4.2.3 Discussion on Meshing Issues

Two different approaches for the meshing of the vehicle were adopted. At first, the simulations were run using a very well defined structure consisting of over 17000 segments, featuring a body fitted triangular wire-grid (very similar to the one presented in Figure 3.13). Reasonable agreement was found in a narrow band of frequencies for these simulations. However, it was observed that the use of a less dense staircase approximation of the model (Figure 4.12(d)) with about 8000 segments, gave considerably better results over a wider frequency band. The triangular mesh faithfully reproduces the contours and details of the real model. However, this level of complex-

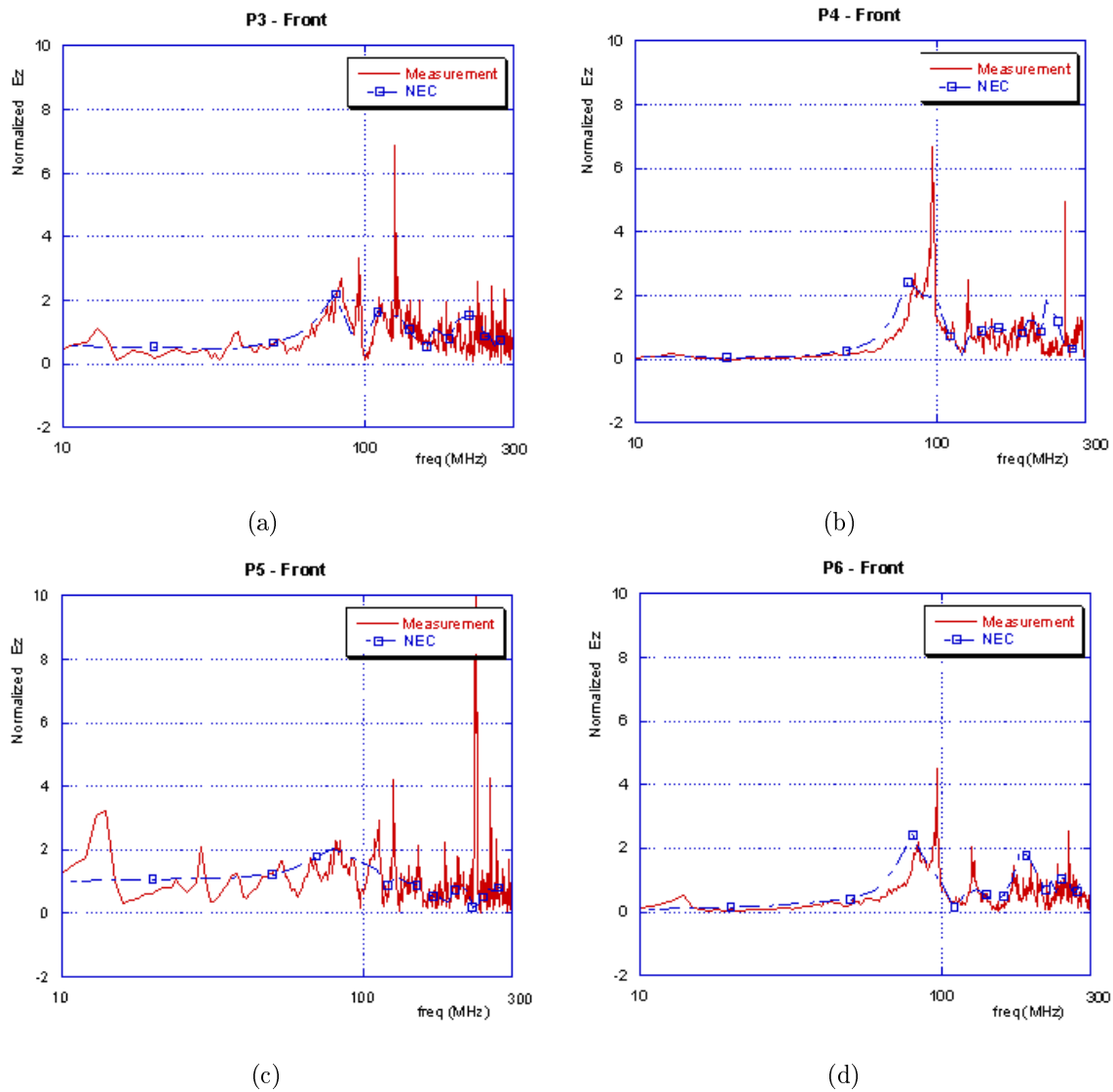


Figure 4.14: Normalized vertical electric field E_z at points P3, P4, P5, and P6. Comparison between measurements and simulations (using parallel NEC) for front illumination. The fields are normalized with respect to the incident field located at the centre of the EMP simulator

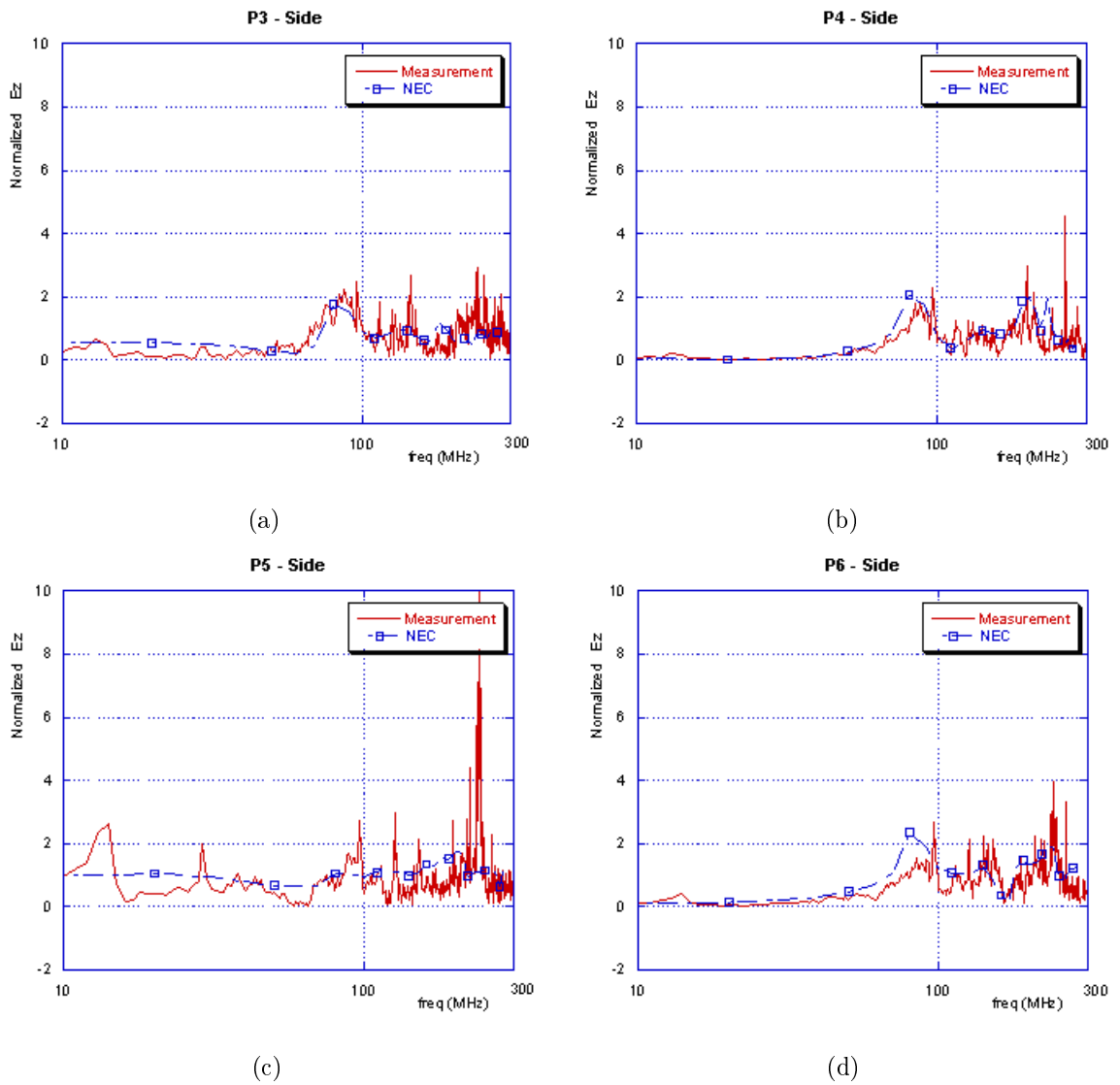


Figure 4.15: Normalized vertical electric field E_z at points P3, P4, P5, and P6. Comparison between measurements and simulations (using parallel NEC) for side illumination. The fields are normalized with respect to the incident field located at the centre of the EMP simulator

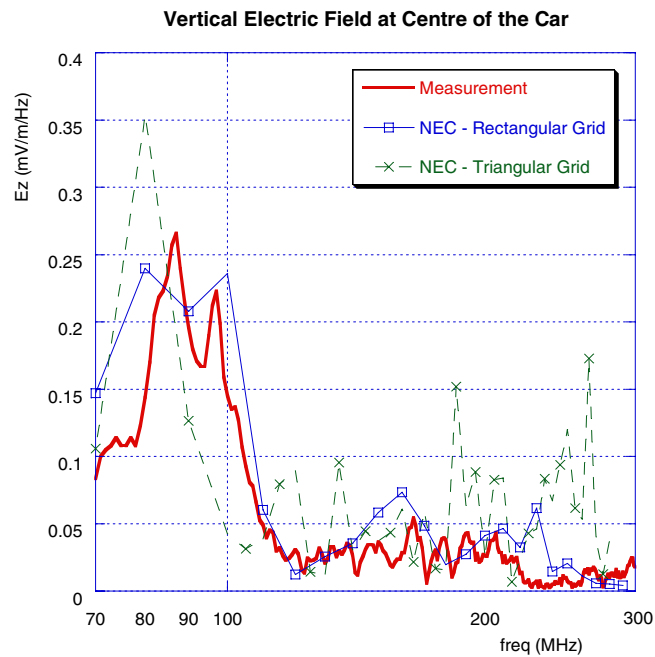


Figure 4.16: Comparison of measurement and simulation for the two different meshes. Adapted from [11]

ity requires some compromises. In fact, while some of the segments were 14 cm long, others were as small as 1 cm. The first attempts at running the body-fitted triangular model (originally composed of over 23000 segments) produced unsatisfactory results. For this reason, a routine was written to eliminate very small segments, in an effort to smooth out the differences in length. In the less dense staircase approximation of the model, all of the segments have the same length and radius. It was found that the simplified version of the model, despite being a less faithful representation of the real car, exhibited far better results when compared to measurements. An example of these results can be seen in Figure 4.16. This figure shows the measured vertical component of the electric field penetrating inside the vehicle illuminated by an EMP simulator. In the same figure, we also present the computed results using the parallel version of NEC [9] and obtained using the triangular and square meshes. It can be seen from Figure 4.16 that the square-mesh model yields very good results, whereas the results obtained using the triangular mesh are not satisfactory over a wide frequency range. The application of the so-called “equal area rule” (discussed in Chapters 5 and 6) and the general guidelines recommended for successful NEC simulation [10], has shown to

give the best results when it comes to perfectly square and homogeneous meshes. In fact, the application of the rule in those cases is also a guarantee that most of the other guidelines in the use of NEC are well respected. A perfectly square and homogeneous mesh will assure that all segments have the same length and radius, a desirable condition for successfully modeling complex 3D surfaces with NEC. On the other hand, the extension of the application of the rule to more complex (and better body fitted) meshing techniques (i.e. a triangular mesh) [12] does not exhibit the same degree of accuracy, possibly due to the fact that large variations of segment length and radius are inevitable. The next two chapters are dedicated to this particular issue.

4.3 Conclusions

Using data collected from the GEMCAR project, the parallel implementation of NEC was tested by comparing simulation results with those obtained by using other numerical methods (TLM, BEM, FDTD) and with measurements carried out using the VERIFY (Vertical EMP Radiating Indoor Facility), an EMP simulator belonging to the Swiss Defense Procurement Agency (Spiez). These measurements were carried out on a real vehicle (a Volvo S80), with 3 different levels of complexity: (1) the “simple test case”, (2) the “medium complexity case” and (3) the “complex case”. Only the first two cases were allowed using the EMP simulator and, from those two, only the simple case results were used in this chapter. The three components of the electric and magnetic fields were measured at 8 different points defined inside the car. Two additional points were used for surface field measurements.

The code was applied to analyze the penetration of electromagnetic fields inside the vehicle body shell (i.e., the simple case). The Parallel NEC results agreed well with those obtained using the other methods and with the experimental data obtained from measurements, which constituted a numerical and an experimental validation of the code.

The application of the code to such a large problem permitted the observation of some issues raised by the application of the so-called Equal Area Rule (EAR) for the calculation of segment length and radii. It was observed, in particular, that the

use of a homogeneous square mesh yields considerably improved results compared to a triangular body-fitted mesh. A more detailed discussion of this issue is presented in Chapter 5.

Bibliography

- [1] A. Ruddle, D. Ward, A. Williams, and A. Duffy. Objective validation of automotive EMC models. In *1998 IEEE International Symposium on Electromagnetic Compatibility*, volume 1, pages 475–479, 1998.
- [2] A. Rubinstein, F. Rachidi, D. Pavanello, and B. Reusser. Electromagnetic Field Interaction with Vehicle Cable Harness: An Experimental Analysis. In *International Conference on Electromagnetic Compatibility, EMC Europe. Sorrento*, volume 1, 2002. Proceedings.
- [3] W.J.R. Hofer. The transmission-line matrix method: theory and applications. In *IEEE Trans. On Microwave Theory and Techniques*, pages 882–892, 1985. Vol 330.
- [4] A. Ruddle. Computed impact of optional vehicle features (sunroof and windscreen heater) on automotive MEC characteristics. In *Proc. of the 15th International Symposium on Electromagnetic Compatibility, Zurich*, 2003.
- [5] X. Ferrières, J.P. Parmantier, S. Bertuol, and A.R. Ruddle. Modeling EM coupling onto vehicle wiring based on the combination of a hybrid FV/FDTD method and a cable network method. In *Proc. of the 15th International Symposium on Electromagnetic Compatibility, Zurich*, 2003.
- [6] S. Alestra, P.N. Gineste, P. Gondota, R. Perraud, and I. Terrasse. Modeling the electromagnetic field coupling into a car using a finite boundary element code. In *International Conference on Electromagnetic Compatibility, EMC Europe. Sorrento*, volume 1, 2002. Proceedings.

-
- [7] N. Whyman, C. Thomas, S. Alestra, X. Ferrières, J.P. Parmantier, R. Perraud, F. Rachidi, A. Rubinstein, and A.R. Ruddle. The EU Framework V Project GEMCAR: Model validation. In *Proc. of the 15th International Symposium on Electromagnetic Compatibility, Zurich, 2003*.
- [8] A. Rubinstein, F. Rachidi, J.-P. Parmantier, X. Ferrières, S. Alestra, R. Perraud, A.R. Ruddle, and B. Reusser. Modélisation de la penetration d'un champ électromagnétique à l'intérieur d'une automobile: simulation et validation expérimentale. In *Colloque CEM, Grenoble, France, March 2002*.
- [9] A. Rubinstein, F. Rachidi, M. Rubinstein, and B. Reusser. A Parallel Version of NEC for the Analysis of Large Structures. In *IEEE Transactions on Electromagnetic Compatibility*, volume EMC-45, pages 177–188, May 2003.
- [10] Edmund K. Miller. PCs and AP and Other EM Reflections. In *IEEE Antennas and Propagation Magazine*, volume 39, 1997.
- [11] A. Rubinstein, F. Rachidi, and M. Rubinstein. On Wire-grid Representation of Solid Metallic Surfaces. In *IEEE Transactions on Electromagnetic Compatibility*. In press.
- [12] C. W. Trueman and S. J. Kubina. Fields of Complex Surfaces using Wire Grid Modeling. In *IEEE Transactions on Magnetics*, volume 27, pages 4262–4267, Sep 1991.

Chapter 5

The Wire-Grid Representation of Solid Metallic Surfaces using the MoM

5.1 Introduction

The use of a wire grid model to approximate a continuous conducting surface was introduced by Richmond in 1966 [1]. By defining expressions for the scattered field of a wire segment, a point-matching solution was found for the scattering of a wire-grid structure by solving a system of linear equations [1]. The paper reports good agreement on simulation results of structures as simple as a conducting plate and as complex as a segmented sphere.

The wire-grid method has been adopted and the fast progress of digital computers has contributed to the evolution and development of even more complicated arbitrarily shaped models. The growth in complexity of the evaluated problems has permitted the observation of certain limitations derived from the fact that a wire-grid is, in fact, a highly simplified representation of reality. It has been observed in particular that the far-field results obtained with a wire-grid representation of a perfectly conducting closed surface are very reliable [2]. On the contrary, the wire-grid has been considered by some authors as a poor model of a closed surface when it comes to interaction calculations (currents and charge densities induced on the surface of a structure) [2], a rather reasonable conclusion, considering the fact that the wire-grid is an equivalent model of the solid surface.

A wire-grid approximation of a solid conducting surface introduces a number of new variables that affect the accuracy of the solution. For instance, the grid spacing must be carefully selected. This is further complicated by the fact that this particular parameter has an impact on the computation time and resource requirements [3]. In addition, the segments representing the solid structure must each be defined in terms of its length, width and position in space. Although the maximum segment length can be readily specified as a function of the frequency, it has been observed by many authors [2, 4, 5, 6, 7] that numerical simulation results are very sensitive to wires radii. As of the writing of this thesis, the calculation of this parameter could still be characterized as an art form or guesswork.

The wire-grid method has evolved and several numerical formulations based on segmented wires, patches or cells are available today for the solution of the electromagnetic scattering problem. One of these numerical solutions is based on the Method of Moments (MoM), for which the most popular incarnation in the frequency domain is the Numerical Electromagnetics Code (NEC) [8].

The “equal area rule” (EAR), also known as the “same surface area” and in some cases as the “twice surface area”, has been for years a rule of thumb for the calculation of segment radius in wire-grid modeling using NEC (e.g. [4, 5, 6, 7]). The rule states that the surface area of the wires parallel to one linear polarization is made equal to the surface area of the solid surface being modeled. Ludwig [4] defines the issue as being “clearly complex” and even though his paper adds new information to the problem by running several variations of a canonical problem (an infinite circular cylinder) it does not provide the final answer to the wire radius question. The author does conclude, however, that “the results certainly enhance confidence in the same surface area wire size rule of thumb”.

The problem of the modeling of an infinite cylinder was revisited by Paknys in 1991 [5]. The author arrives at the conclusion that the equal area rule gives the best accuracy for the E-field for this particular problem. However, the author also observes that the EAR does not always work and attempts to explain why a unique criterion has not yet been found.

In 1991, Trueman and Kubina [6] summarized a series of rules for wire-grid simu-

lation and produced a group of wire-grid modeling guidelines. They also considered a nonrectangular grid for which they derived a general expression allowing the calculation of the segment radius as a function of the two adjacent mesh surfaces to which it belongs.

The aim of the present chapter is to analyze the degree of accuracy achieved by the EAR for uniform rectangular and body-fitted wire-grids.

The EAR, as it is known today, is described in Section 5.2. Also in that section a particular form of the rule of thumb for squared meshes is presented as well as the generalized formula developed later for arbitrary meshes. In Section 5.3, we give a numerical example of the application of the EAR and we present a particular case for which the generalization fails to give satisfactory results.

5.2 The Equal Area Rule

As mentioned in the introduction, the simulation of a solid surface by means of a wire-grid approximation requires the proper selection of a certain number of parameters. The segment length is determined by the frequency at which the model needs to be evaluated. An appropriate selection of the segment length results in a more computer efficient model. The use of too large a number of segments may produce unacceptably costly models in terms of memory and computing power. On the other hand, the use of a small number of segments may have an impact on the accuracy of the solution. The wire radius, on the contrary, does not affect in any way the computing power or memory requirements, but, as we shall see, may have a significant effect on the quality of the solution.

The rule of thumb for the selection of the wire radius which has been applied for more than a decade was obtained by empirical observation while testing several different radii on a canonical problem. As the optimal radius was found, it was observed that a numerical relationship appears to exist between the value of this radius and the area of the solid surface being modeled [4, 5, 6, 7]. Consider a square patch of side Δ . The simplest wire-grid representation of this structure would be the one formed by four single wires on the four sides of the square as seen in Figure 5.1. According

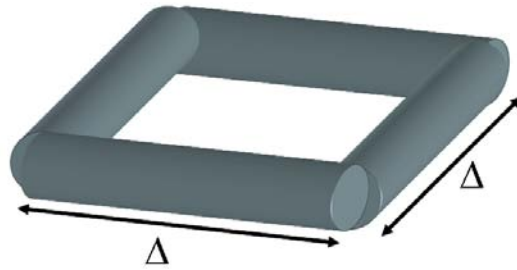


Figure 5.1: Four single wires representing a solid square patch. Adapted from [9]

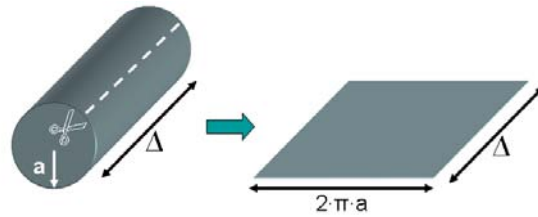


Figure 5.2: Surface area of a wire. Adapted from [9]

to the EAR, the optimum wire radius for one single segment is the one obtained by calculating the surface area of the wire (Figure 5.2) and setting this area equal to the solid surface being modeled, in this case, the one already shown in Figure 5.1. As a result, the circumference of the cross section of the cylindrical conductor must be made equal to the segment length Δ and, therefore, the radius given by the EAR may be obtained as:

$$a = \frac{\Delta}{2 \cdot \pi} \quad (5.1)$$

This version of the EAR appears to have worked well for many problems over the years (e.g. [4, 5, 10]). On the other hand, the Method of Moments, on which NEC is based, allows the use of body-fitted meshes that nicely reproduce the geometry of the object. Clearly, in many cases, a square-mesh representation of a 3D structure will result in a rather rough model, from which we would expect less precision and, therefore, larger errors. Additionally, obtaining a square-mesh representation of an existing object is not always a simple task. In fact, complex structures may be represented by the CAD files that were created and used during design and construction. These CAD files often use triangular or even arbitrarily shaped meshes that better represent the real contours and small details of the geometry.

For arbitrarily shaped meshes, a general expression for the calculation of the wire

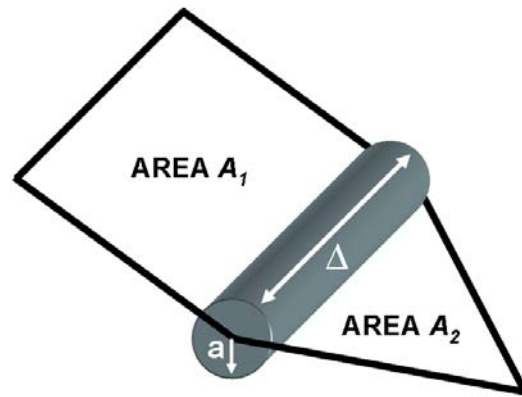


Figure 5.3: Equal Area Rule for an arbitrarily shaped mesh. Adapted from [9]

radius has been presented in [6]. The formula takes into account the surface area of the two shapes adjacent to the segment (A_1 and A_2) for which the radius is required (Figure 5.3). The result is also dependent on the segment length Δ :

$$a = \frac{A_1 + A_2}{4 \cdot \pi \cdot \Delta} \quad (5.2)$$

For the particular case where both adjacent surfaces are square of side Δ , the two areas become Δ^2 and we obtain the expression for the EAR of a rectangular mesh as already presented in (5.1).

5.3 A Numerical Example using Parallel NEC

A model represented by a perfectly squared and homogeneous mesh guaranties that other rules in the construction of a NEC model are well respected. Indeed, a NEC model should avoid adjacent segments featuring large variations of segment length and radius. Some variations are allowed as long as they are smooth [8]. Clearly a perfectly square model will exhibit no changes at all in segment length and radius.

When a model is constructed using an arbitrarily shaped mesh, respecting the existing guidelines which include not having abrupt changes of length and radius in adjacent segments becomes an almost impossible task to accomplish for realistic body-fitted models. Obviously, some models can be constructed with complex meshes that exhibit homogenous segment lengths, but this only applies to particular figures and in no way does it apply to extracted CAD data for practical applications. Another

problem derives from the difficulty in calculating the appropriate wire radii by applying the EAR general formula. This requires the determination of the surface area of the two shapes adjacent to the segment under consideration and, therefore, additional and sometimes complicated post processing of the mesh is necessary.

Let us examine in what follows a simple example of a closed metallic cube illuminated by a plane wave characterized by an E-field with an amplitude of 1 V/m and a frequency of 300 MHz ($\lambda = 1$ m). Two different polarizations were taken into account (1) vertical and (2) oblique polarization. The side of the cube is 40 cm long. The cube was meshed using a perfectly square and homogenous grid of 4 cm length (Figure 5.4). If the surfaces of the cubic Faraday cage are well represented by their wire grid homologues, illuminating the cube with a plane wave and then measuring the E field anywhere in the interior should give a result very close to zero. Several versions of the cube were created with different radii, including the one predicted by the EAR formula. We added diagonal segments cutting each square patch of the grid in half, creating a triangular mesh out of the same cube (Figure 5.5). At first, one would imagine that this should improve the accuracy of the wire-grid representation of the cube. All the radii were recalculated so that they would comply with the EAR general formula (Equation 5.2). Since all of the triangles of the resulting mesh are isosceles (i.e. two equal sides) and identical, the resulting model exhibited two different radii. Again, several versions of this cube were created by systematically changing the values of these two radii keeping the proportionality factor between them ¹. The E field calculated at the center of the square-mesh cube as a function of the wire radius is presented in Figure 5.6 for vertical and oblique polarizations of the incident field. Since the triangular model is characterized by two different radii (corresponding to the vertical/horizontal wires and to the diagonal ones, respectively), we presented its corresponding results in Figure 5.6 as a function of the radius of the vertical/horizontal segments only. The values for the radii predicted by the EAR formula (for both rectangular and triangular meshes) are also shown in that figure. As it can be seen, the prediction of the EAR for the rectangular case corresponds with the minimum of the total field evaluated at the center of the square meshed cube. This minimum was, as expected, very close to zero.

¹We found basically no fundamental differences using other frequencies up to 1 GHz

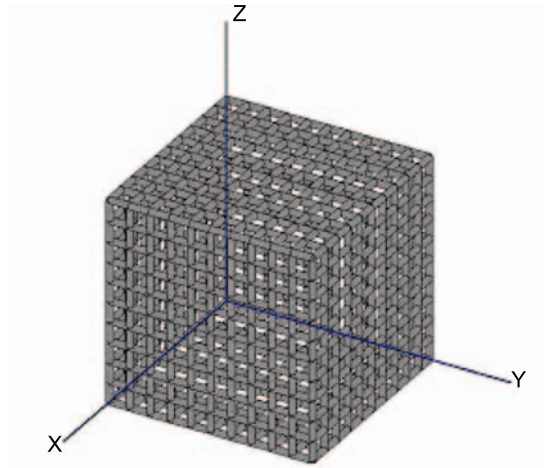


Figure 5.4: Cube with rectangular Mesh. Adapted from [9]

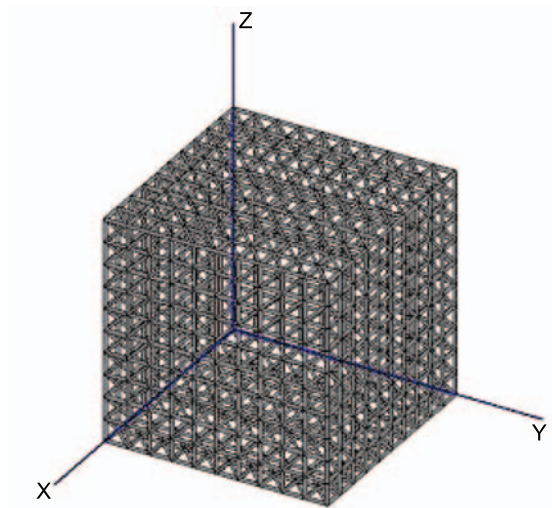


Figure 5.5: Cube with triangular Mesh. Adapted from [9]

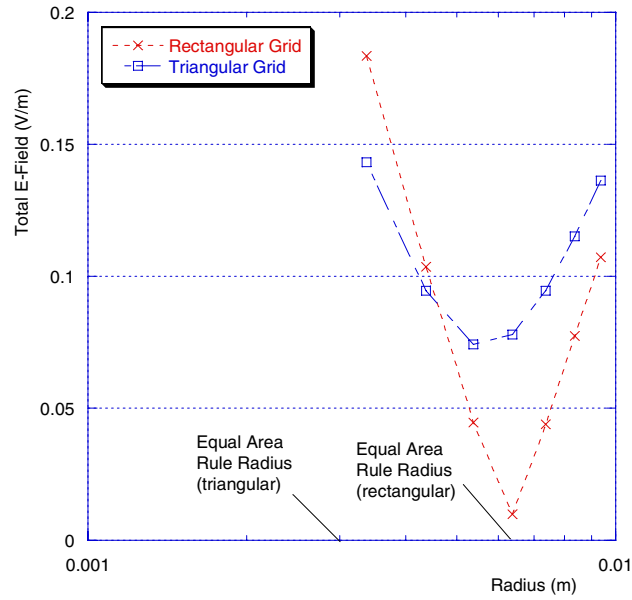
Surprisingly, the application of the radius predicted by the EAR for a square mesh to the vertical and horizontal segments in the triangular case appears to give nearly optimum results. Moreover, the radius predicted by the EAR for the triangular mesh is far from the optimum radius. Contrary to our expectations, the triangular model was far less effective than the simple square model (see Figure 5.6(a)). Using an oblique polarization for the incident field (Figure 5.6(b)), we obtain a similar behavior in that the radius predicted by the general formula of the EAR for the triangular mesh is different from the optimum value.

A possible interpretation of this rather unanticipated result could be the following. The idea behind the EAR is that we suppose that a metallic surface could be accurately represented by an equivalent wire grid model with proper values for segment lengths and radii. In other words, we substitute the original geometry (a closed metallic surface) by an equivalent one (a wire grid model). In this case, adding new elements to the grid making the holes smaller does not improve the performance of the whole surface because the size of the holes is not the only parameter involved. For this particular example, there might exist an optimum combination of parameters (segment lengths, radii) that would render the triangular version even better than the rectangular one, at the same given frequency. However, this combination of parameters includes segment radius as probably the most important value, and the existing EAR formula appears not able to properly predict it².

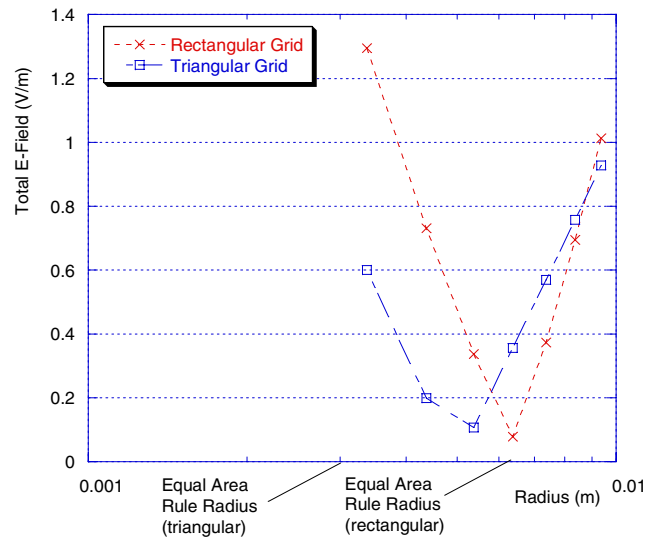
5.4 Conclusions

In this chapter, we discussed the wire-grid representation of metallic surfaces in numerical electromagnetic modeling. Considering a simple geometry namely cube, we showed that the Equal Area Rule is accurate as long as the wire-grid consists of a simple square mesh. For more complex body-fitted meshes, such as triangular ones, the Equal Area Rule appears to be less accurate in reproducing the electromagnetic field scattered by metallic bodies. Chapter 6 describes a new method to derive more accurate criteria to specify the parameters of the wire-grid model for complex geometries.

²As a further example, the reader may consider the two models of an automobile presented in Subsection 4.2.3.



(a) Incident plane wave has vertical polarization.



(b) Incident plane wave has oblique polarization.

Figure 5.6: Simulated E-field as a function of the wire radius for a rectangular (squared) and a triangular meshes. Adapted from [9]

Bibliography

- [1] J. H. Richmond. A Wire-Grid Model for Scattering by Conducting Bodies. In *IEEE Transactions on Antennas and Propagation*, volume AP-14, pages 782–786, Nov 1966.
- [2] K. S. H. Lee, L. Marin, and P. Castillo. Limitations of Wire-Grid Modeling of a Closed Surface. In *IEEE Transactions on Electromagnetic Compatibility*, volume EMC-18, pages 123–129, Aug 1976.
- [3] Joseph T. Mayhan. Characteristic Modes and Wire Grid Modeling. In *IEEE Transactions on Antennas and Propagation*, volume 38, Apr 1990.
- [4] A. C. Ludwig. Wire Grid Modeling of Surfaces. In *IEEE Transactions on Antennas and Propagation*, volume AP-35, pages 1045–1048, Sep 1987.
- [5] R. J. Paknys. The Near Field of a Wire Grid Model. In *IEEE Transactions on Antennas and Propagation*, volume 39, pages 994–999, Jul 1991.
- [6] C. W. Trueman and S. J. Kubina. Fields of Complex Surfaces using Wire Grid Modeling. In *IEEE Transactions on Magnetics*, volume 27, pages 4262–4267, Sep 1991.
- [7] Edmund K. Miller. PCs and AP and Other EM Reflections. In *IEEE Transactions on Antennas and Propagation Magazine*, volume 39, 1997.
- [8] G. Burke and A. Poggio. Numerical electromagnetics code - method of moments. In *Report No. UCID-18834*, 1981. Livermore CA: Lawrence Livermore National Laboratory.

- [9] A. Rubinstein, F. Rachidi, and M. Rubinstein. On Wire-grid Representation of Solid Metallic Surfaces. In *IEEE Transactions on Electromagnetic Compatibility*. In press.
- [10] R. K. Najm B. A. Austin. Wire-grid Modeling of Vehicles with flush-mounted Antennas. In *Seventh International Conference on Antennas and Propagation*, volume 2, 1991. Livermore CA: Lawrence Livermore National Laboratory.

Chapter 6

Improved Surface Modelling. The New Equal Area Rule (NEAR)

6.1 Introduction

Modelling of a surface using the Method of Moments (MoM) and, in particular, using the Numerical Electromagnetics Code (NEC), can be achieved by two different approaches. Though the NEC manual [1] states in the Structure Modelling Guidelines that straight segments are used for modelling wires and flat patches for modelling surfaces, it also mentions the use of wire-grid modelling with “varying success”.

Since computer power by the time NEC was developed did not allow the computation of large problems, the application of the code was devoted mainly to antenna simulations. Attempts to model very complex structures using a wire-grid approach exceed available memory and calculating power.

The geometrical considerations for the construction of a successful model are clearly stated in the manual for the modelling of simple wire structures such as antennas. Some of these considerations, however, do not apply to the use of wires for the simulation of surfaces and, consequently, a new set of guidelines was introduced in 1991, by Trueman and Kubina [2], based on the so-called Equal Area Rule (EAR) (see, for example, [3]). The original formulation of the EAR comes from empirical observation and, as of today, no physical interpretation has ever been given to the rule.

The contents of this chapter is based on very preliminary work regarding a physical

interpretation of the EAR. In the first part of the chapter, a derivation is presented that leads to the rectangular form of the EAR proposed by Miller [3]. This derivation represents, to the best of our knowledge, the first attempt at a physical interpretation of the Equal Area Rule. The same methodology, when applied to a non-rectangular mesh yields a new expression that differs from the results given by the generalization of the EAR formula proposed in [2]. The chapter ends with simulation results that are used to compare the EAR with the newly proposed expression.

6.2 Theoretical basis for the classical Equal Area Rule (EAR) and proposed New Equal Area Rule (NEAR)

As already mentioned in the introduction, the derivation presented here represents a first attempt at providing a physical interpretation for the empirical EAR. Although crude approximations are made throughout the derivation, the results are encouraging and they are presented here as a basis for future work.

When an incident field E_i impinges on a perfectly conducting surface, currents are induced on it. These induced currents produce, in turn, a scattered electric field that cancels out the tangential electric field on the conductor's surface. This is so, since the total (incident plus scattered) tangential field on the surface of a perfect conductor must always equal zero. The situation is illustrated in Figure 6.1 for a metallic slab.

We will now assume that the slab is made of a material with a finite but high conductivity. In that case, most of the induced current flows close to the surface of the conductor due to the skin effect. The current can be written as

$$I_s = \sigma_A E_s w = \sigma_A E_i w \quad (6.1)$$

where w is the width of the slab, σ_A is the surface conductivity of the slab, and E_s and E_i are the magnitudes of the scattered and the incident field, respectively. The surface conductivity can be defined as

$$\sigma_A = \sigma \delta \quad (6.2)$$

where σ is the conductivity of the material and δ is the skin depth of the conductor.

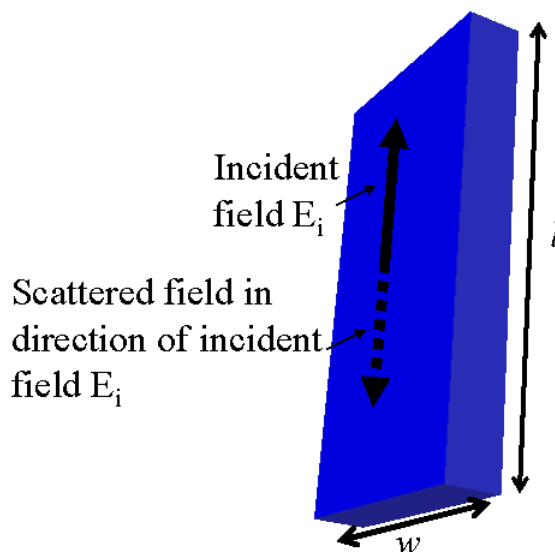


Figure 6.1: Scattered field generated by a perfect conductor in response to an incident electric field

Radiation due to the scattered current is proportional to the product of the current times the length l of the slab as long as the length and the width are much smaller than the wavelength. We will call that quantity the slab's total dipole moment p_{Slab_tot} . It can be calculated by way of

$$p_{Slab_tot} = \sigma_A E_s w l \quad (6.3)$$

Note that the magnitude of p_{Slab_tot} equals the product of the surface conductivity times the incident electric field (which is identical to the scattered field) times the surface area of the slab, wl . Equation 6.3 will actually be applied to surfaces that are of the order of or even greater than the wavelength. We will nevertheless press ahead with the derivation.

Let us now repeat the exercise of finding the total moment for a surface represented by a rectangular mesh of cylindrical wire segments as shown in Figure 6.2

We will first concentrate on one of the segments of length Δ_1 that compose the wire grid. The geometry is illustrated in Figure 6.3, to which the following derivation refers.

Let us call the incident electric field E_i as in the case of the slab. In this case, we will assume that the incident field and the cylindrical conductor's axis are not necessarily parallel. Let us call the angle between the conductor and the incident electric field θ .

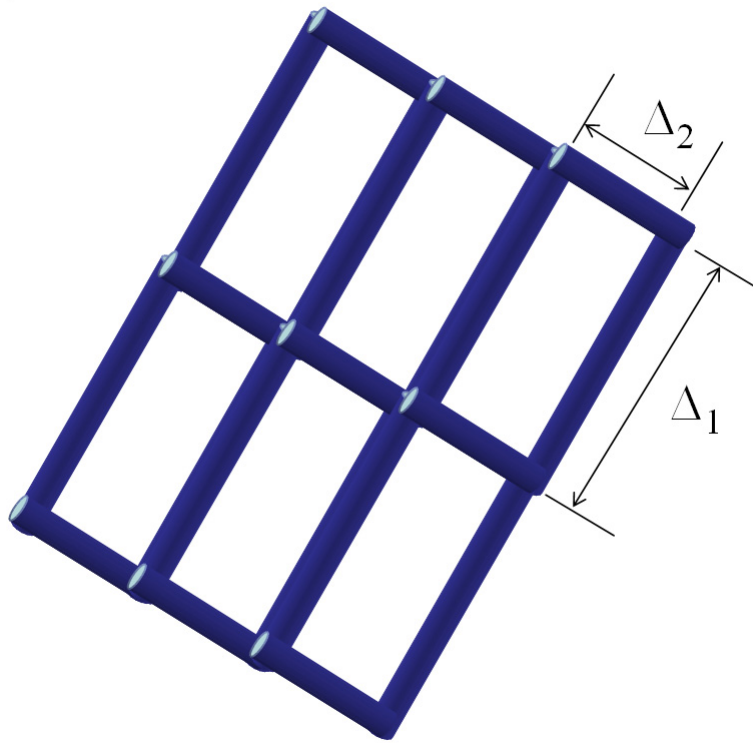


Figure 6.2: A wire grid representation of the slab using rectangles

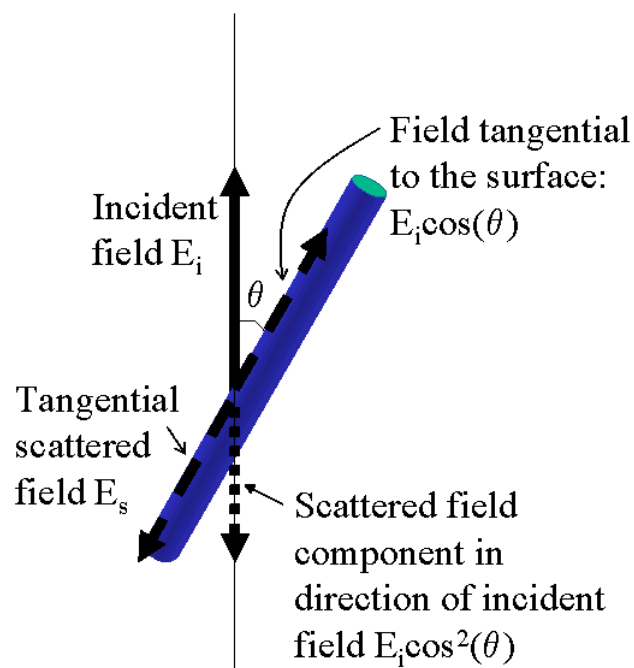


Figure 6.3: Geometry of the problem for one of the segments

The component of the incident electric field tangential to the surface of the conductor is given by

$$E_t = E_i \cos(\theta) \quad (6.4)$$

The scattered electric field has the same magnitude but opposite direction. Its magnitude is therefore

$$E_s = E_i \cos(\theta) \quad (6.5)$$

Assuming that the scattered field is uniform around the circumference of the conductor, and using the fact that the induced current flows near the surface of the conductor, we can calculate the total scattered current as follows

$$I_s = 2\pi a \sigma_A E_i \cos(\theta) \quad (6.6)$$

where a is the radius of the conductor and σ_A is the surface conductivity of the wire, whose definition was already given above, and which is assumed to be equal to that of the slab.

The dipole moment of the wire segment is given by the product of the scattered current and the length of the segment,

$$p_{Segment} = 2\pi a \sigma_A \Delta_1 E_i \cos(\theta) \quad (6.7)$$

The component of the dipole moment in the direction of the incident field is

$$p_{Segment} \cos(\theta) = 2\pi a \sigma_A \Delta_1 E_i \cos^2(\theta) \quad (6.8)$$

We can easily obtain the dipole moment in the direction of the incident field for the segments of length Δ_2 (see Figure 6.2) as follows:

$$p_{Segment} \sin(\theta) = 2\pi a \sigma_A \Delta_2 E_i \sin^2(\theta) \quad (6.9)$$

where we have used the fact that the angle between the present segment's axis and the incident electric field is $\pi/2 - \theta$.

The total moment in the direction of the incident field for a grid that has a width of $w = m\Delta_2$ and a height of $l = n\Delta_1$ is, therefore,

$$p_{Grid_tot} = 2m(n+1)\pi a \sigma_A \Delta_2 E_i \cos^2(\theta) + 2n(m+1)\pi a \sigma_A \Delta_1 E_i \sin^2(\theta) \quad (6.10)$$

We will now assume that, to approximate the scattering behavior of the slab by way of the wire-grid model, the total moments must be equal. Equating equations 6.3 and 6.10 and cancelling out terms that appear on both sides of the equation, we obtain

$$mn\Delta_1\Delta_2 = 2m(n+1)\pi a\Delta_1 \cos^2(\theta) + 2n(m+1)\pi a\Delta_2 \sin^2(\theta) \quad (6.11)$$

Let us assume that the grid is square, $\Delta_1 = \Delta_2 = \Delta$, and that $m = n$. Under those conditions, we can rewrite Equation 6.11 as

$$m^2\Delta^2 = 2m(m+1)\pi a\Delta(\cos^2(\theta) + \sin^2(\theta)) \quad (6.12)$$

which, after solving for the radius a , can be written as

$$a = \frac{m\Delta}{(m+1)2\pi} \quad (6.13)$$

If $m \gg 1$ so that $m+1 \cong m$, a reduces to the well known equal area rule formula

$$a = \frac{\Delta}{2\pi} \quad (6.14)$$

6.3 Application to other patterns

The derivation presented in the previous section can be applied to wire-grids made of polygons other than squares. In this section, we illustrate the derivation of the NEAR (new equal area rule) for a triangular grid in response to a vertically polarized incident electric field.

Consider the surface shown in Figure 6.4. As in the case of the slab of the previous section, the total moment is the product of the surface conductivity times the incident electric field times the surface area.

To calculate the surface area, we divide the surface into triangles as shown in Figure 6.5.

The total surface area is given by the product of the number of triangles times the area of each individual triangle. The number of triangles is readily seen to be $2mn$. The area of a triangle, on the other hand, is given by

$$s = \frac{\Delta^2 \tan(\alpha)}{4} \quad (6.15)$$

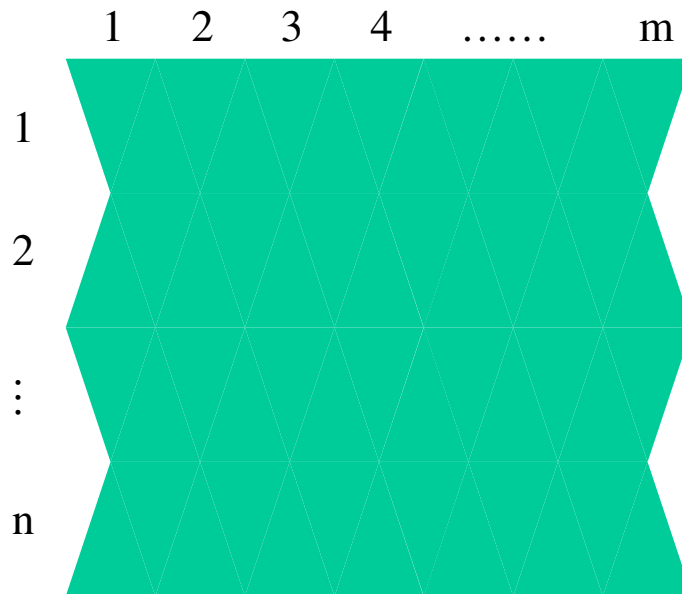


Figure 6.4: Surface chosen for the derivation of the NEAR formula for a triangular mesh

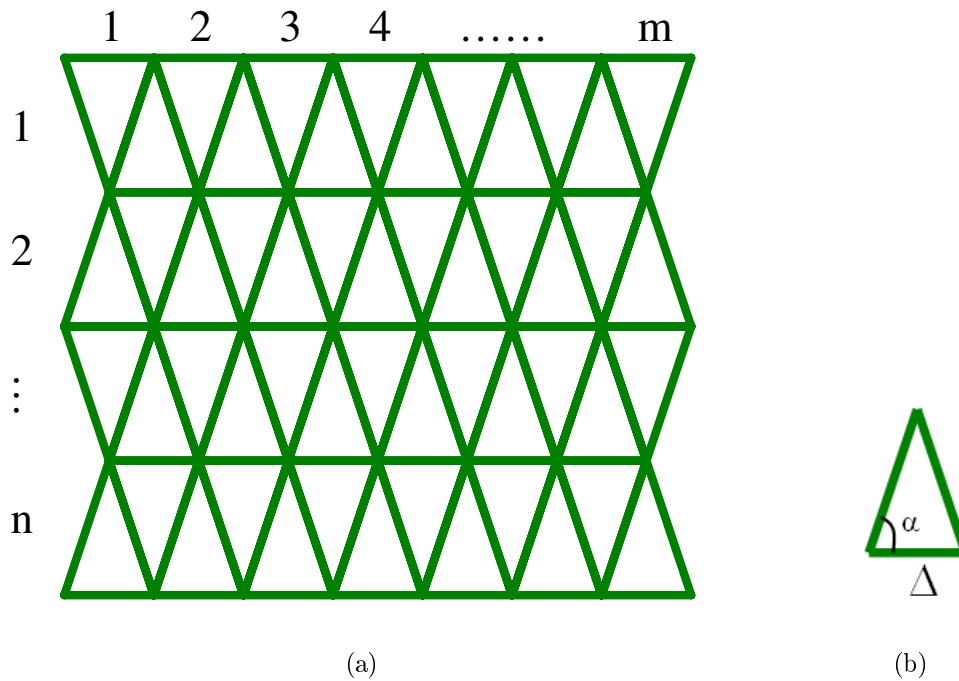


Figure 6.5: (a) The triangular mesh corresponding to the surface under consideration and (b) the geometry of one triangle

and the total moment of the surface is

$$p_{surface_total} = 2mn\sigma_A E_i \frac{\Delta^2 \tan(\alpha)}{4} \quad (6.16)$$

Let us now calculate the total moment for the wire-grid version of the surface. The wire-grid consists of horizontal and non-horizontal segments. The moment from the horizontal segments is zero as can be seen from Equation 6.7, where, in this case, $\theta = \pi/2$.

For the non-horizontal segments, on the other hand, the length of the segments is $\frac{\Delta}{2 \cos(\alpha)}$ and the angle between the incident electric field and the axis of the segments is $\theta = \pi/2 - \alpha$. The moment in the direction of the incident field is therefore given by

$$p_{Segment} = 2\pi a \sigma_A \frac{\Delta}{2 \cos(\alpha)} E_i \sin^2(\alpha) = \pi a \Delta \sigma_A E_i \tan(\alpha) \sin \alpha \quad (6.17)$$

The total moment for the wire-grid is obtained by multiplying the moment given in Equation 6.17 by the total number of non-horizontal segments which, from Figure 6.5, can be seen to be $2nm$. The result is

$$p_{Grid_total} = 2mn\pi a \Delta \sigma_A E_i \tan(\alpha) \sin \alpha \quad (6.18)$$

Equating now the moments for the surface and for its wire-grid representation, we obtain

$$2mn\pi a \Delta \sigma_A E_i \tan(\alpha) \sin \alpha = 2mn E_i \sigma_A \frac{\Delta^2 \tan(\alpha)}{4} \quad (6.19)$$

from which the radius a can be found to be

$$a = \frac{\Delta}{4\pi \sin(\alpha)} \quad (6.20)$$

For equilateral triangles, $\alpha = \pi/3$ and

$$a = \frac{\Delta}{2\pi} \quad (6.21)$$

Interestingly, the radius is the same as that obtained for the square grid and, as we will see in the next section, it is different from that predicted by the classical EAR.

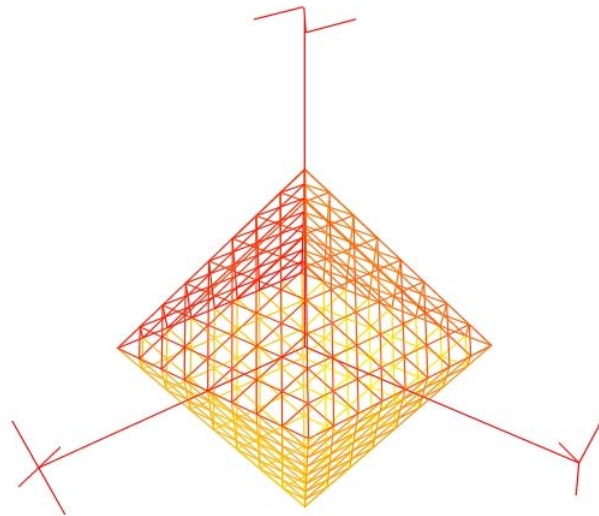


Figure 6.6: Model of an octahedron meshed with a triangular grid

6.4 Comparison Between the Classical and the New EARs

The objective in this section is to test the merits of the new equal area rule (NEAR) relative to the classical rule. A closed surface was chosen for the simulations since the field inside is known to be zero. Consider the octahedron model shown in Figure 6.6. The field point to be used for the comparison was chosen inside the octahedron. The sides of the polyhedron were modeled using equilateral triangles formed by individual segments of 1 *cm* length each. The range of frequencies used for the analysis is such that the segments satisfy the NEC's length requirements. The following straightforward test was performed: The field inside the octahedron was calculated both, using the radius predicted by the classical equal area rule, and using that predicted by the new rule described in the previous section, and the results were compared.

6.4.1 The Radius Predicted by the Classical Equal Area Rule (EAR)

As already mentioned in Chapter 5, Equation 6.22 has been proposed by Trueman and Kurbina [2] as the general formula for the calculation of the wire radius for an

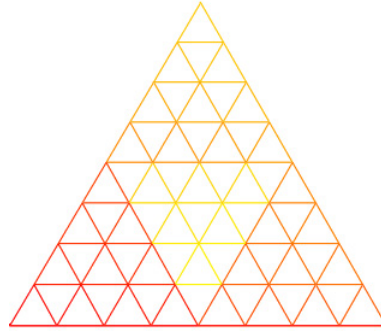


Figure 6.7: Triangular mesh of a face of the Octahedron

arbitrarily shaped mesh. For convenience, the formula is repeated here

$$a = \frac{A_1 + A_2}{4 \cdot \pi \cdot \Delta} \quad (6.22)$$

where A_1 and A_2 are the surface areas of the two shapes adjacent to the segment for which the radius is required (Figure 5.3), and Δ is the segment length.

Since the triangles are equilateral of side Δ , their surface areas, A_1 and A_2 , can be obtained as follows

$$A_1 = A_2 = \frac{1}{4} \sqrt{3} \Delta^2 \quad (6.23)$$

Substituting Equation 6.23 into Equation 6.22 and using the fact that $\Delta = 0.01$ m, we obtain the segment radius a predicted by the EAR

$$a = 7.9577 \cdot 10^{-4} \text{ m} \quad (6.24)$$

6.4.2 The Radius Predicted by the New Equal Area Rule (NEAR)

To find the radius of the segments, we followed the procedure presented in Section 6.3. Refer to the triangle in Figure 6.7, which represents one of the eight faces of the octahedron. We first found the total moment for a solid triangular surface by multiplying the incident electric field E_i times the surface conductivity σ_A times the surface area of the triangle:

$$P_{TotalTriangle} = E_i \sigma_A \frac{l^2 \sin(60)}{2} \quad (6.25)$$

where l is the length of one side of the triangle. We will now find the total moment from the segments. Each segment has a length of $\Delta = l/8$. The contribution of the

horizontal segments is zero since the field is vertically polarized (see Equation 6.7). The moment in the direction of the incident field for each one of the other segments, of which there are 72, is

$$p_{Segment} = E_i \cos(30)^2 \sigma_A 2\pi a \frac{l}{8} \quad (6.26)$$

The total moment for the 72 segments is

$$p_{72 \text{ Segments}} = 72 E_i \cos(30)^2 \sigma_A 2\pi a \frac{l}{8} \quad (6.27)$$

Equating the total moments from the solid surface and from the grid, we get

$$E_i \sigma_A \frac{l^2 \sin(60)}{2} = 72 E_i \cos(30)^2 \sigma_A 2\pi a \frac{l}{8} \quad (6.28)$$

Solving for the radius a , we get

$$a = \frac{l}{18\pi\sqrt{3}} \quad (6.29)$$

Since the side of a face of the octahedron is composed of 8 segments, $l = 0.08 \text{ m}$ and the radius predicted by the NEAR is

$$a = 8.1678 \cdot 10^{-4} \text{ m} \quad (6.30)$$

We ran NEC using the model from Figure 6.6 and the values of the radii obtained from Equations 6.22 and 6.29. The calculated total E field at the center of the Octahedron is displayed in Figure 6.8.

As we can see from Figure 6.8, the fields obtained using the New Equal Area Rule radius are closer to zero than those obtained using the classical EAR. This shows that the EAR does not provide the best possible radius for the simulation of surfaces using wire-grids. Of course, this does not prove that the NEAR radio is optimum either but it does suggest that it is better.

6.5 Conclusions

We have presented a theoretical development that leads, for the case of a square grid representation of a surface, to the same formula proposed by the equal area rule. This

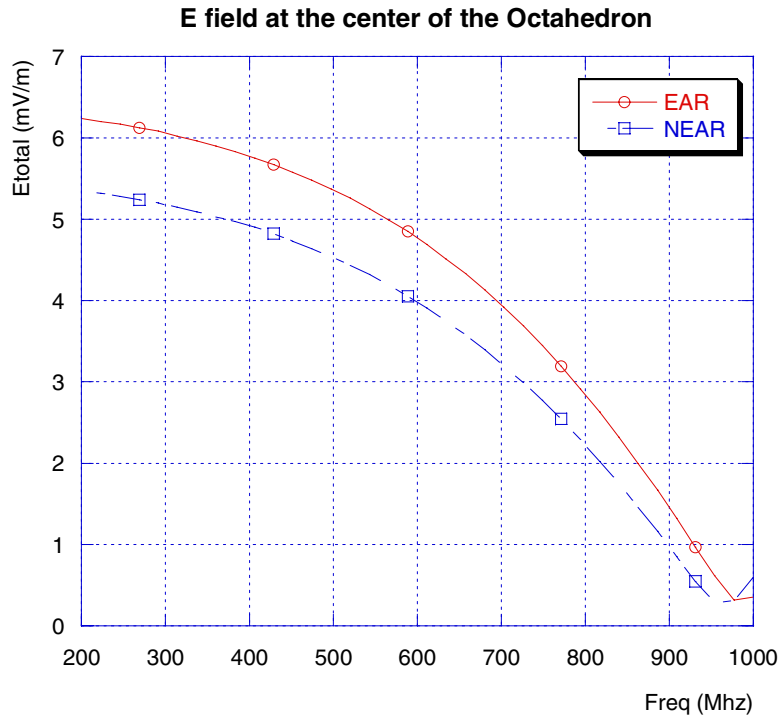


Figure 6.8: Comparison of the total E field calculated using the Classical (EAR) and the New (NEAR) formulas

development is, to the best of our knowledge, the first mathematical derivation and physical interpretation of the EAR as of today.

Our development shows, however, a different value for the radius of the segments if the representation of the surface uses a triangular mesh. To compare the two methods (the traditional versus the new EAR), we carried out a simple numerical test using an octahedron. Although the NEAR yields better results for the case studied in this chapter, further work is needed before any definitive conclusion can be drawn.

The original EAR for square grids does not depend on the polarization of the source. This makes this formula relatively easy to apply as it only depends on segment lengths. On the other hand, geometries coming from CAD data are difficult to adapt and very sophisticated software must be used to modify the mesh. The square representation also fails in reproducing the very fine details of the geometry, which has a negative impact on near field results.

The developed NEAR is more difficult to apply than the classical formula as it depends on the angle of polarization. This means that a change in the position or

even the polarization of the source may require a new calculation of the parameters. A body-fitted geometry from CAD data could be used but it requires pre-conditioning. Furthermore, since the radius must be individually calculated for segment groups as a function of several parameters, including the angle of polarization, the results may lead to conflicts with NEC's general geometry construction guidelines. Further work is in progress.

Bibliography

- [1] G. Burke and A. Poggio. Numerical electromagnetics code - method of moments. In *Report No. UCID-18834*, 1981. Livermore CA: Lawrence Livermore National Laboratory.
- [2] C. W. Trueman and S. J. Kubina. Fields of Complex Surfaces using Wire Grid Modeling. In *IEEE Transactions on Magnetics*, volume 27, pages 4262–4267, Sep 1991.
- [3] Edmund K. Miller. PCs and AP and Other EM Reflections. In *IEEE Transactions on Antennas and Propagation Magazine*, volume 39, 1997.

Chapter 7

Conclusions and Perspectives

There exist a number of methods to numerically simulate electromagnetic phenomena. Different methods require different computer resources, but all of them exhibit exceedingly long running times when it comes to modeling electrically large, complex structures such as automotive vehicles. Some of the methods require large amounts of memory as well.

Different strategies have been proposed to improve the performance of these methods and to make them applicable to large, complex problems. One of these strategies involves the application of different tools to different parts of the large problem, and the linking of the thus obtained partial solutions (which are usually stored in large external files) into a single, global solution.

For the linking of the partial solutions, two strategies have been proposed. The first one uses scattering matrices that are used to network the partial solutions together, and the second one uses the incident fields and the coupling model.

A second strategy is called hybridization. It merges different numerical techniques inside a single code. This strategy has the advantage over the multiple domain approach of not needing the large external files. It exhibits, on the other hand, the disadvantage of requiring full runs even if only minor changes are made to the geometry.

A third strategy, applicable to frequency domain codes, is to optimize the selection of the frequencies at which the simulation is run. This could be done, for example, with the help of the Blumer method.

A fourth strategy, called parallelization, is to divide the work and the required

memory among a number of processors.

All of these strategies can be combined to improve the overall performance of the simulation.

Although NEC, based on the Method of Moments, has been used for decades to successfully model antennas and other relatively small structures, it remained inapplicable to electrically large problems, mainly due to its memory requirements, but also to the required runtime. We have produced a parallel version of NEC that overcomes these limitations.

Optimal performance requires a very specific distribution of the matrix elements known as the bi-dimensional block-cyclic distribution.

Assuming the array of processors as a two-dimensional grid, it has been shown that a rectangular distribution assures a theoretically-optimum load balance among the processors.

Too high a number of processors can actually lower the overall performance of the computer cluster in terms of running time, but it still improves the memory performance, since the memory requirement is divided by the total number of processors.

A substantial reduction of the running time for large problems comes from the fact that the sharing of the memory requirements eliminates the need for disk swapping. This point should not be underestimated as we have observed, in one example at least, that it can account for over 90% of the running time. This percentage is actually impossible to predict since it is a function of a number of factors that are random in nature, such as, fragmentation of the disk, efficiency and memory usage of the operating system, disk access times, etc.

Most of the running time is consumed by two tasks in the NEC code: the construction of the interaction matrix and its factorization. It is for that reason that those two tasks have been parallelized.

Although the largest model that has been successfully run using Parallel NEC at the time of the writing of this thesis consists of over 30000 segments, the actual limit is only imposed by the combined memory of all the processors in the cluster. This is an important conclusion since it implies that any size model can be run if enough processors are used.

Parallel NEC produces accurate simulation results as evidenced by numerical and experimental validations carried out in this thesis. The experimental validation was carried out using measurements of electric and magnetic fields inside a real vehicle (a Volvo S80). These measurements were carried out at 8 different points inside the car although only four were used for the actual validation. Three different sources were used to illuminate the car: (1) a Log Periodic antenna, (2) a Biconilog antenna and (3) the *VERIFY* EMP simulator belonging to the Swiss Defence Procurement Agency, located at Spiez. The data used for the validation were collected with the EMP Simulator. The uniformity of the field was verified by establishing a map of the E-field produced by the simulator by measuring the vertical electric field at a height of 1 m above the ground and at square intervals of 1 m.

The Equal Area Rule can be used to represent solid surfaces only as long as the wire-grid consists of a square mesh. For more complex body-fitted meshes, such as triangular grids, the Equal Area Rule appears to be less accurate in reproducing the electromagnetic field scattered by metallic surfaces. An important observation is that the general Equal Area Rule does not necessarily provide the optimum radius for meshed other than square.

We have presented a theoretical development that leads to the same formula proposed by the Equal Area Rule (EAR), for the case of a square grid representation of a surface. To the best of our knowledge, this is the first physical interpretation of the EAR as of today.

The physical interpretation of the EAR produces different results if the mesh is not square.

According to our derivation of the New Equal Area Rule (NEAR), the radii of the wires are, in general, a function of the polarization of the incident electric field. The dependence drops for the case of a square mesh.

It is possible to obtain a better representation of a surface using a radius that is different from that predicted by the EAR, at least for the case of a non square grid.

Perspectives

A number of areas are of interest for future research work.

One of these areas is the utilization of patches. Although the use of patches is subject to limiting constraints, such as the condition that the model forms a totally closed surface, its parallelization would allow the running of even more complex simulations, provided the modeled structure (or at least part of it) satisfies the constraints.

Another area where further work is of interest is the inclusion of the Blumer Method into Parallel NEC. The calculation of the Blumer index in real time would allow the end user to know at any time the precision of the spectrum already calculated. The next frequency steps for the ongoing calculation could be dynamically selected by the code in order to increase the accuracy of the spectrum so that the user would only need to specify the start and end points of the frequency interval and the desired Blumer Index to be obtained. This could be done by evaluating the derivative of the spectrum and then requiring that the number of new points to be added to the spectrum be proportional to that derivative.

A third area where further research is needed is the representation of surfaces using wire-grids. The derivation presented in this thesis could be improved and tested by closely examining the approximations made. A better physical understanding and mathematical formulation of the wire-grid surface representation parameters would allow the utilization of better fitted meshes from CAD data.

Appendix - Use of the Blumer Index

This section draws heavily from [1].

The Blumer index is useful for adapting the sampling density of a calculated or measured spectrum to reduce the errors.

We start with a set of frequencies for representing the spectrum which can be equally-spaced over the selected bandwidth ω_{min} to ω_{max} for convenience. For each of these frequencies, the response of the spectrum (calculated or measured) is saved. As seen in Figure 1, once the initial spectrum has been determined, Equation 2.16 is used to calculate the Blumer index B . This resulting value of B is compared with a user specified threshold value, which will be used as the routine exit condition. Once this condition is attained, the calculation process finishes and the existing spectrum is then used for the desired purpose (i.e., for further analysis). On the contrary, if the value of B is less than the threshold value, the existing list of frequencies is augmented in a specified way, increasing the number of frequency points in the spectrum. The new data points are located so that they fall in a region where they will be most effective in describing the spectrum. The value of B is again computed and compared and the whole process is repeated until the value of B is sufficiently high, or until too many iterations have occurred.

Modification of the Spectral Frequency Points

Selected frequency points are included in order to increase the accuracy of the spectrum.

One method to suggest where additional points should be located is to use the derivative of the spectrum [1]. As an example, consider the sample spectrum of a

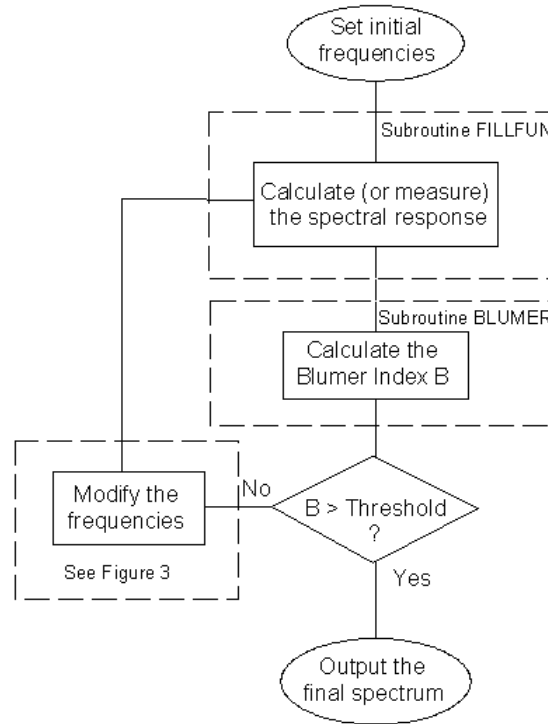


Figure 1: Flow diagram for the use of the Blumer Index. Adapted from [1]

time-shifted, damped sine wave given by

$$F(\omega) = \frac{\omega_0}{\omega_0^2 + (j\omega + \alpha)^2} e^{-j\omega t_0}, \quad (1)$$

which is shown in Figure 2(a) for the particular case of $\alpha = 0.1$ Hz, $\omega_0 = 1.0$ Hz, and $t_0 = 20$ s. It can be seen that frequencies around the resonance at $\omega = 1.0$ Hz contribute the most to the integrals in Equation 2.16, and it is in this region where a higher density of point should be used so that the function is evaluated accurately.

One way of doing this is locating new frequency points in the vicinity of the peak by evaluating the derivative of the spectrum and then requiring that the number of new points to be added be proportional to the derivative. Figure 2(b) shows the magnitude of the derivative of the sample function which, as it can be seen, provides useful information about the possible location of new points.

Considering the discrete spectrum function $F(\omega_i)$ for $i = 1$ to N_p , within the $(i - 1)^{th}$ and i^{th} frequency points, the local derivative can be approximated as

$$\frac{dF}{d\omega_i} \approx \frac{F(\omega_i) - F(\omega_{i-1})}{\omega_i - \omega_{i-1}}. \quad (2)$$

Assuming that for the entire spectrum, the maximum and minimum derivative

magnitudes are given as

$$\left| \frac{dF}{d\omega} \right|_{max} \quad \text{and} \quad \left| \frac{dF}{d\omega} \right|_{min} \quad (3)$$

the number of additional frequency points between ω_{i-1} and ω_i can be calculated as

$$N_{new} = 1 + \mathbf{int} \left[3 \times \frac{|dF/d\omega|_i - |dF/d\omega|_{min}}{|dF/d\omega|_{max} - |dF/d\omega|_{min}} \right], \quad (4)$$

where $\mathbf{int}()$ denotes the integer function. In this way, in regions where the spectrum is not varying much, $|dF/d\omega|_i \approx |dF/d\omega|_{min}$, and the number of new points N_{new} between ω_{i-1} and ω_i is 1. Near the peak, where $|dF/d\omega|_i \approx |dF/d\omega|_{max}$, $N_{new} = 4$. This way, points are added in the vicinity of the peak.

The numerical value 3 in Equation 4 is kind of a tuning parameter that affects the number of new points added to the spectrum in each iteration. Only one new data point is added between each of the old points, uniformly across the frequency band when the value is set to zero. Using a higher number puts successively more points near the peaks in each iteration. The determination of the optimum value of this parameter can be done empirically.

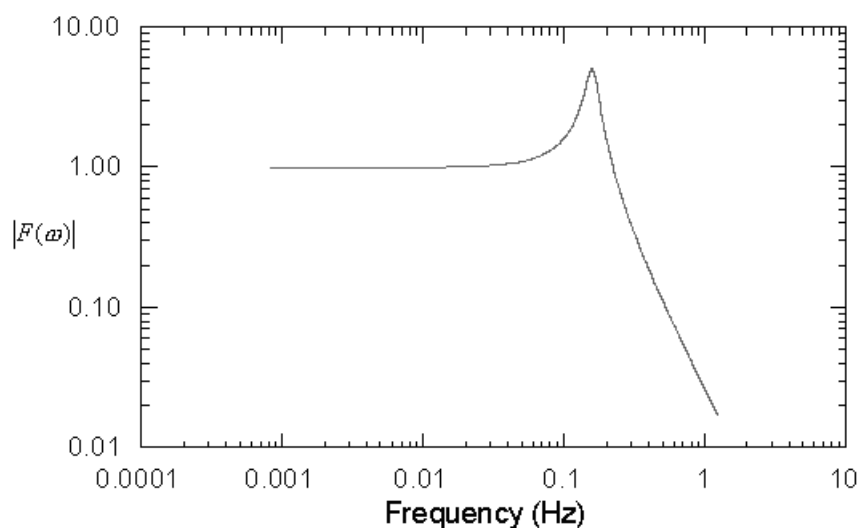
Figure 3 illustrates the steps for determining the new frequency points and constitute the calculations performed in the box labeled ‘‘Modify the frequencies’’ in Figure 1 [1]. The old spectral points are saved so that they can be reused when the spectrum is recalculated.

As an example, a series of calculations was employed using the analytically represented spectrum in Equation 1 with 3 initial frequency points. The calculation of B and the choice of new points was performed following the steps depicted in Figure 1. A total of 8 iterations were carried out.

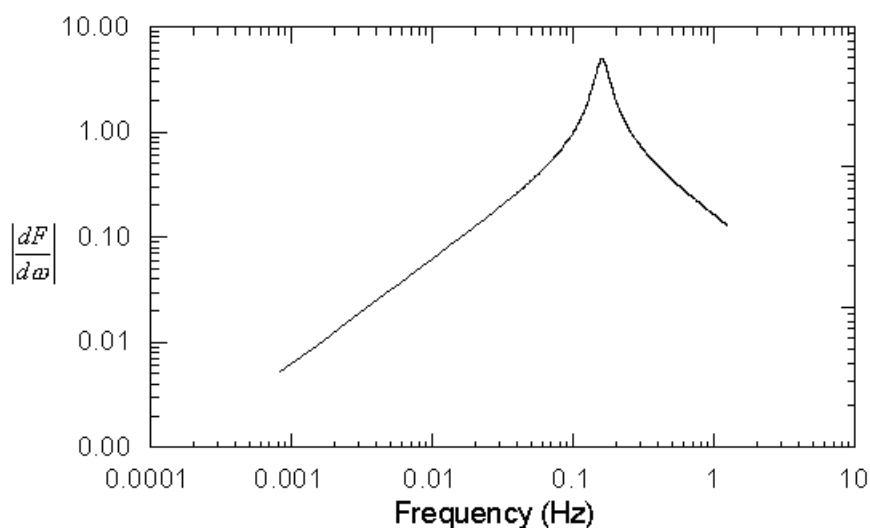
Figure 4 plots the spectral magnitudes for the numerically sampled spectrum for each iteration, illustrating the convergence of the spectra to the correct value. Table 1 illustrates the resulting Blumer index B and the corresponding number of sample points for each iteration of the spectrum.

Application to the GEMCAR model

The Blumer method was successfully applied to a model of the car used within the GEMCAR project. We used the Blumer index to establish the accuracy of a simulation



(a)



(b)

Figure 2: Plots of (a) the spectral magnitude of the damped sine waveform, and (b) the magnitude derivative of the spectrum. Adapted from [1]

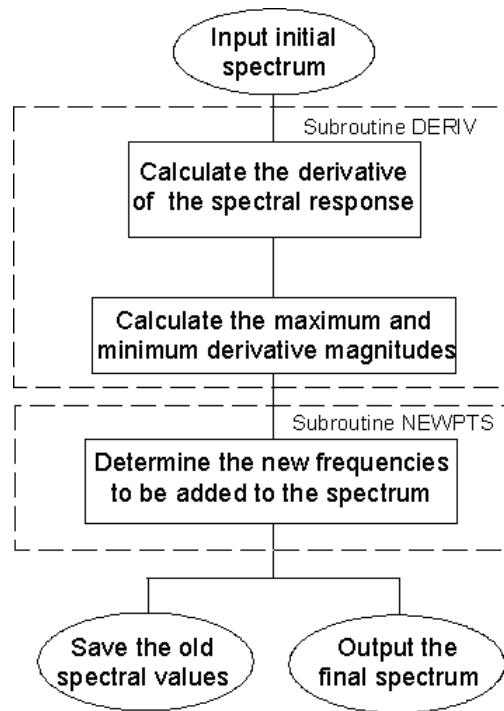


Figure 3: Event flow for determining new frequency points in the spectrum. Adapted from [1]

Iteration	No. of Points	Blumer Index
1	3	0.40
2	7	34.95
3	18	59.54
4	42	78.34
5	94	99.58
6	222	99.91
7	564	99.98
8	1573	99.99

Table 1: Blumer index for the spectrum of Figure 4 as a function of the iteration number

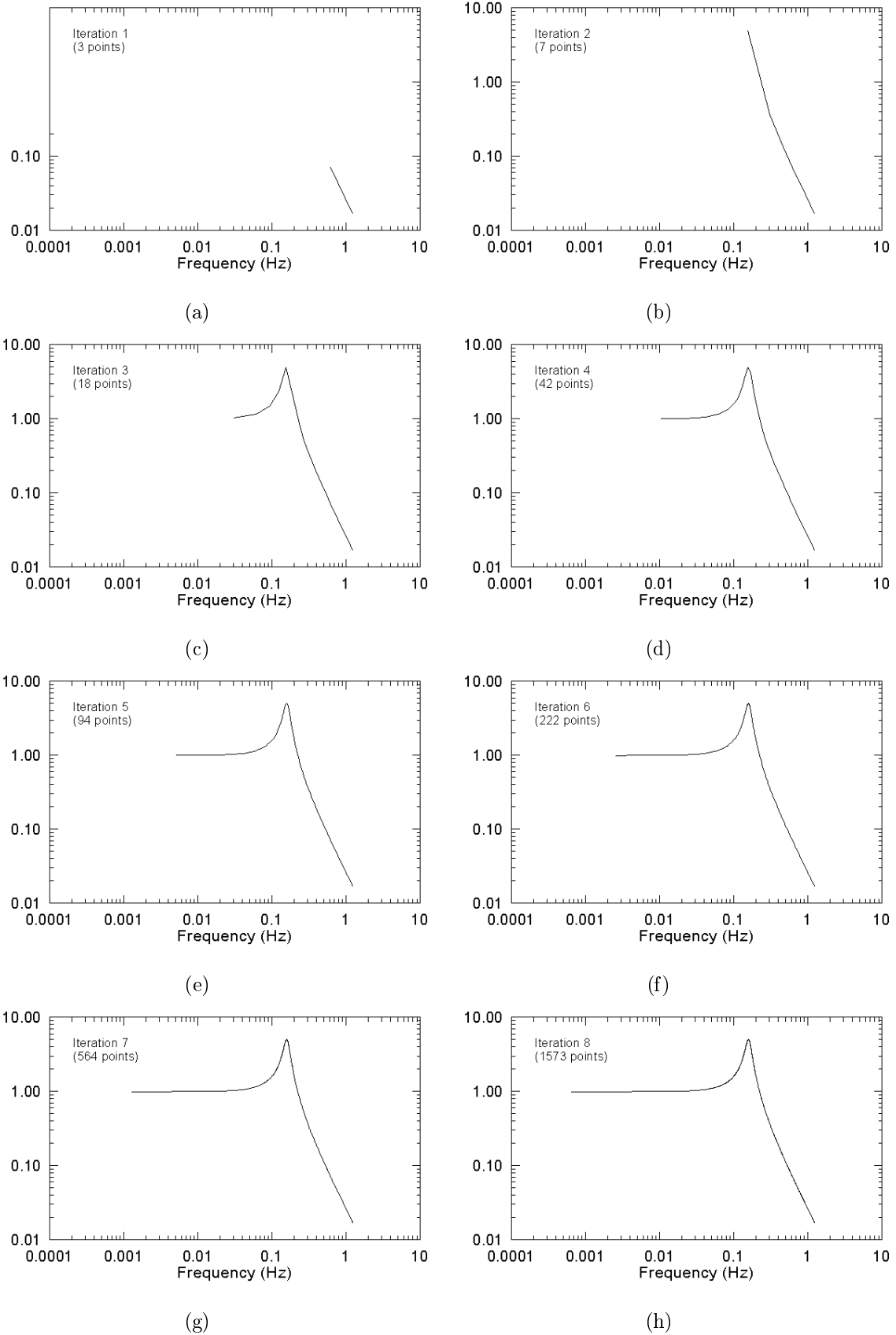


Figure 4: Spectral magnitude for iterations 1 - 8 (note that there is also a spectral point at $\omega_{min} = 0$, which is not evident on the log-log plots). Adapted from [1]

of the model explained in Chapter 4 featuring initially 29 equally spaced frequency steps between 10 MHz and 290 MHz . The Blumer method was then applied to try to ameliorate the quality of the results while adding a minimum number of points.

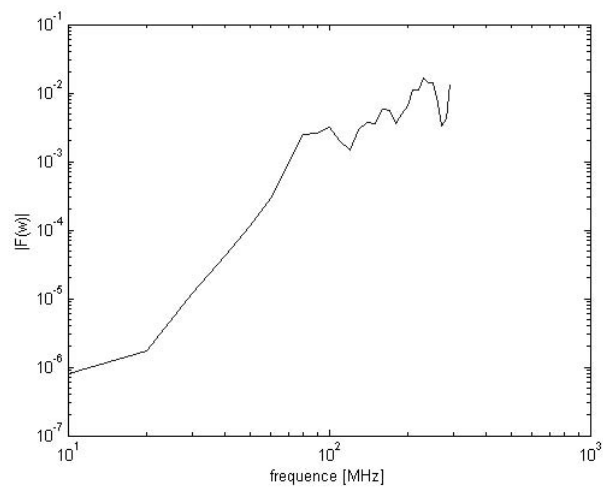
Starting from the existing simulation, three iterations were calculated. The computed results for each iteration are displayed in Figure 5 and the respective Blumer index values are displayed in Table 2.

Iteration	No. of Points	Blumer Index
1	29	53.0830
2	71	78.0191
3	162	94.9862

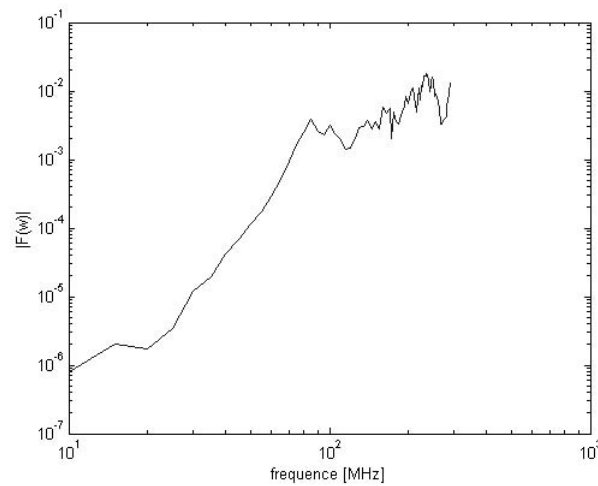
Table 2: Blumer index for the spectra of Figure 5 as a function of the number of iterations

As expected, the newly calculated frequency steps resulting from the application of the method are mostly concentrated in the higher frequency part of the spectrum, which is where resonances are located and thus, the better part of the information.

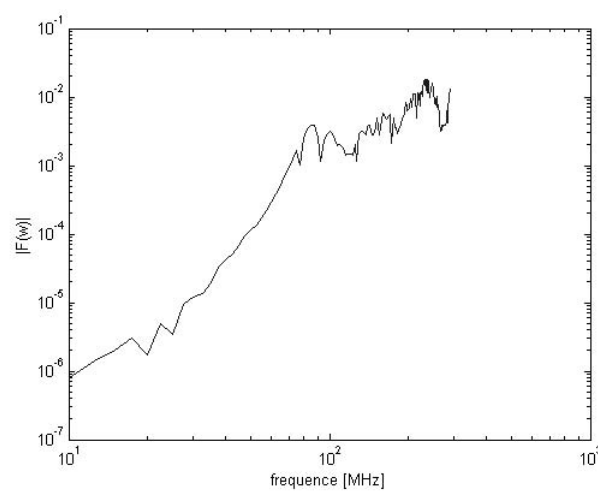
Work is in progress in order to integrate the Blumer method into parallel NEC.



(a) Iteration 1: 29 frequencies



(b) Iteration 2: 71 frequencies



(c) itération 3: 162 frequencies

Figure 5: Frequency spectrum of the vehicle simulation after each iteration

Bibliography

- [1] F. M. Tesche. Suggestions for the Implementation of an Adaptive, Nonuniform Sampling Scheme for CW Data Acquisition. In *Internal Report for the Swiss Defense Procurement Agency*, Dallas, TX, 1995.

Glossary of Terms

AutoEMC: European project EMC simulation for automotive applications.

BEM: Boundary Element Method.

CFIE: Combined Filed Integral Equation.

EAR: Equal Area Rule.

EFIE: Electric Field Integral Equation.

EMC: Electromagnetic Compatibility.

EMP: Electromagnetic Pulse.

EPFL: École Polytechnique Fédérale de Lausanne.

FAC: Fully Anechoic Chamber.

FDTD: Finite-Difference Time-Domain.

FFT: Fast Fourier Transform.

FMM: Fast Multi-pole Method.

FVTD: Finite-Volume Time-Domain.

FWHM: Full Width at Half Maximum.

GEMCAR: Guidelines for Electromagnetic Compatibility Modelling for Automotive Requirements.

GPS: Global Positioning System.

LAN: Local Area Network.

LAPACK: Linear Algebra Package.

MFIE: Magnetic Field Integral Equation.

MoM: Method of Moments.

MPI: Message Passing Interface.

NEAR: New Equal Area Rule.

NEC: Numerical Electromagnetics Code.

OATS: Open Air Test Site.

PC: Personal Computer.

PDE: Partial Differential Equation.

PLM: Perfectly Matched Layer.

PVM: Parallel Virtual Machine.

RCS: Radar Cross Section.

SAC: Semi Anechoic Chamber.

SCALAPACK: Scalable Linear Algebra Package.

TLM: Transmission Line Matrix.

VERIFY: Vertical EMP Radiating Indoor Facility.

WLAN: Wireless Local Area Network.

Curriculum vitae

Personal Information

Abraham RUBINSTEIN SCHARF
Route de la Maladière 20
CH-1022 Chavannes-près-Renens (VD)

Tel.: 41 21 691 2294
E-Mail: abraham.rubinstein@epfl.ch

Born September 14, 1971 in Bogota
Single, polish

Education

- 2004 Ph.D. from the EPFL
- 2000 Electrical Engineering Diploma from the “Universidad del Zulia”, Maracaibo

Professional Experience

- 2000-2004 Research and Teaching Assistant at the Power Systems Laboratory (LRE) of the EPFL
- Numerical computation of electromagnetic fields for EMC applications in automotive design
 - Research on lightning and EMP interaction with automobiles
 - Parallel Computing programming
 - Participation in laboratories and courses on EMC and Electric Circuits
 - Supervision of student projects
 - Development and maintenance of the EMC Group Web page
 - Development and maintenance of the Web page of the “Section d’électricité” of the EPFL
 - LRE’s Calculation Server system administrator
- 1998-2000 Project Engineer and System Integrator at COPLAN C.A., Maracaibo (Venezuela)
- Design, programming and Implementation of Remote Terminal Units (RTU) for Power Generation Plants
 - Design of detection and monitoring systems for explosive gases
 - Automation of Gas Compression Plants for venezuelan national oil company PDVSA
 - Head of the Human-Machine Interface (HIM) programming department
- 2 weeks (1997) Assistance and technical consulting at Telecom PTT, Bern

- Development of computer programs for the selection and design of cabling systems for data communications

2 months (1996) Professional Training Course at the Power Systems Laboratory (LRE) of the EPFL

- in Development and correction of software for the simulation of lightning electromagnetics

Distinctions

Best Thesis in Venezuela for obtaining the Degree of Electrical Engineering granted by INELECTRA, Caracas (Venezuela)

Certificate of Recognition for Excellent Academic Performance, appeared on the List of Honor of the College of Engineering of the "Universidad del Zulia", Maracaibo (Venezuela)

Maraven (Venezuelan National Oil Company) Prize of Academic Excellence, Maracaibo (Venezuela)

Certificate of Recognition for Outstanding Performance in Calculus III, granted by the "Universidad del Zulia", Maracaibo (Venezuela)

Certificate of Recognition for Outstanding Performance in Informatics, granted by the "Universidad del Zulia", Maracaibo (Venezuela)

Certificate of Recognition for Outstanding Performance in Linear Algebra, granted by the "Universidad del Zulia", Maracaibo (Venezuela)

Certificate of Recognition for Outstanding Performance in Physics II, granted by the "Universidad del Zulia", Maracaibo (Venezuela)

Certificate of Recognition for Outstanding Performance in the Course: "Study and Comprehension of Mankind", granted by the "Universidad del Zulia", Maracaibo (Venezuela)

Certificate of Recognition for Outstanding Performance in Calculus I, granted by the Department of Mathematics, College of Engineering of the "Universidad del Zulia", Maracaibo (Venezuela)

Certificate of Recognition for having attained the best Grade Point Average for the Senior year of High School in 1987-1988, granted by the "Unidad Educativa José Ramón Yepes", Maracaibo (Venezuela)

Certificate of Recognition for Excellence Performance in Literature for the year of Middle School in 1983-1984, granted by the "Escuela Básica Aragua", Maracay (Venezuela)

Certificate of Excellence in Academic Performance for the year of Middle School in 1983-1984, granted by the "Escuela Básica Aragua", Maracay (Venezuela)

Publications Parts of the present work have been published in the following papers:

Journal Papers

A. Rubinstein, F. Rachidi, and M. Rubinstein. A Physical Interpretation of the Equal Area Rule. In *To be submitted to IEEE Transactions on Electromagnetic Compatibility*, 2004.

A. Rubinstein, F. Rachidi, and M. Rubinstein. On Wire-grid Representation of Solid Metallic Surfaces. In *IEEE Transactions on Electromagnetic Compatibility*, 2004. In press.

A. Rubinstein, F. Rachidi, M. Rubinstein, and B. Reusser. A Parallel Version of NEC for the Analysis of Large Structures. In *IEEE Transactions on Electromagnetic Compatibility*, volume EMC-45, pages 177–188, May 2003.

Conference Proceedings

N. Whyman, C. Thomas, S. Alestra, X. Ferrières, J.P. Parmantier, R. Perraud, F. Rachidi, A. Rubinstein, and A.R. Ruddle. The EU Framework V Project GEMCAR: Model validation. In *Proc. of the 15th International Symposium on Electromagnetic Compatibility, Zurich, 2003*.

S. Alestra, X. Ferrières, J.P. Parmantier, R. Perraud, F. Rachidi, A. Rubinstein, A.R. Ruddle, and N. Whyman. The EU Framework V Project GEMCAR: CEM techniques investigated. In *Proc. of the 15th International Symposium on Electromagnetic Compatibility, Zurich, 2003*.

A. Rubinstein, F. Rachidi, and M. Rubinstein. Development of an Optimized Parallel Numerical Electromagnetics Code (NEC) and Its Implementation on the Swiss-T1 and Eridan Parallel Supercomputers. In *Annual Review of Progress in Computational Electromagnetics. Monterey*, 18-22 March 2002.

A. Rubinstein, F. Rachidi, J.-P. Parmantier, X. Ferrières, S. Alestra, R. Perraud, A.R. Ruddle, and B. Reusser. Modélisation de la penetration d'un champ électromagnétique à l'intérieur d'une automobile: simulation et validation expérimentale. In *Colloque CEM, Grenoble. France*, March 2002.

A. Rubinstein, F. Rachidi, D. Pavanello, and B. Reusser. Electromagnetic Field Interaction with Vehicle Cable Harness: An Experimental Analysis. In *International Conference on Electromagnetic Compatibility, EMC Europe. Sorrento*, volume 1, 2002. Proceedings.

A. Rubinstein, F. Rachidi, and B. Reusser. Modeling of the penetration of an electromagnetic field inside an automaobile using a parallel version of NEC: simulation and experimental validation. In *URSI General Assembly, Maastricht, the Netherlands*, August, 2002.

A. Rubinstein, D. Pavanello, F. Rachid, M. Ianoz, B. Reusser, E. Petrache, and J. L. Bermudez. The GEMCAR project : Preliminary experimental results on a simple test case using an EMP simulator. In *International Workshop on EMC Measurement Techniques for Complex and Distributed Systems. Lille, France*, June 2001.

E. Petrache, F. Rachidi, M. Ianoz, JL Bermudez, A. Rubinstein, M. Paolone, C.A. Nucci, A. Borghetti, J.A. Gutiérrez, and B. Reusser. An experimental test for the validation of time domain codes for the analysis of transient field coupling to transmission line networks. In *International Workshop on EMC Measurement Techniques for Complex and Distributed Systems. Lille, France*, June 2001.

Reports

A. Rubinstein. GEMCAR: EMP Measurements - Medium Test Case. Technical report, EPFL, September 2001.

A. Rubinstein. GEMCAR: EMP Measurements - Simple Test Case. Technical report, EPFL, November 2000.

Supervised graduate and undergraduate projects

F. Faivre. Implémentation d'un système d'échantillonnage adaptatif non uniforme. Projet de semestre, EPFL, February 2003.

D. Pavanello. Electromagnetic field interaction with modern vehicles: application of the Method of Moments. Bachelor's thesis, Politecnico di Torino, Facoltà di Ingegneria dell'Informazione, 2002.

I. Sidibe. Compatibilité électromagnétique dans les voitures modernes. Projet de semestre, EPFL, February 2000.